Vestibular Evoked Myogenic Potentials: Physiology, Variability, and Statistical Characteristics

By

Srinivasamurthy Ravi Prakash

M.E. Electrical Communication Engineering
Indian Institute of Science, Bangalore. 1990

Submitted to the Harvard-MIT Division of Health Science and Technology
in partial fulfillment of the requirements for the degree of

DOCTOR OF PHILOSOPHY

at the

MASSACHUSETTS INSTITUTE OF TECHNOLOGY
JUNE 2009

Signature of Author:_____

Harvard-MIT Division of Health Science and Technology
May 15th, 2009

Certified by:_____

Steven D. Rauch, M.D.
Professor of Otology and Laryngology, Harvard Medical School

Accepted by: _____

Ram Sasisekharan, Ph.D.
Director, Harvard-MIT Division of Health Science and Technology
Edward Hood Taplin Professor of Health Science and Technology and Biological Engineering

Vestibular Evoked Myogenic Potentials: Physiology, Variability, and Statistical Characteristics

Srinivasamurthy Ravi Prakash

Submitted to the Harvard-MIT Division of Health Science and Technology on June 5th, 2009 in partial fulfillment of the requirements for the degree of Doctor of Philosophy

Abstract

Vestibular Evoked Myogenic Potentials (VEMPs) are electrical signals recorded from the skin overlying skeletal muscles of the head and neck in response to high-intensity acoustic stimuli. VEMPs have been observed in stimulus locked averages of the electromyogram in a majority of human subjects, and are thought to originate in the otolith organs of the inner ear, which are balance organs responsible for sensing acceleration and orientation with respect to gravity. Otolith reflexes interact with the motor drive to a contracted muscle to give rise to the VEMP signal. In the last few years these signals have been used in the clinic as an indicator of peripheral vestibular function and a test based on VEMP from neck muscles (cervical, or cVEMP) is currently the only clinically feasible means of assessing the functioning of the saccule and its innervation. However, the usefulness of the test is limited by the inter-subject and test-retest variability of the response, and the unclear relationship between specific response features and vestibular pathophysiology.

In this thesis, our goal is to measure VEMP variability, assess the influence of non-vestibular factors on the VEMP, and to develop a signal processing strategy to estimate response parameters that are both statistically stable, and physiologically meaningful.

In the first part of the thesis, we systematically measure VEMPs from a small clinically normal population, and quantify the variability of the response, particularly the dependence on contraction effort. We also assess approaches to normalizing the response by estimates of the effort.

In the second part of the thesis, we develop a computational model of VEMP physiology, and use the model to separate external sources of variability from internal noise. The model outputs are also used to define a statistical measure, the inverse coefficient of variation (iCOV), which correlates with altered vestibular sensitivity, but is relatively robust to other changes.

When applied to the experimental data, the iCOV is found to yield estimates of vestibular sensitivity that are more stable than the conventional VEMP amplitude. This measure also reveals a diversity of response threshold and growth characteristics within the clinically normal population. These findings suggest that the proposed approach could lead to the development of an improved clinical tool, but could also yield new insights into the physiological mechanisms of vestibular pathology.

Thesis Supervisor: Steven D. Rauch, M.D.

Professor of Otology and Laryngology, Harvard Medical School

Acknowledgements

In doing this work I have relied on the encouragement, support, guidance and the well-meaning criticism of many. Among them have been friends, family, colleagues and mentors, and I owe each of them an enormous debt of gratitude. When we moved from California to Massachusetts, trading a life of relative order and comfort for the uncertainty of graduate student life, we were warmly embraced by the community at MIT, at the Mass. Eye and Ear Infirmary, and in our adopted hometown of Arlington, and this sustained us along the long journey through school. Meanwhile, the friends and family in California, in India and around the world have stood by us all along.

Dr. Rauch's warmth, humor, and keen clarity of thought and expression have been a reliable aid in my efforts. While caring for his patients and students, he has been unfailingly encouraging and generous of his time, and in his assessment of my abilities at time when I doubted them most. I could not ask for a better advisor and friend.

My thesis committee was much more than that: they were a diverse group of clinicians and scientists who met to discuss how to make a better test of balance, and in passing, to assess, guide and encourage my tortuous progress through the PhD. Dr. John Guinan has been an inspiration in his methodical approach to problems, breadth of knowledge and insight, and truly fearsome work ethic. He has been a very big part of the thesis, and my discussions with him have been critical to the direction of the work. More than anything, he taught me that a model's success is built on a foundation of well-understood experimental data. Dr. Barbara Herrmann's experience with evoked potentials and her intuitive understanding of the nature of VEMP provided much-needed clarity and perspective. She introduced me to the problem of VEMP variability, and taught me to make careful, systematic measurements on those really difficult animals, humans. Dr. Uri Eden was a late recruit to the committee, and agreed enthusiastically to guide me even though the topic was a little removed from his main body of research. His input has been crucial in understanding the mathematical basis for the behavior of the model, and I hope to continue working with him in that direction well beyond this thesis. I would like to thank Dr. Yvette Smulders from Maastricht for her help in collecting the data, and all the subjects who participated in the study.

My thanks go to the faculty, staff, post-docs and students at MEEI and EPL for their support and guidance. In particular I would like to thank Dr. Jennifer Melcher for being a wonderful academic advisor, coach and friend, and Dr. Chris Shera, Dr. John Rosowski, Dr. Bertrand Delgutte, Dr. Nelson Kiang and Dr. Ruth Anne Eatock for many helpful discussions. I should also thank the EPL Engineering staff, particularly Frank Cardarelli for help with LabView programming.

The Speech and Hearing program of HST is a program extraordinary breadth, and attracts students with a wide range of interests and talents. It has also provided me with some of my closest friends

and colleagues – I am proud and privileged to have known them: Adrian, Daryush, Brad, Anne, Anton, Amanda Yoko, Sasha, Erik, Cara, Asa, Jocelyn, Radha and Ray.

On the home front, I would like to thank and remember Dr. Anuradha Rao, who was very special to all of us. I miss you.

Our neighbors in Arlington have been deeply supportive and encouraging of this whole enterprise – it helps that half of them have been through grad school themselves. Particular thanks to the Trvalik, Delbanco, Daly, Brigham, Pajevic and the Sawai families, and to Lalitha and Vidyamurthy.

We could count on the support of the family we left behind: Krishna, Chaya, Sujatha, Kumar and their children in California, and my parents-in-law, my brother and my parents in India.

One of the joys of being in school has been to be able to spend time with Nishant and Kayshav, watching them go through pre-school to middle school. Along the way, they have shared – and endured – the ups and downs of my research with humor and fortitude.

Hard as this work has been neither the start, nor the end, nor the long middle of this adventure would have been possible without the courageous support and love I received from my wife. Shyamala has been the rock, the prime mover and the love of my life. Thank you for everything.

Table of Contents

Chapter 1. Outline

There are some enterprises in which a careful disorderliness is the true method
~Hermann Melville

Vestibular Evoked Myogenic Potentials (VEMPs) are electrical signals recorded from the skin overlying skeletal muscles of the head and neck in response to high-intensity acoustic stimuli. These have been observed in a majority of human subjects, and are thought to originate in the otolith organs of the inner ear, which are vestibular (balance) organs responsible for sensing acceleration and orientation with respect to gravity. Otolith reflexes interact with the motor drive to a contracted muscle to give rise to the VEMP signal. In the last few years these signals have been used in the clinic as an indicator of peripheral vestibular function and a test based on VEMP from neck muscles (cervical, or cVEMP) is currently the only clinically feasible means of assessing the functioning of the saccule and its innervation. In the rest of this thesis, we will use the term VEMP to refer to cervical VEMP only.

1.1 The problem

The usefulness of the VEMP test is limited by two factors. First, the response waveform and its amplitude are highly variable, even within the normal population, and even from session to session within the same subject. Second, the relationship between specific response features and peripheral vestibular mechanisms are poorly understood. As a result, despite numerous studies measuring various response features (e.g. amplitude or latency) in normal and pathological populations, there is no corresponding improvement in the understanding of peripheral pathophysiological processes that could produce changes in those features.

1.2 Goals and scope of the study

Our research had two inter-related goals:

(i) To experimentally study the nature and causes of variability in VEMP responses within a normal population and to critically examine approaches to reducing this variability.

(ii) To incorporate the current knowledge of the physiology underlying VEMP into a model that can be studied using computational and analytical methods. We could use this model to identify a statistic that can be computed from the surface measurements which reflects a clinically significant

aspect of the peripheral vestibular response. To the extent that this statistic is independent of other (non-vestibular) influences, we can expect improved inter-subject and inter-session variability

Our knowledge of the vestibular reflex mechanisms underlying VEMP is by no means complete. There remain many open questions, particularly relating to signal transmission to the saccule, transduction processes within the saccule, neural coding of the response at the periphery and neural transformations in the vestibular nuclei. While many of these questions are of great clinical significance, they were not the subject of this study. Instead, we focused at the other end of the signal chain, where the vestibular response interacts with the motor system. This emphasis was appropriate because the clinical problems motivating this study relate to the wide variability of the response among *normal* subjects. In this population, it is reasonable to assume that every ear responds to identical stimuli in a similar manner, and examine potential sources of variability outside the vestibular system.

We also note that this study, with its small sample size and focus on the physiological basis of VEMP and VEMP variability in normals, is complementary to conventional clinical studies where measurements from large populations of identified normal and pathological subjects are studied, correlations between pathology and measured parameters are evaluated, and the range of expected parameter values for each population is established. We hope that our results help guide the design of future clinical studies and help in the interpretation of the results of those studies.

1.3 Approaches

In the experimental phase of the study, we recorded VEMPs from a small, clinically normal population using a recording and storage setup that allowed us to manipulate individual responses (traces) and compute different statistical measures on the recorded data. By sorting and scaling the measured data based on different attributes, we could create new ensembles of traces and compare the VEMP derived from each ensemble with the conventional VEMP average of consecutive traces.

In the modeling phase, we summarized the physiology of the vestibular reflex, the cortico-motor drive, the muscle and the measurement system in a simplified conceptual model. We translated this conceptual model into a computational model using Matlab routines to generate ensembles of synthetic signals which we could manipulate in the same manner as recorded data. We also translated the concepts into a mathematical model, from which we could predict the behavior of VEMP under different conditions. Unlike experimental data, the model outputs allowed us to examine the influence of specific changes in the vestibular periphery on the statistics of the VEMP.

Finally, we will applied the statistical measures developed from the modeling study to the experimental data and looked for similarities and systematic differences within our normal subject pool.

1.4 Key findings of the study

Our experimental data confirmed the problem with VEMP: the average VEMP waveform shows large differences between subjects and between measurement sessions. Our simulation studies suggested that a significant proportion of these differences arise from inter-subject and inter-session differences in the electrical response of the muscle, its surrounding tissues, and the electrode geometry, as opposed to arising from differences in the vestibular response.

Our experiments also confirmed the dependence of the magnitude of the VEMP average on contraction effort, but we found that data obtained even with relatively weak contraction have a measurable signal component, suggesting a potential benefit of normalization by an effort estimate. We were able to use the simulation studies to develop the appropriate filter for extracting the contraction effort estimate to drive a normalization scheme. However, we found that variations in contraction effort make a relatively small contribution to the intra-session variability of VEMP, compared with the variability intrinsic to the stochastic nature of the signal. Therefore, even an ideal normalization scheme should be expected to yield only minimal improvements in test-retest variability. Nevertheless, normalization allows us to relax the requirement of sustaining an intense contraction effort that makes VEMP a demanding test for many patients.

In the simulation study, we examined the outputs of a computational model of the muscle, its motor drive, and the acoustic inhibition. We sought a statistical measure of the amount of inhibition produced by a given stimulus, which would be relatively immune to differences in inter-subject and inter-session characteristics. We found that the mean amplitude of an ensemble of measurements scaled by the standard deviation of the ensemble of measurements is less vulnerable than the amplitude alone to changes in subject- and session-specific characteristics. When this statistic (which we term inverse coefficient of variation, or iCOV) was applied to experimental data, it was found once again that the mean-to-standard deviation ratio measured across sessions, across different degrees of contraction effort and across repeated measurements within a session, shows much smaller variability than the raw amplitude of the VEMP average. As a result, when the iCOV is used as a metric of the size of the inhibitory response, different stimulus intensities are more clearly distinguished compared with conventional amplitude growth functions. We conclude that the iCOV is a superior metric for identifying pathologies characterized by altered sensitivity of the vestibular periphery.

From a practical standpoint, the outcome of this study is a simple algorithm for processing the VEMP responses that has been shown to yield improved performance in our experimental and simulated data. We propose a real-time implementation of this algorithm and its application on a larger clinical population to clarify its potential for identifying pathophysiological changes in the vestibular system.

From a conceptual standpoint, the success of the computational model in replicating features of the experimental VEMP strengthens our understanding of the physiological mechanisms of VEMP. At the same time, we have a deeper understanding of how a breakdown of the conventional additive Gaussian noise model can affect the processing and interpretation of the signals. These lessons may be applicable to a wider class of physiological signals whose underlying statistical models are similar to VEMP and the electromyogram.

1.5 Organization of the thesis

In the following chapters, we discuss the study and its outcomes in detail. Chapter 2 describes the physiology of vestibular reflexes and the physiology of skeletal muscle necessary to understand the experiment and model development. In Chapter 3, we describe our systematic survey of the variability of cVEMP measurements among normal subjects, and a qualitative and quantitative examination of the factors that influence the VEMP response. Chapter 4 develops a computational model of the VEMP reflex, examines the statistics of the simulated VEMP signals as a function of the magnitude of the vestibular response, and develops a signal processing algorithm that yields stable magnitude estimates. We conclude in Chapter 5 by looking at the implications of the study on the vestibular and muscle physiology, clinical applications, and describe the directions of future work suggested by this study.

Chapter 2. Background

In this chapter we will briefly describe some of the physiological systems that are involved in the generation of the VEMP response. Rather than an exhaustive description of the vestibular and motor systems, the chapter provides a brief outline of these systems at the level of complexity necessary for the understanding and modeling of the physiology of VEMP. The reader is referred to texts such as Baloh and Honrubia [1] for the vestibular system, or the Handbook of Physiology [2] sections on nerve and muscle physiology for additional background if needed.

2.1 The Vestibular system

The vestibular system provides the principal sensory input that enables the human body to control its posture, orientation and gaze direction and to plan coordinated muscle actions such as locomotion. At various centers in the brainstem and the mid-brain, inputs from the vestibular system are integrated with inputs from the visual and somatosensory systems, such that a consistent percept of position, motion and orientation is created in higher cortical centers. At the same time, descending projections from these brainstem and mid-brain centers to muscles of the eye, neck, torso and limbs help control the position of the eyes and the body in face of voluntary movements and external perturbations. It is these mechanisms of fast motion compensation that allow us to perform complex tasks such as reading a signboard from within a moving train.

The peripheral vestibular system consists of the vestibular labyrinth in the inner ear, five sensory organs within each labyrinth and the associated nerve bundles. Three of the sensory organs are arranged in the semi-circular canals that respond to rotational motion. Two of the sensors are in the "otolith" organs, the saccule and the utricle, which respond to linear acceleration and orientation with respect to gravity. A comprehensive review of the functional anatomy and neurophysiology of the vestibular system may be found in [3].

2.1.1 Clinical issues of vestibular testing

When a patient presents with vertigo or dizziness, the disorder, in majority of cases, is found to be in the peripheral vestibular system [4]. In order to guide the treatment, the physician is usually interested in answers to the "where" and "what" (i.e., the site of lesion and the pathophysiological mechanism) of the disorder. The patient's subjective percepts and the neurological signs combine sensory inputs from both ears and from the visual and somatosensory systems and it is often difficult to disambiguate these influences. Therefore, although considerable information can be obtained from the patient history and clinical examination by a skilled physician, there is a need for

quantitative functional testing of the vestibular system [5]. A fairly current review of quantitative tests of vestibular function [6] points out the difficulties of assessing otolith function compared with canal organ function. Since translational acceleration is difficult to apply in a confined setting and cannot be applied unilaterally, tests of the utricle involve complex stimuli combining rotational and translational motion. Because the saccule responds to acceleration in the vertical plane and to the gravity vector, it is even more difficult to test. The only feasible means of testing the saccule and the branch of the vestibular nerve that serves the saccule (the inferior vestibular nerve) is the VEMP test.

2.1.2 Stimulation of the saccule

Like the caloric test applied to the horizontal semicircular canal, the VEMP test involves a stimulus that is unrelated to the motion-sensing function of the saccule. It relies on the "leakage" into the vestibular system, of part of the energy of an acoustical signal transmitted through the external and middle ear. It is a matter of considerable debate whether the acoustic response of the saccule has functional significance; a hearing role for the saccule has long been posited for some reptiles and amphibia (see references in [7]) and some authors have speculated that this role persists in humans [8]. For the purposes of the VEMP test, it is sufficient to note that the saccule has been directly observed to respond consistently to acoustic stimulation in different species (guinea pig [9], cat [10], and squirrel monkey [11]), and can therefore be presumed to have an acoustic response in humans as well.

The mechanical details of the acoustic coupling are also not very well understood, although the elevation of VEMP amplitude (i.e. elevation of saccular response) in instances where the semicircular canal wall has a dehiscence (a hole or a soft spot) suggests that motion of the stapes initiates fluid movement across the saccule into the rest of the vestibular labyrinth. Since there are no direct measurements of the saccular response in humans, we do not know the normal magnitude of the response to a given stimulus. We also do not know how much this response magnitude varies across the normal population. The use of VEMP as an assay of vestibular sensitivity is premised on the idea that different ears couple roughly the same proportion of the acoustic energy of the stimulus to the saccule, and inter-subject differences in the size of the VEMP response arise from differences in the saccule's sensitivity to linear acceleration.

2.1.3 The vestibulocollic reflex

As our example of reading a signboard from a train illustrates, control of the body involves two separate components: the voluntary motor drive (to neck and eye muscles in order to track the moving signboard) and reflex signals (that move the muscles of the eye and the body to compensate

for the non-smooth motion of the train). The net activity of a muscle arises from the interaction of these voluntary and reflex components.

These 2- and 3-synapse reflex loops from the vestibular system include the vestibulo-ocular reflex to the muscles of the eye, vestibulocollic reflexes to the neck muscles, and vestibulospinal reflexes to the lower body. The VEMP arises as a consequence of the effect of vestibulocollic reflexes on the surface electrical activity produced by muscles responsible for neck rotation, particularly the sternocleidomastoid (SCM) muscle. Specifically, it is believed that *when the ear is excited by a brief acoustic stimulus, the response of the saccule is carried on vestibulocollic reflex pathways, causes a brief inhibition of the motor neurons of the ipsilateral SCM, and results in a stimulus-locked modulation of the surface electrical potential that we call VEMP.*

The pathways connecting the saccule with the neck muscles have been studied in detail by different investigators (see [12, 13] for a comprehensive review). In Figure 2.1, we briefly outline three key studies that support our current understanding of the physiology of vestibulocollic reflexes and VEMP.

2.2 VEMP

The introduction of the stimulus-triggered signal averaging in the 1950s [14, 15] made it possible to extract weak physiological responses despite contamination by large amounts of both physiological and instrument noise. This led to an explosion of interest in the physiology, pathophysiology and clinical application of surface potentials evoked by sensory stimuli (e.g. [16], and other papers in those Annals). Sound-evoked potentials, in particular, were studied over a variety of scalp electrode montages and stimulus paradigms, yielding responses over a wide range of latencies and amplitudes. Stable and reproducible responses over the 0-5 ms post-stimulus period were soon recognized as neurogenic far-field potentials from the auditory nerve and brainstem [17], and now constitute the auditory brainstem response (ABR) used in clinical audiology [18]. Meanwhile, potentials with peaks in the 7-50ms range recorded over the mastoid and over the inion [19] were found to include components which changed in amplitude depending on changes in head position, posture and muscle tone [20], leading to the conclusion that these responses originated in the activity of head and neck muscles [21]. Such myogenic components recorded over the temporal bone (the post-auricular muscle potential) were found to be cochlear in origin [22], while the inion response was evoked by stimulation of the vestibular system [23].

Over the following few decades, electrophysiological studies of the vestibular periphery [10, 11], brainstem nuclei [24], and neck muscle units [21, 25], as discussed in Section 2.1.3, helped delineate the sources and the pathways responsible for the vestibular components of the auditory evoked response which are now referred to as the vestibular evoked myogenic potential. In recent years, vestibular evoked myogenic responses have been recorded from other muscle groups, in particular

those involved in eye movement. These are generally referred to as the ocular VEMP, or oVEMP. The mechanisms of these responses are not the focus of this study, and the term VEMP in this thesis will refer to cervical VEMPs or cVEMPs. Figure 2.1 summarizes the key pieces of evidence supporting the current understanding of the origin of the clinical VEMP response. Briefly,

- The saccule has a phasic response to a punctate acoustic stimulus
- The saccule response activates an inhibitory reflex from the vestibular nuclei to the sternocleidomastoid (SCM) motoneurons.
- This inhibition modulates the ongoing activity of motor units of the SCM muscle under voluntary contraction
- The modulation results in changes of the statistics of the surface electromyogram (EMG).
- Changes in the mean of the EMG estimated using stimulus-locked averages of the EMG, constitute the VEMP response.

This relationship between the VEMP and the vestibular periphery has led to the use of VEMP as a clinical test of the functioning of the saccule and its afferent innervation. The history of VEMP is extensively reviewed in [26], [27] and [28], while the physiology and clinical application are reviewed in [29].

2.2.1 VEMP in the clinic

Since the mid-1990s, the VEMP test has been developed along the methods outlined in [21], and is now an established part of the vestibular test battery at a number of clinics. Despite differences in the details, all VEMP tests follow the same basic procedure:

- Surface electrodes are placed on the skin over the sternocleidomastoid (SCM) muscle on one side of the neck.
- The subject tenses the muscle under test either by turning the head or by lifting the head from a supine position.
- The subject maintains maximum voluntary tension on the muscle, and is assisted by direct or indirect feedback of the ongoing EMG level.
- Brief acoustic stimuli (tonebursts or clicks) are applied to the ear ipsilateral to the muscle being recorded at a rate between 5 and 15 stimuli/sec.
- The electrical signal from the electrodes is amplified, band-pass filtered, and recorded in synchrony with the stimulus. A waveform of running average of the EMG signal over an approximately 50 ms post-stimulus interval is computed and displayed.

- When sufficient averaging has been performed that a stable response waveform is obtained - or no such response is found – the recording is terminated.

The typical output of a VEMP test is a set of waveforms stacked by stimulus intensity (Figure 2.2). Each VEMP waveform represents the averaged EMG at different time points relative to the stimulus, and is computed by averaging the individual post-stimulus EMG signals. Normal VEMPs generally show a characteristic biphasic pattern with an initial latency of 11-15 ms, and duration of 15-30 ms, and peak-peak amplitudes between 20 μV and >200 μV depending on the stimulus level and contraction effort.

Reviews of clinical applications of VEMP, including measures of variability of various response parameters may be found in [29-32] and [33].

The processing and interpretation of VEMP in the clinic is often done along the lines similar to neurogenic potentials such as ABR. In evaluating a typical evoked potential,

- The responses are recorded using a standard clinical protocol developed for the test.
- The responses are averaged until a section of the response emerges above the surrounding noise.
- Features of the averaged response are identified based on comparison with the "canonical" shape of the response waveform.
- The resulting waveform features, is examined for salient parameters such as peak amplitudes, peak latencies, response threshold, etc.
- These parameters are compared against normative ranges established from clinical studies that compare normal and pathological populations.
- The departures from normal values are interpreted using pathophysiological models that relate the response features such as identified peaks to generator sites, and specific types of changes to pathological processes at those sites.

For auditory evoked potentials, this process is well established and described in clinical textbooks [18, 34]. When applied to VEMP, however, the process is much less successful for three reasons: the variability of the response waveform, its dependence on extraneous factors such as contraction effort, and the lack of well-established pathophysiological models. These difficulties of using VEMP have not been systematically described, but are a common feature of the experience with VEMP in the clinic at the Massachusetts Eye and Ear Infirmary. In a published report on VEMP variability, Ochi, Ohashi and Nishino [32] describe this problem:

> Latency of pI and nII were stable, whereas pInII amplitude was varied. The input–output function of pI latency and nII latency were not stable. Although the muscle tonus affects

pInII amplitude significantly, no statistically significant improvement was observed in test–retest investigation after adjustment using muscle tonus.

Thus the response parameter that responds most reliably to stimulus level (i.e. whose input-output function was stable) is also the parameter that shows the greatest variability and sensitivity to contraction strength.

The fact that the VEMP is a fundamentally different response from neurogenic evoked potentials has been recognized only peripherally in most clinical reports. A notable exception is the work by Wit and Kingma [35] who explicitly model VEMPs along lines similar to those we have explored in this thesis. However, they do not use the model to understand the statistical properties off VEMP, and to address the underlying clinical questions; its usefulness is therefore limited.

2.3 Physiology of muscle

An important part of the model of VEMP in this study is the structure of the muscle whose activity generates the EMG as well as the VEMP. This muscle, the SCM, is a large skeletal muscle primarily responsible for the rotation of the head in the horizontal plane. The muscle is anchored at the cranial end to the temporal bone and at the caudal end to the sternum and clavicle, so that contraction of the muscle results in rotation of the head toward the contralateral shoulder. The muscle is primarily innervated by a branch of the accessory nerve (CN XI) whose α-motor neurons originate in the spinal root at segments C1-C3 of the cervical spine [36]. The innervation zone of the SCM is found to be midway between the insertion points on the belly of the muscle [37]. The gross anatomy of the SCM in humans has been reviewed in [38] and the microarchitecture of primate neck muscles has been described in [39]. EMG studies of the function of neck muscles have been reported in humans [40], and in other primates [41]. These studies have been used in our investigation as the basis for defining the muscle size parameters of the computational model of VEMP, and to guide the placement of electrodes in the experimental study.

The mechanical action of a muscle is due to the contraction of individual muscle fibers initiated by an action potential on the α-motor neuron that innervates it. Each fiber is served by a single motor neuron, but a motor neuron usually projects onto a number of muscle fibers which contract in unison. The motor neuron and the set of fibers it innervates, collectively called a *motor unit*, constitute a key functional building block of the muscle. The wave of electrical activity propagating along the length of the muscle as the fibers of a motor unit depolarize in response to an action potential on the motor neuron is called a *motor unit action potential.* The fibers of the motor unit may be distributed across the cross-section of the muscle and interspersed with the fibers of up to dozens of other motor units. The basic architecture and physiology of mammalian muscle are described in most standard neurophysiology texts [42]. There are few detailed studies on the

number, the size and depth distribution of human motor units specifically for neck muscles, and the parameters we used were extrapolated from broader studies such as the one by Buchthal and Schmalbruch [43].

Since the interest in this study was on electrical activity induced by the muscle contraction at the skin surface, we examined the large body of literature on the modeling and analysis of electromyograms. A detailed review of these studies is outside the scope of this thesis; a comprehensive survey may be found in [44]. The EMG modeling studies largely fall into three broad categories: (i) Idealized signal models that treat the EMG as a filtered Gaussian noise process with a noise variance parameter representing contraction effort (e.g. [45]), (ii) Models that include motor unit spiking and treat the EMG as a filtered point process (e.g. [46]), where the effort is translated into spike statistics using models of motor unit recruitment , and (iii) Extended signal models, which replace the generic filter with a detailed volume conductor model incorporating factors such as motor unit distribution, tissue geometry, electrical properties of tissue (e.g. [47]). Our study uses a detailed statistical model of the motor unit pool and the spiking process but for computational simplicity, it subsumes details of the motor unit action potential and the volume conductor into a single filter transfer function. Thus it includes features of models of type (ii) and (iii) above.

2.4 Figures

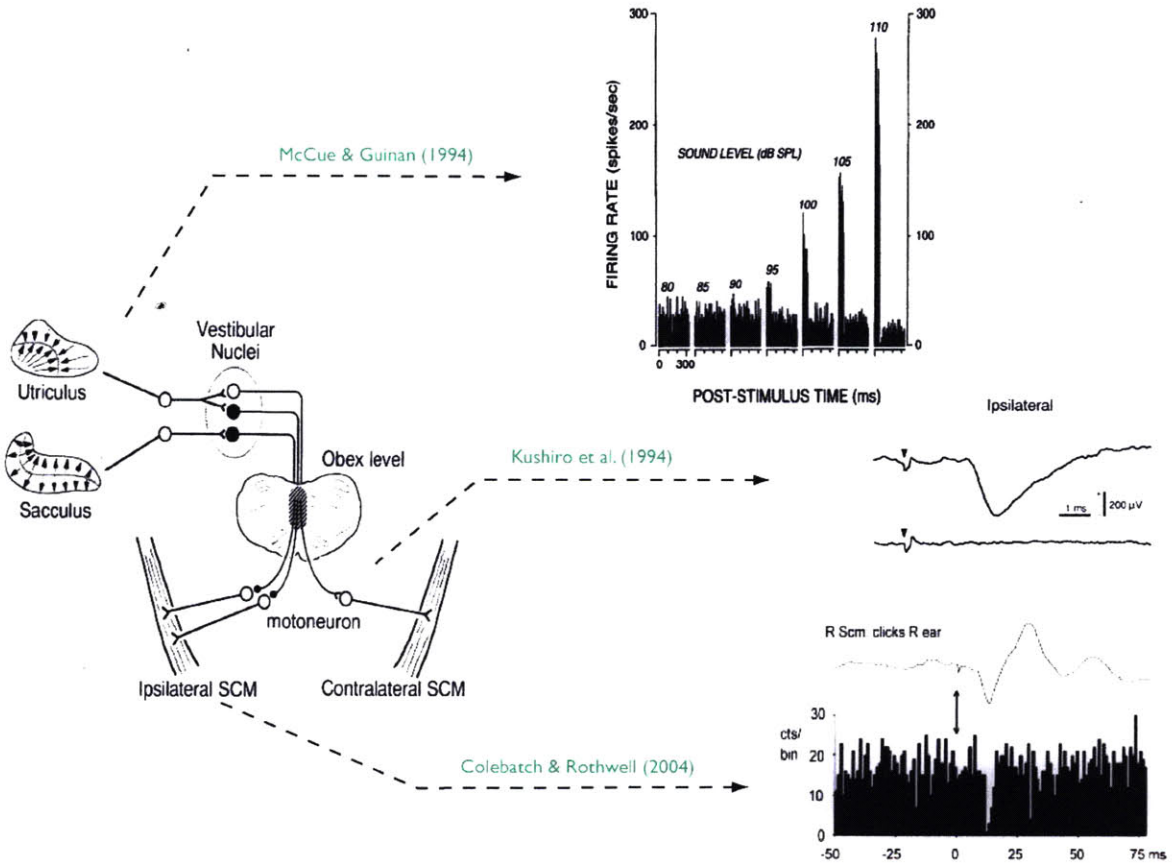

Figure 2.1 Key studies of vestibulocollic reflex physiology

Figures from three different studies that examined the pathways linking acoustic stimulation of the saccule to surface electric potentials from neck muscle. (i) McCue and Guinan [10] showed that saccule afferents in the cat demonstrate graded excitation in response to acoustic clicks of increasing intensity, (ii) Kushiro et al. [24] showed that stimulation of cat saccule afferents evoked inhibitory post-synaptic potentials in motor neurons of cranial nerve XI, and (iii) Colebatch and Rothwell [25] showed that motor units of the SCM in the human showed stereotyped changes in firing rate following a click stimulus, and that these firing rate changes were associated with changes in stimulus-locked averages of the surface potential measured over the SCM.

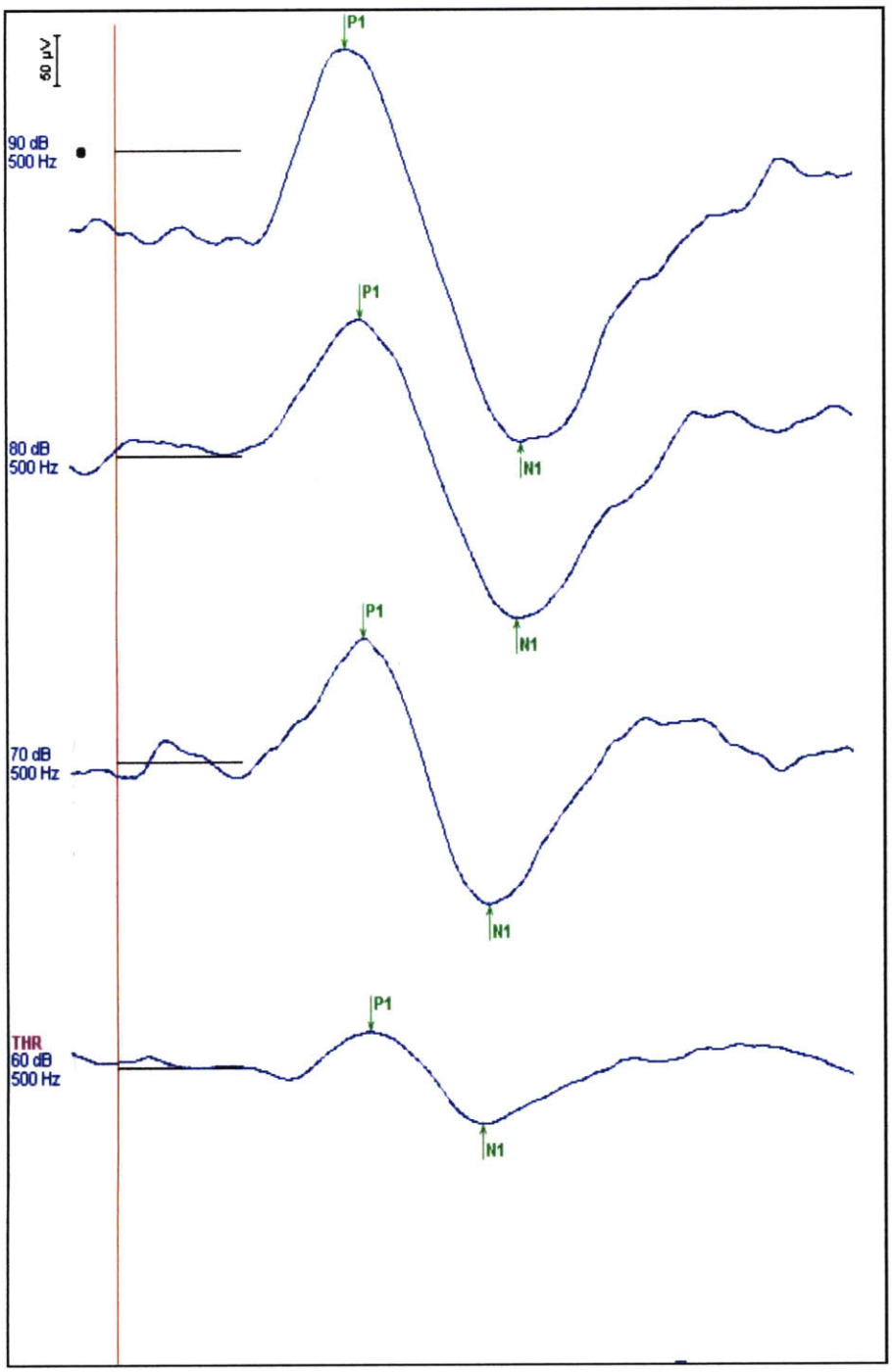

Figure 2.2 Output of a typical clinical VEMP test

This figure shows the result of a typical VEMP test conducted at the Audiology Department of Massachusetts Eye and Ear Infirmary. The curves represent the averages of different numbers of traces (determined by the audiologist making the measurement) from one ear at four different stimulus intensities of a 500 Hz, 8 ms toneburst.

2.5 References

1. Baloh, R.W. and V. Honrubia, *Clinical neurophysiology of the vestibular system*. Contemporary neurology series. 1979, Philadelphia: F. A. Davis Co. ix, 230 p.
2. Brookhart, J.M., V.B. Mountcastle, and H.W. Magoun, *The Nervous system (Handbook of Physiology)*. Vol. 5. 1977, Bethesda, Md.: American Physiological Society.
3. Highstein, S.M., R.R. Fay, and A.N. Popper, *The Vestibular System*. Springer Handbook of Auditory Research. 2004, New York: Springer. xvi, 560 p.
4. Hoffman, R.M., D. Einstadter, and K. Kroenke, *Evaluating dizziness*. American Journal of Medicine 1999; **107**(5):468.
5. Fife, T.D., et al., *Assessment: Vestibular testing techniques in adults and children: Report of the Therapeutics and Technology Assessment Subcommittee of the American Academy of Neurology*. Neurology 2000; **55**(10):1431.
6. Wuyts, F.L., et al., *Vestibular function testing*. Current opinion in neurology 2007; **20**:19.
7. Ashcroft, D.W. and C.S. Hallpike, *On the function of the saccule*. The Journal of Laryngology and Otology 2007; **49**(07):450.
8. Todd, N.P., F.W. Cody, and J.R. Banks, *A saccular origin of frequency tuning in myogenic vestibular evoked potentials? implications for human responses to loud sounds*. Hear Res 2000; **141**(1-2):180.
9. Didier, A. and Y. Cazals, *Acoustic responses recorded from the saccular bundle on the eighth nerve of the guinea pig*. Hear Res 1989; **37**(2):123.
10. McCue, M.P. and J.J. Guinan, *Acoustically Responsive Fibers In The Vestibular Nerve Of The Cat*. Journal Of Neuroscience 1994; **14**(10):6058.
11. Young, E.D., C. Fernandez, and J.M. Goldberg, *Responses of squirrel monkey vestibular neurons to audio-frequency sound and head vibration*. Acta oto-laryngologica 1977; **84**(5-6):352.
12. Wilson, V.J., et al., *The vestibulocollic reflex*. J Vestib Res 1995; **5**(3):147.
13. Wilson, V.J. and R.H. Schor, *The neural substrate of the vestibulocollic reflex. What needs to be learned*. Exp Brain Res 1999; **129**(4):483.
14. Dawson, G.D., *A summation technique for the detection of small evoked potentials*. Electroencephalography and clinical neurophysiology 1954; **6**(1):65.
15. Barlow, J.S., *An Electronic Method For Detecting Evoked Responses Of The Brain And For Reproducing Their Average Waveforms*. Electroencephalography And Clinical Neurophysiology 1957; **9**(2):340.
16. Katzman, R., *Introduction to the special issue on Evoked Potentials*. Annals Of The New York Academy Of Sciences 1964; **112**(A1):3.
17. Jewett, D.L. and J.S. Williston, *Auditory-evoked far fields averaged from the scalp of humans*. Brain 1971; **94**(4):681.
18. Katz, J., R.F. Burkard, and L. Medwetsky, *Handbook of clinical audiology*. 5th ed. 2002, Philadelphia: Lippincott Williams & Wilkins. xvi, 814 p.

19. Geisler, C.D., L.S. Frishkopf, and W.A. Rosenblith, *Extracranial Responses To Acoustic Clicks In Man*. Science 1958; **128**(3333):1210.
20. Davis, H., et al., *Evoked Responses To Clicks Recorded From The Human Scalp*. Annals of the New York Academy of Sciences 1964; **112**:224.
21. Colebatch, J.G., G.M. Halmagyi, and N.F. Skuse, *Myogenic Potentials Generated By A Click-Evoked Vestibulocollic Reflex*. Journal Of Neurology Neurosurgery And Psychiatry 1994; **57**(2):190.
22. Yoshie, N. and T. Okudaira, *Myogenic evoked potential responses to clicks in man*. Acta oto-laryngologica 1969; **252**:89.
23. Townsend, G.L. and D.T. Cody, *The averaged inion response evoked by acoustic stimulation: its relation to the saccule*. Ann Otol Rhinol Laryngol 1971; **80**(1):121.
24. Kushiro, K., et al., *Saccular and utricular inputs to sternocleidomastoid motoneurons of decerebrate cats*. Experimental Brain Research 1999; **126**(3):410.
25. Colebatch, J.G. and J.C. Rothwell, *Motor unit excitability changes mediating vestibulocollic reflexes in the sternocleidomastoid muscle*. Clinical Neurophysiology 2004; **115**(11):2567.
26. Ferber-Viart, C., C. Dubreuil, and R. Duclaux, *Vestibular evoked myogenic potentials in humans: a review*. Acta Oto-Laryngologica 1999; **119**(1):6.
27. Halmagyi, G.M., et al., *Vestibular responses to sound,* in *Clinical And Basic Oculomotor Research: In Honor Of David S. Zee*. 2005. p. 54-67.
28. Zhou, G. and L.C. Cox, *Vestibular Evoked Myogenic Potentials: History and Overview*. Am J Audiol 2004; **13**(2):135.
29. Welgampola, M.S. and J.G. Colebatch, *Characteristics and clinical applications of vestibular-evoked myogenic potentials*. Neurology 2005; **64**(10):1682.
30. Akin, F.W., O.D. Murnane, and T.M. Proffitt, *The effects of click and tone-burst stimulus parameters on the vestibular evoked myogenic potential (VEMP)*. Journal of the American Academy of Audiology. 2003; **14**(9):500.
31. Colebatch, J.G., *Vestibular evoked potentials*. Current Opinion In Neurology 2001; **14**(1):21.
32. Ochi, K., T. Ohashi, and H. Nishino, *Variance of vestibular-evoked myogenic potentials*. Laryngoscope 2001; **111**(3):522.
33. Basta, D., I. Todt, and A. Ernst, *Normative data for P1/N1-latencies of vestibular evoked myogenic potentials induced by air- or bone-conducted tone bursts*. Clinical Neurophysiology 2005; **116**(9):2216.
34. Hall, J.W., *New handbook of auditory evoked responses*. 2006, Boston, Mass.: Pearson.
35. Wit, H.P. and C.M. Kingma, *A simple model for the generation of the vestibular evoked myogenic potential (VEMP)*. Clinical neurophysiology 2006; **117**(6):1354.
36. Routal, R.V. and G.P. Pal, *Location of the spinal nucleus of the accessory nerve in the human spinal cord*. J Anat 2000; **196 (Pt 2)**:263.
37. Falla, D., et al., *Location of innervation zones of sternocleidomastoid and scalene muscles - a basis for clinical and research electromyography applications*. Clinical Neurophysiology 2002; **113**(1):57.
38. Kamibayashi, L.K. and F.J.R. Richmond, *Morphometry of human neck muscles*. Spine 1998; **23**(12):1314.
39. Richmond, F.J.R., K. Singh, and B.D. Corneil, *Neck Muscles in the Rhesus Monkey. I. Muscle Morphometry and Histochemistry*. J Neurophysiol 2001; **86**(4):1717.
40. Blouin, J.S., et al., *Neural control of superficial and deep neck muscles in humans*. Journal of neurophysiology 2007; **98**(2):920.

41. Corneil, B.D., et al., *Neck muscles in the rhesus monkey. II. Electromyographic patterns of activation underlying postures and movements*. Journal Of Neurophysiology 2001; **86**(4):1729.
42. Burke, R., *Motor units: anatomy, physiology, and functional organization.*, in *Handbook of physiology: the nervous system, section 1*, V. Brooks, Editor. 1981, American Physiological Society: Bethesda, MD. p. 345-422.
43. Buchthal, F. and H. Schmalbruch, *Motor Unit Of Mammalian Muscle*. Physiological Reviews 1980; **60**(1):90.
44. Merletti, R. and P. Parker, *Electromyography: physiology, engineering, and noninvasive applications*. IEEE Press series in biomedical engineering. 2004, [Hoboken, NJ]: IEEE/John Wiley & Sons. xxii, 494 p.
45. Hogan, N. and R.W. Mann, *Myoelectric signal processing: optimal estimation applied to electromyography--Part I: derivation of the optimal myoprocessor*. IEEE Trans Biomed Eng 1980; **27**(7):382.
46. De Luca, C.J., *Physiology and mathematics of myoelectric signals*. IEEE Trans Biomed Eng 1979; **26**(6):313.
47. Farina, D. and R. Merletti, *A novel approach for precise simulation of the EMG signal detected by surface electrodes*. Ieee Transactions On Biomedical Engineering 2001; **48**(6):637.

Chapter 3. Phenomenology

What is not surrounded by uncertainty cannot be the truth
~Richard Feynman

The purpose of the experimental study of EMG and VEMP is to characterize the basic properties of the response, its dependence on stimulus parameters, the dependence on non-stimulus physiological variables, and the statistical variability inherent in the signal. In keeping with the focus of the study on normative data, we studied a population of clinically normal subjects, and in order to study the test-retest variability, each subject was measured under identical conditions multiple times over the course of the study and multiple times during each recording session.

A unique feature of our measurement system is the capability to record the response to each stimulus presentation (each trace), and store the traces so that they can be retrieved in any order. Using this capability, we can form new ensembles of traces and study the properties of the resulting average waveforms. For example, using ensembles selected on the basis of estimated contraction effort, we can compare various schemes for trace rejection and normalization.

3.1 Experimental methods

The goal of each experimental recording session was to form an ensemble of stimulus response waveforms (traces) which could be manipulated off-line in different ways. The test consisted of recording toneburst-evoked cVEMP responses from the sternocleidomastoid (SCM) muscle under a set of different stimulus level and muscle contraction conditions. The experimental procedure was designed to be similar to that currently used for diagnostic purposes at the Massachusetts Eye and Ear Infirmary (MEEI).

In this procedure, the subject provides sustained tension of the SCM by turning the head away from the side under test, while seated upright in a chair. Tone-burst stimuli are applied to the ear ipsilateral to the test muscle at the rate of 13 per second, and the stimulus locked EMG is averaged over a number (usually 100-200) of stimulus presentations. The actual number is determined by the tester, who controls the start and end of each measurement. The running average of the EMG waveforms is displayed along with the root-mean-squared (rms) value of the EMG. The tester monitors the rms EMG level and provides verbal feedback to the subject about the amount of contraction desired to maintain a level close to maximum.

By monitoring the running average of the EMG, the tester determines whether a discernible response exists, and based on the stability of the waveform decides when a sufficient number of traces have been averaged. This averaged waveform, as well as sub-averages formed by selecting

responses at different ranges of rms EMG level are stored and can be displayed to assist in determining the quality of the recorded response. In a typical clinical VEMP test, this process is repeated for tonebursts of different frequencies between 250 Hz and 1 kHz.

In our experiment, we used a limited version of this clinical test, where only 500 Hz toneburst stimuli were used. Thus, the only stimulus parameter that was varied was the stimulus intensity. Further, while the clinical test generally estimates the threshold of VEMP onset at each stimulus frequency, we do not directly seek to estimate the threshold; our goal is to collect the response waveforms at fixed stimulus levels, and to analyze the response growth characteristics offline. This may lead to threshold estimates in cases where the stimulus range covers the threshold, but more important, the data may help obtain new insights into the physiology of the response threshold.

We will now look at various components of the experimental system in detail.

3.1.1 Subject selection and study design

The goal of the experiment was to collect repeated measurements from a pool of normal subjects. A pool of five subjects, with 5 separate recording sessions on each subject was determined to be the appropriate size for the scope of this study. Each subject was to be recorded over 5 identical sessions spaced approximately 1 week apart, and the same test ear and electrode montage used each time.

The subjects were recruited from among the students and faculty at MEEI, and were clinically normal in that they had no history of otologic, balance or neuromuscular disorders, and had normal hearing as measured by an initial audiogram and screening distortion product otoacoustic emission (DPOAE) test. Since the stimulus intensity in our experimental protocol was limited to 90 dB HL, we also required that the subject have a detectable cVEMP response at 90 dB HL using the standard clinical VEMP procedure. Subjects numbered 1, 2, 6, 7 and 8 qualified for inclusion under these criteria and completed the entire series of measurements; the rest of the analysis in this study was based on data recorded from these five subjects. The cohort included 2 male and 3 female subjects, between the ages of 20 and 60 years.

Five separate sessions were recorded from subjects 1, 2, 6 and 7, and four sessions were recorded from subject 8. The final recording session of the experiment, session 5 of Subject 8 could not be conducted due to a flood that destroyed a major portion of the experimental setup. All data from session 5 of each subject was omitted from further analysis and the rest of the study was conducted using a 5x4 matrix of subjects and sessions.

All measurements were made on the right ear of each subject (and correspondingly, the right SCM was the muscle used for EMG measurements). No inter-ear comparisons were conducted in this study.

We conducted a DPOAE screening test on both ears at the beginning and end of each session to ensure there were no large auditory changes as a result of the acoustic stimulation.

At the start of each session, signals were recorded for brief (~20-30 second) periods without stimuli being presented, under various control conditions: (i) without electrodes, (ii) with a 10 KΩ dummy load resistor across the leads, (iii) with electrodes attached to the subject, but no head turning, (iv) with half, three-quarter, and maximum head turns, as well as (v) a single maximum-effort contraction with no stimulus. We also made recordings with a portable signal generator across the leads of the head-stage amplifier. The aim of collecting these reference signals was to help detect and correct anomalies that might be discovered during off-line processing of the stimulus responses. The main use of these initial recordings during the post processing was in estimating the noise level on each channel, and measuring the DC offset in the measurements.

Each session consisted of 15 head-turning maneuvers (contractions) each lasting about 40 seconds, corresponding to roughly 500 toneburst presentations at a fixed stimulus level. A set of 5 contractions was recorded at stimulus intensities of 90, 85, 80, 75 and 70 dB HL presented in random order. This was repeated for two more sets to yield a total of 15 contractions. During the first and third set of contractions, the subject was instructed to exert maximum voluntary effort, and was given feedback to maintain the EMG at a correspondingly high level (> ~1 mV rms, as monitored on the clinical VEMP system). During the second set of contractions, the subject was instructed to maintain "moderate" effort, and the rms EMG was maintained (again via verbal feedback to the subject) in a broad range between 100 and 500 μV. Between contractions, the subject was allowed to relax the neck and rest, but at no time during a session were the electrodes disconnected and reattached.

Prior to each contraction, a new acquisition was started on the trace-by-trace recording system (see Section 3.1.3). This streamed the sampled stimulus and response waveforms onto the disk as a single array of numbers, stored as a file tagged by the subject, session and file number. A paper record of each session associated each file number with the corresponding recording conditions (e.g. stimulus intensity and set number).

After at least 500 traces have been acquired, the trace recording system was stopped, the clinical VEMP system was halted, and the subject was then allowed to relax the contraction.

The data files from each session were saved and processed offline as described in Section 3.1.4.

3.1.2 Stimulus characteristics

The stimulus for each contraction consisted of a series of tonebursts of alternating polarity presented at a rate of 13/sec. The 500 Hz tonebursts were generated using a Blackman window with a two-cycle rise and fall and no plateau. The stimulus intensity delivered by the system was calibrated prior to the study and not separately monitored during the recording.

3.1.3 Signal output and acquisition

Figure 3.1 outlines the experimental setup used in this phase of the study. A major portion of the equipment, including (i) the stimulus generation, amplification and delivery, (ii) the surface EMG electrodes and amplifiers, and (iii) the computer and software controlling the generation of stimulus and acquisition of the conventional VEMP average, was identical to the VEMP recording system used in the clinic. This portion (the "clinical VEMP system") is shown in the figure as the grey shaded box, and is largely described in [28]. The acquisition system developed specifically for this study (the "trace recording system") tapped the analog stimulus and response signals just prior to their conversion from and to digital signals in the clinical system. These signals were separately digitized and stored using the system outlined in the blue shaded box, which includes a separate computer running a LabView virtual instrument (VI) that controls the acquisition of the stimulus and EMG signals.

The stimulus waveform was generated by the clinical VEMP system using National Instruments 6052-E boards. The analog signal at a fixed level was amplified by a Virtual Model 320 audiometer power amplifier, whose gain and attenuation were set to yield the specified stimulus intensity. The stimulus was delivered over Telephonics TDH-49 circumaural headphones.

The surface EMG of the SCM muscle was measured using adhesive surface electrodes (Ultratrace Adult ECG electrodes). The skin surface was cleaned with alcohol, and gently abraded to improve the electrical contact. A single-differential electrode montage was used: active electrode on the muscle belly, reference electrode on the sternal insertion of the muscle and ground on the forehead (Figure 3.1).

The electrode outputs were amplified by a Tucker-Davis Bioamp system (TDT-HS4 head stage & TDT-DB4 amplifier). This analog signal was sent to both the clinical VEMP system and the trace recording system.

In the trace recording system, the stimulus waveform as well as the amplified EMG were simultaneously sampled at 25kHz and streamed to disk using two National Instruments NI6052-E boards and the custom LabView VI. The two acquisition boards operated on a common sampling clock to avoid offsets in the stimulus and EMG sampling instants. This clock was free-running, and independent of the clock used in the clinical VEMP system. During the initial testing of the acquisition system, two problems were discovered in the equipment: Board 1 had a noise floor that was larger than the Board 2, while Board 2 had a fixed DC offset that was present in all measurements regardless of the signal source. We continued the study using these boards, taking care to use Board 1 only for the stimulus, where the amplitude of the signal made the noise insignificant, and used Board 2 only for the EMG, where the fixed offset could be subtracted from all the measured samples.

When a trace recording VI was halted, a Matlab script converted the streamed samples into an array of numbers and saved the array. Figure 3.2 shows a segment of such a recorded array (from Subject1, Session3, File16), and illustrates details of the stimulus described in Section 3.1.2.

The gains on the signal pathway from the head-stage to the EMG array were fixed for all sessions. To calibrate the scale for the recorded samples, we measured this gain by recording from a signal generator whose output was monitored using an oscilloscope. The gain, which translated a 400μV input into a sampled value of 1.0, was found to be flat from 100Hz to 1kHz.

3.1.4 Signal processing

Each recording session produced a series of data files containing stimulus and EMG waveforms. These files were processed off-line using a series of Matlab scripts, and all results reported in this chapter are the product of this analysis.

The stimulus recording was parsed into individual stimuli by detecting the zero-crossing at the center of the each toneburst. The identified stimulus positions were used to segment the EMG recording (since the samples of the stimulus and EMG were acquired synchronously) into individual traces each trace being roughly 70ms (approx. 1700 samples) long. Each contraction at a given stimulus intensity and effort level yielded an array of about 500 EMG traces. The DC offset was subtracted from the EMG signal prior to parsing it, making the signal zero-mean. The resulting 2-dimensional array of EMG traces from each recording was saved into a file that identified the subject number, session number, set number (of the two maximal and one moderate effort contractions), and the stimulus intensity.

Figure 3.3 illustrates the result of a typical recording (for Subject2, Session1, Set1, 90dB stimulus). The figure shows 5 EMG traces as well as the average waveform of all 622 traces in the recording. Note the large difference in the amplitudes of individual EMG waveforms and the amplitude of the average EMG.

3.2 Results

We now survey the results of our experiment. We have already seen, in Figure 3.3, that the EMG traces average out to a waveform that is much smaller in amplitude than the individual traces. Since the EMG is a zero-mean signal, this behavior is not surprising, and the average waveform could be interpreted as the residual noise. However, repeated measurements of the average indicate that there are systematic variations in the post-stimulus mean of the EMG. These variations constitute the VEMP response, which we examine in Figure 3.4.

3.2.1 Diversity of response waveforms

The average of the ensemble of traces from one recording at 90 dB stimulus level is shown for each subject and session in Figure 3.4. We see that there is considerable inter-subject variation in the morphology and the salient features (amplitude, peak latencies, etc.) of VEMP average, even though it was obtained under the conditions most favorable to a robust response (viz., maximum stimulus level and contraction effort). We also observe inter-session differences of different sizes – some subjects (e.g. Subj. 2) have very repeatable average, whereas others (e.g. Subj. 6) show large inter-session differences in all waveform features. Part of the difference between sessions could be due to the inherent noise of the VEMP average. We are interested in the relationship of this noise to the inter-session variability and to inter-subject differences in this variability.

We examine this question by looking at differences between averages of sub-ensembles of the EMG in Figure 3.5. The two subjects chosen for the comparison are ones whose inter-session behavior was seen to be different in Figure 3.4. A comparison between the two sides of Figure 3.5 suggests that the subject with larger inter-session variability also shows larger intra-session variability. However, the sub-averages from each session show consistent features that are different from other sessions; i.e. the intra-session variability contributes to only a part of the observed inter-session variability. In turn, the inter-session variability contributes to the difference in the VEMP waveform seen between subjects.

A closer look at the intra-session variability (or noise) is offered in Figure 3.6, which shows the VEMP average as well as a 95% confidence interval band. Again, we see large inter-subject differences and systematic inter-session differences, both in mean response and in the size of the noise component.

3.2.2 Growth of response with stimulus intensity

The clinical utility of VEMP lies in the growth of the response with stimulus intensity. Later in the study, we examine the growth characteristic quantitatively. In Figure 3.7 we look qualitatively at the VEMP response (averaged over all the traces of a single recording) for each of 5 stimulus intensities between 70 and 90 dB HL for all subjects and sessions.

We found that with increasing stimulus intensity, the amplitude of the response waveform became larger, and the response was more easily delineated from the noise in the EMG. We found that the growth of the response was different for different subjects: Subject 2, for example had a detectable response at 80 dB in all sessions, whereas Subject 7 appeared to have a response only to 85 and 90 dB stimuli. In all subjects, we saw different degrees of variation among sessions in the level corresponding to response onset. Thus, even within a normal population, the relationship between stimulus level and the response size was far from uniform, when the response metric was the amplitude of the VEMP average waveform.

3.2.3 Dependence of response on contraction effort

It is well known that the VEMP response amplitude is influenced by the voluntary contraction effort [29]: the stronger the contraction, the larger the VEMP amplitude. We can examine how this relationship holds across subjects and sessions by using a conventional metric of motor effort, the root-mean-square (rms) level of the surface EMG. With each trace in an ensemble, we can associate a value of the rms EMG, which is computed from the samples of the trace. This method includes the VEMP response in each trace as well in the computation of rms EMG, but as we have seen in Figure 3.3, the amplitude of the VEMP component is much smaller than the EMG traces, so the error is negligible. We show the resulting rms EMG sequence superposed on the original EMG signal in Figure 3.8 A. In Figure 3.8 B, we show the rms EMG sequence for two "maximum contraction" and one "moderate contraction" recording.

In order to understand the influence of contraction effort on the VEMP, we collected all the traces at a given stimulus intensity (here, we choose 90 dB) for a given subject and session, sorted the traces according to their rms EMG level, and formed groups of traces with similar EMG values. By comparing the VEMP averages from these groups, we could assess how the VEMP changed with the average EMG level (and hence, presumably, the motor effort) corresponding to the signals in the ensemble. Figure 3.9 and Figure 3.10 show such a comparison for all the sessions of two subjects, #2 and #7. Here, we collected traces from all contractions, maximum effort as well as moderate effort, sorted the EMGs, and divided the traces into 5 equal bins, and plotted the average of each bin at a height equal to the mean rms EMG level of the traces in that bin.

From the data for Subject 2, we see that (i) the VEMP amplitude grew steadily with the EMG level, (ii) this growth was similar for all the sessions, and (iii) the basic shape of the response was present at all EMG bins, including the lowest effort bin. In contrast the, data for subject 7 show non-uniform growth of the response with EMG level, large inter-session differences in the growth behavior, and some bins that do not appear to have a VEMP waveform component. The bottom panels of Figure 3.9 and Figure 3.10 show the dependence of peak-to-peak amplitude on EMG level for these two subjects aggregated across sessions and sets.

If (i) the effort variability makes a significant contribution to the VEMP variability, and (ii) if the VEMP average were linearly related to the effort, then normalizing the traces by a measure of the effort should yield more stable (less variable) response waveforms. We have seen some evidence of (ii) in Subject 2, but to assess (i), we needed to compare the variability of rms EMG over the contraction, and the variability of the VEMP average.

3.2.4 Variability of contraction effort

Figure 3.11 shows the variation of rms EMG over a recording for different subjects and sessions. (For clarity, we smooth each rms EMG sequence over a 1 second sliding window). We found that

from subject to subject, there are wide differences in the ability to maintain the rms EMG (and therefore the motor effort) at a constant level. This is consistent with our observations in Figure 3.9 and 3.10 where we found that the range of rms EMG values for Subject 2 was much smaller (69 mV to 183 mV), compared with the range for Subject 7 (50 mV to 287 mV). While a comparison of the right and left panels of Figure 3.11 indicates that the subject with the smallest rms EMG variations also has the smallest inter-session and intra-session variability of the VEMP, there is no evidence of a broader rule relating EMG variability and VEMP variability across subjects.

3.2.5 Comparison of normalization schemes

Based on the known dependence of VEMP amplitude on contraction effort, many current VEMP implementations employ a form of normalization using the rms value of the EMG from the contracted muscle prior to the stimulus being applied. Since we have found that the dependence on rms EMG exists among the traces of each recording, we could test a trace-by-trace normalization scheme. Figure 3.12 shows a comparison of the normalization on different EMG bins within a single subject/session, and Figure 3.13 compares the effect of normalization on inter-subject and inter-session variability. We see that the inter-subject and inter-session differences are largely unaffected by normalization. However, does normalization produce a significant improvement in the within-session variability? We examined this question in Figure 3.14, and found little difference as a result of the normalization. The key metric for comparison is the relative sizes of the VEMP average and the confidence interval. Although the amplitudes of the average response have been changed in some instances, the confidence interval, particularly for the problematic case of Subject 6 was not greatly reduced.

3.3 Discussion

The experimental results show us the extent of inter-subject differences in the VEMP waveform within a clinically normal pool of subjects. We also see that the growth of the response with stimulus level is different for different subjects. Where do these differences come from? Various sources suggest themselves, and are summarized in the table below:

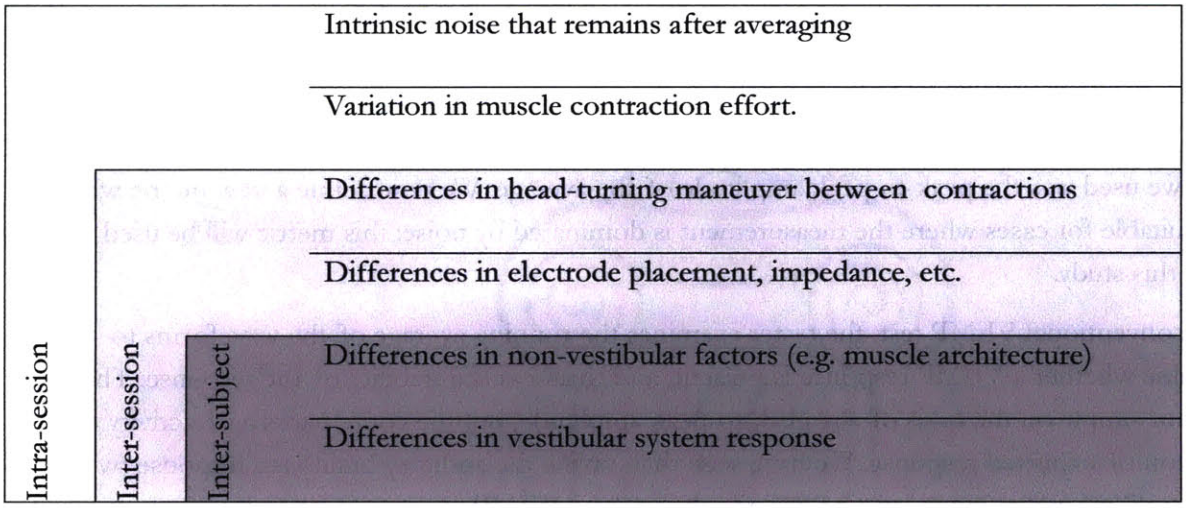

As we see, intra-session variations contribute to inter-session and inter-subject differences, and inter-session differences contribute to the differences in response between subjects.

We found that there were systematic differences between subjects that could not be attributed simply to inter-session and intra-session sources; subjects differ not only in the VEMP waveform, but also in how variable the waveform is from session to session and within sessions. When two subjects were compared, the subject whose VEMP average waveform was less reliable (as measured by comparing sub-averages of the traces) in one session, generally yielded less reliable waveforms on other sessions; and for such a subject the VEMP average also showed larger differences from session to session.

We identified one subject (#1) who had reliable VEMP averages, but whose VEMP waveforms showed systematic differences between sessions. This was one instance where differences in electrode placement may have been a significant factor. The subject, a 562in tall female, had the shortest neck length in the subject pool, and could be expected to have a larger sensitivity to variations in electrode placement. We also identified one instance (Subject 6, session 1), where all the measured data, VEMP as well as rms EMG, appeared to be smaller in magnitude than in the other sessions. This could have been due to a poor electrode contact.

In this chapter, we have tried to qualitatively assess the three classes of difference and in particular, to assess the effects of variation in contraction effort. We can conceive of other tests to further clarify the sources of variability; for example, one could systematically study the effect of changes in the precise placement of electrodes, or one could survey a large diverse subject pool and examine correlations between VEMP response and parameters of neck anatomy. However, this study focused on the sources of intra-session variability, namely the intrinsic noise in each measurement, and the variation in contraction effort.

3.3.1 A metric for response strength

In analyzing the results thus far, we have looked at the waveforms of the VEMP averages and sub-averages. In the few instances where we needed a quantitative measure of response strength, the metric we used was the peak-to-peak amplitude of the average. We now define a new metric which is more suitable for cases where the measurement is dominated by noise; this metric will be used in the rest of this study.

In the conventional VEMP test, the tester examines the running average of the waveforms to determine whether a VEMP response is present, and to assess the stability of the response. This is done, not simply on the basis of the peak-to-peak amplitude, but the entire pattern of activity over the region of expected response. We have seen that, unlike the auditory brainstem response (where a "canonical" normal response can be described), a robust VEMP response from two different subjects or sessions can be very different in shape. The tester takes this into account by implicitly using a template of the "expected" response shape and matching the running average against the template. In a threshold determination, for example, the judgment of whether the response is present or absent in the measurement is based on the similarity of the current average to the ones obtained during the same session at greater stimulus intensities.

Following the same approach, we define the response level associated with a waveform as the inner product (or equivalently, the correlation at lag 0) of the waveform with a prototype waveform. This prototype waveform is the response recorded in the same subject and session at the largest stimulus intensity under maximal voluntary contraction. In signal processing terms, this is seen to be the output of a matched filter at a single time instant.

A great advantage of this metric is that it is linear, and therefore can be applied to individual traces, to sub-averages of traces and entire ensembles very simply, without computing the waveform averages at each stage. When the measured waveforms consist of a fixed signal component that is identical in shape to the prototype but with unknown magnitude, and additive white Gaussian noise, this metric gives the optimum estimate of the signal magnitude. When the noise is not additive, for example, if the measurements consist of a fixed signal component with variable delay (i.e. timing jitter) from trace to trace, this metric may underestimate the size of the signal.

3.3.2 Limitations of normalization

We have seen earlier that trace-by-trace normalization by rms EMG does not greatly improve the inter-session or intra-session variability despite the known dependence of the signal level on contraction effort. We will use the response level metric to understand why this happens.

The top panel of Figure 3.15 shows a scatter-plot of the response level of each trace with the EMG level of the trace. As the error bars show, the mean response level increases with EMG level, as

expected from our observations and from prior studies of the VEMP. In light of this figure, the argument in favor of normalization can be stated as follows: (i) The conventional VEMP average combines the responses from traces with different EMG levels. (ii) Traces in different EMG ranges have different means. (iii) The set of responses that is being averaged is thus drawn from a mixture of probability distributions (iv) The standard error of the mean of this mixture is larger than if the responses were drawn from a single distribution (v) By normalizing the traces with the EMG level, we can get the distributions to line up with the same mean and the resulting average will be less variable. This is illustrated in the bottom panel of the figure, where the response means for the normalized data are seen to be similar.

We also see that the variance of the response changes with EMG level. This is not necessarily a bad thing: if the mean and variance co-vary, then the normalized data will have the same variance and mean regardless of the EMG level, and a simple average is the best estimate of the response level.

The reason normalization does little to improve the reliability of the average response is that the mean response level is dwarfed by the variance in the responses. In the limit of very large numbers of traces, the standard error of the mean may be small enough that the improvement due to normalization becomes apparent, but in the ensemble sizes being considered, this improvement is small. In the particular case of the subject and session shown in Figure 3.15, even if we use all 1500 traces from the three contractions, the standard error of the mean is 5.2% of the mean before normalization, and is reduced to 4.8% of the mean after normalization.

3.4 Figures

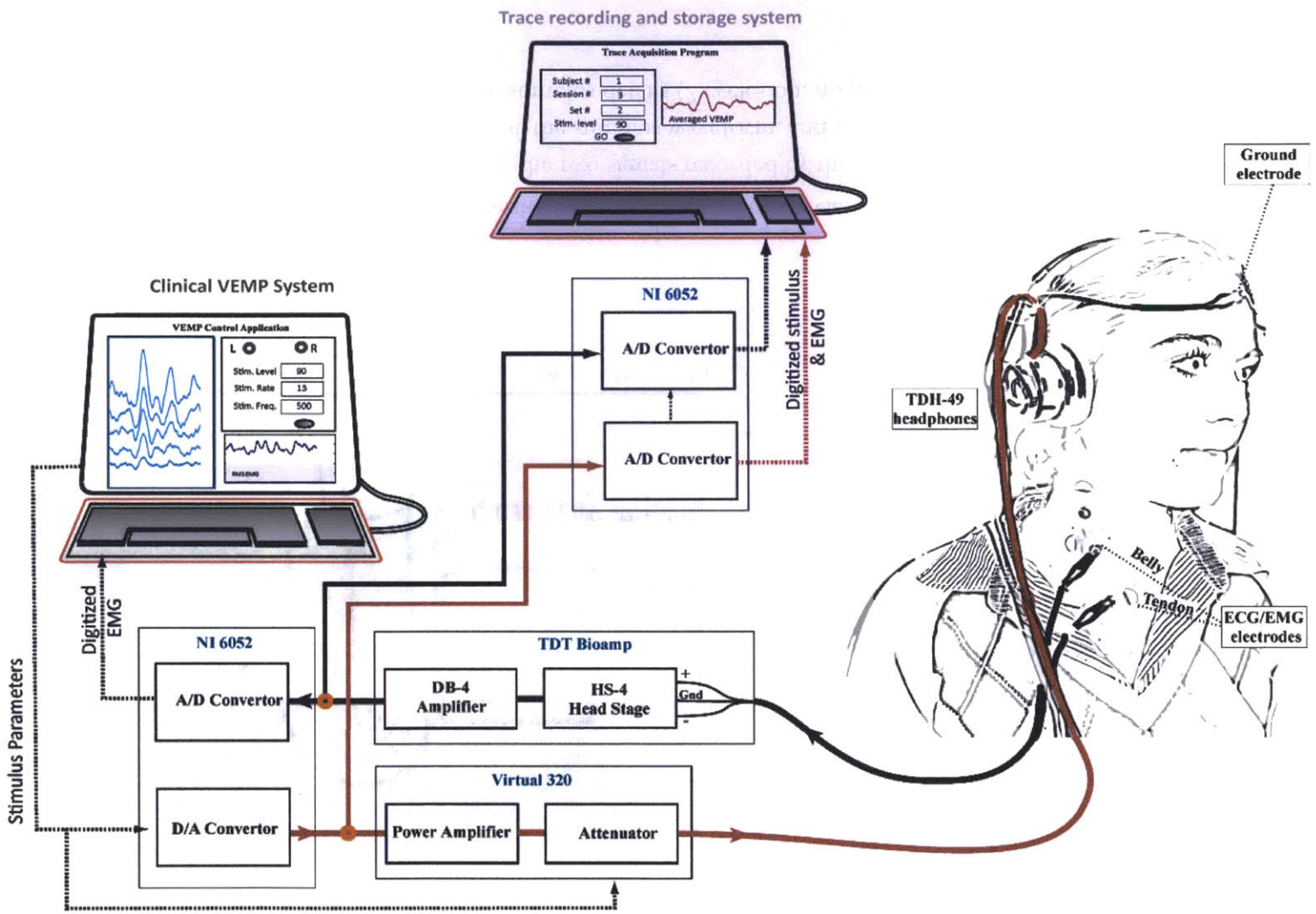

Figure 3.1 Recording system used in this study including the clinical VEMP setup (grey box) and the added trace-by-trace recording system (blue box).

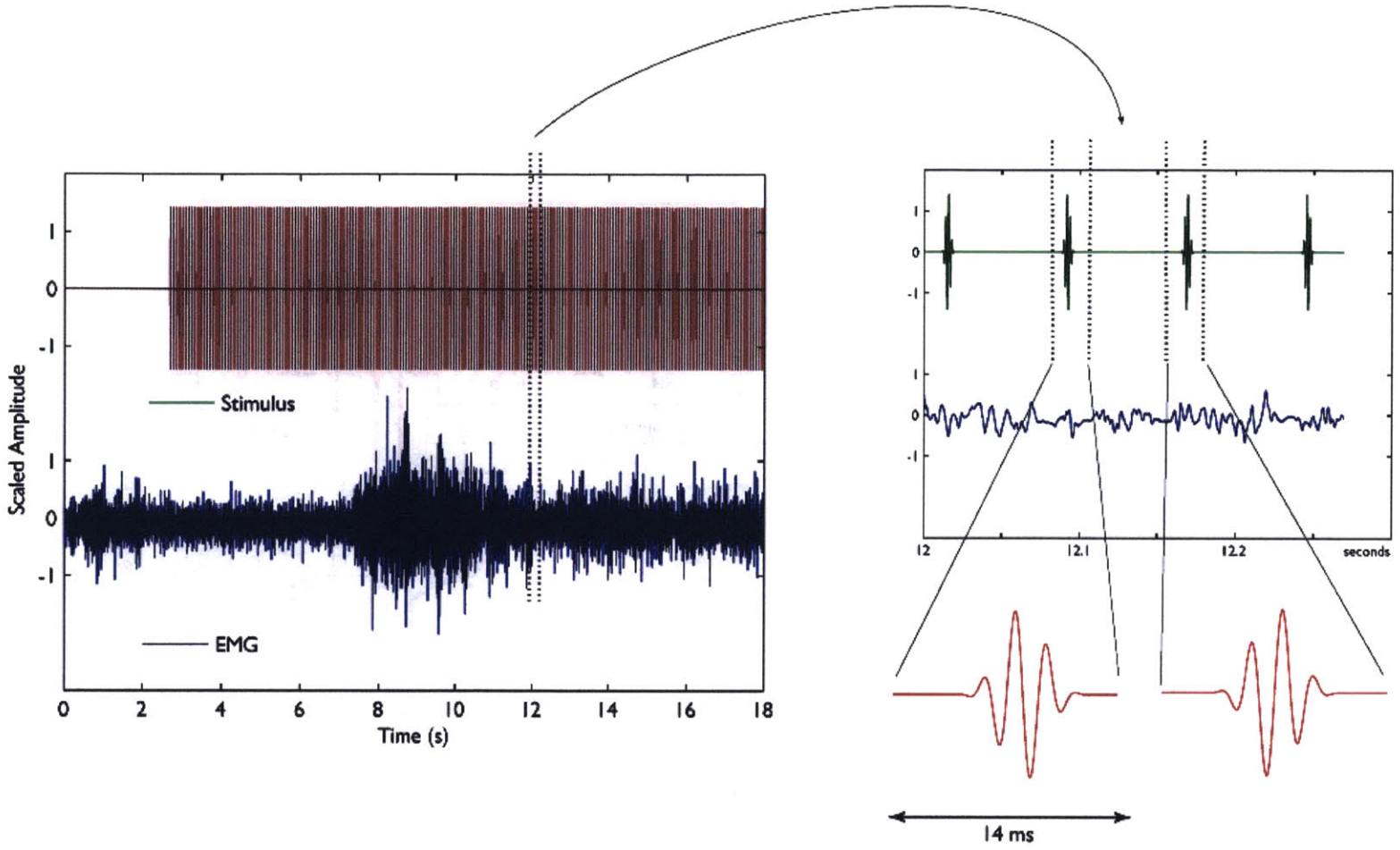

Figure 3.2 Example of stimulus and EMG signals recorded by the trace recording system

This figure on left shows an 18-second segment of the two signals recorded by the trace recording system at the start of a recording. A detail of the signals illustrates the periodic nature of the stimulus waveform, and the low-pass character of the EMG signal. A closer inspection of two adjacent tone-bursts reveals the stimulus details (2 cycles on, no plateau, 2 cycles off, alternating polarity).

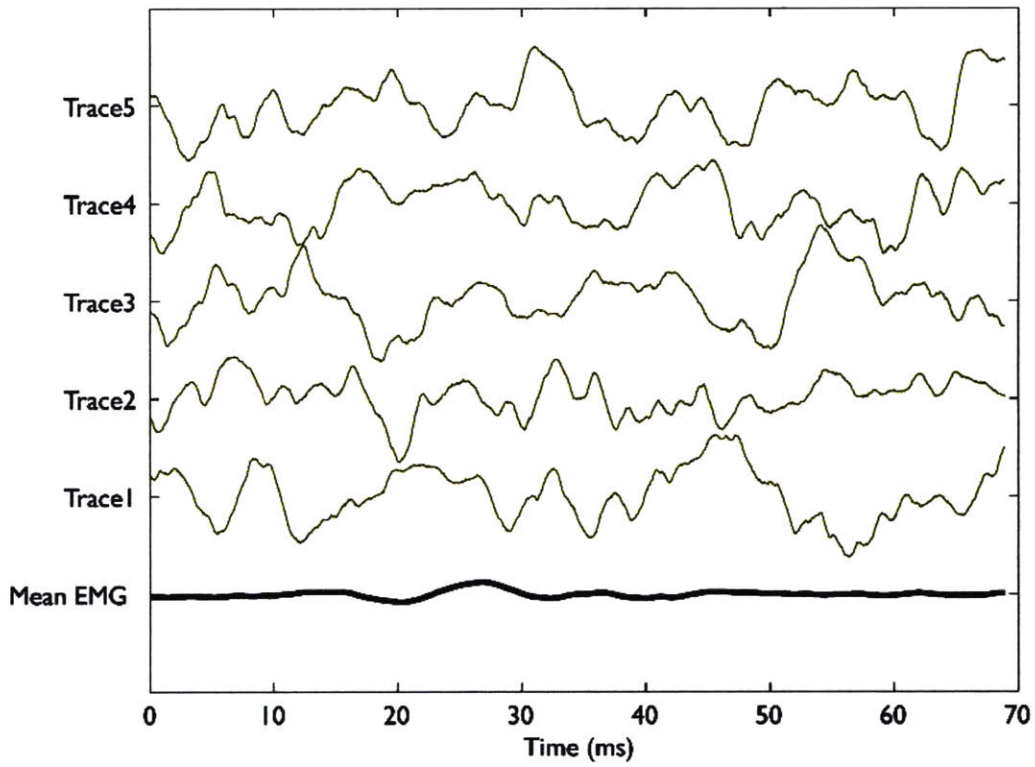

Figure 3.3 Five individual EMG traces (red) and the VEMP average (black) of 620 traces

This figure shows the first 5 traces of the EMG record for Subject 2, Session 1, Set1 (maximum contraction), at a 90dB stimulus level. The red traces do not show any obvious common stimulus-locked. In contrast, the bottom trace (black) shows the average of all 620 traces in the recording. Note that the amplitude of the average response is much smaller compared with the size of individual traces. The x- axis refers to post-stimulus time in ms.

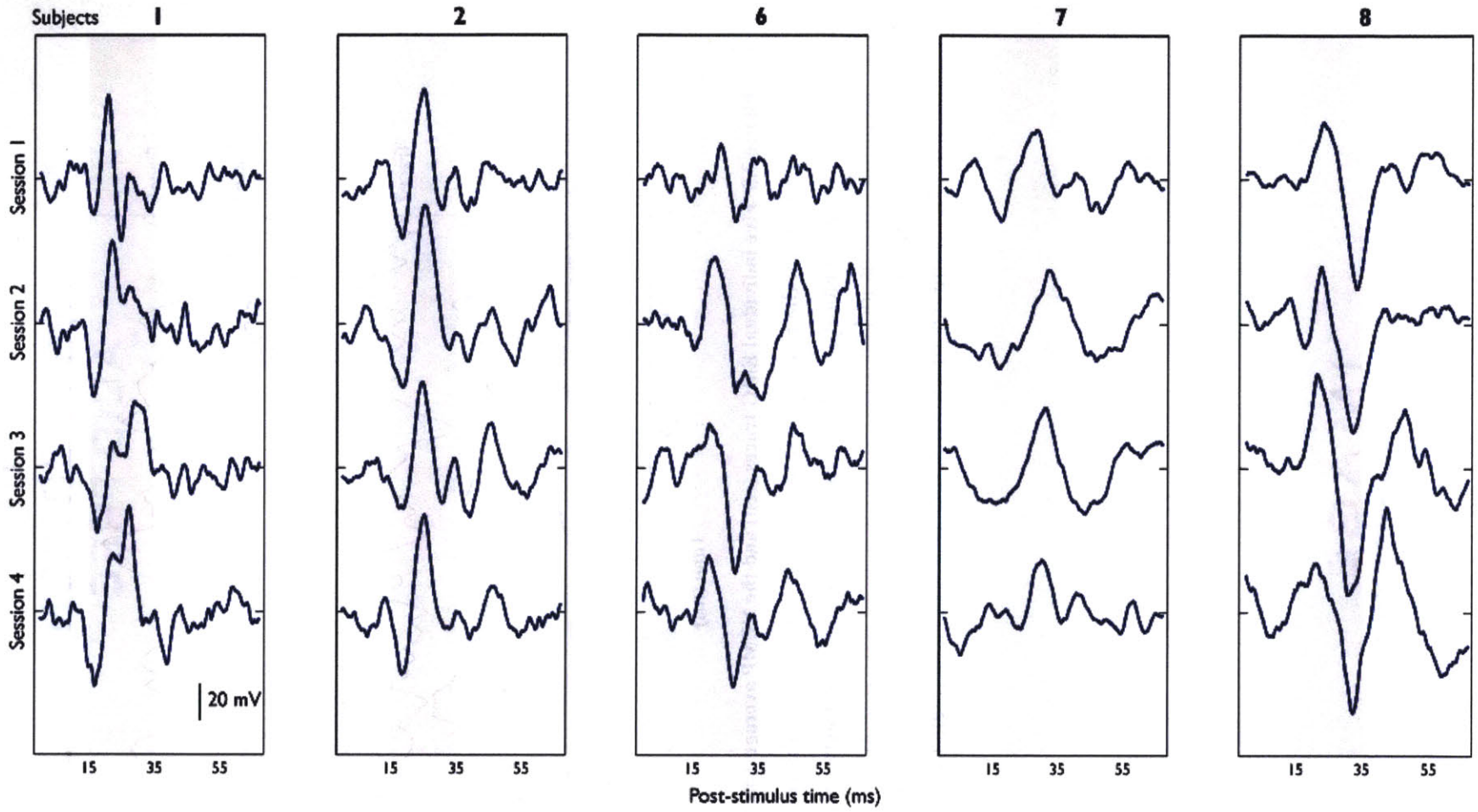

Figure 3.4 Comparison of VEMP averages across subjects and sessions

Each curve shows the average of all EMG traces from one maximum-effort recording (Set 1) at a 90 dB stimulus intensity. The figure illustrates the diversity of VEMP responses from subject to subject as well as the inter-session variability of each subject. The grey shaded region from 15 to 35 ms post-stimulus time is the range of the response typically reported in VEMP literature.

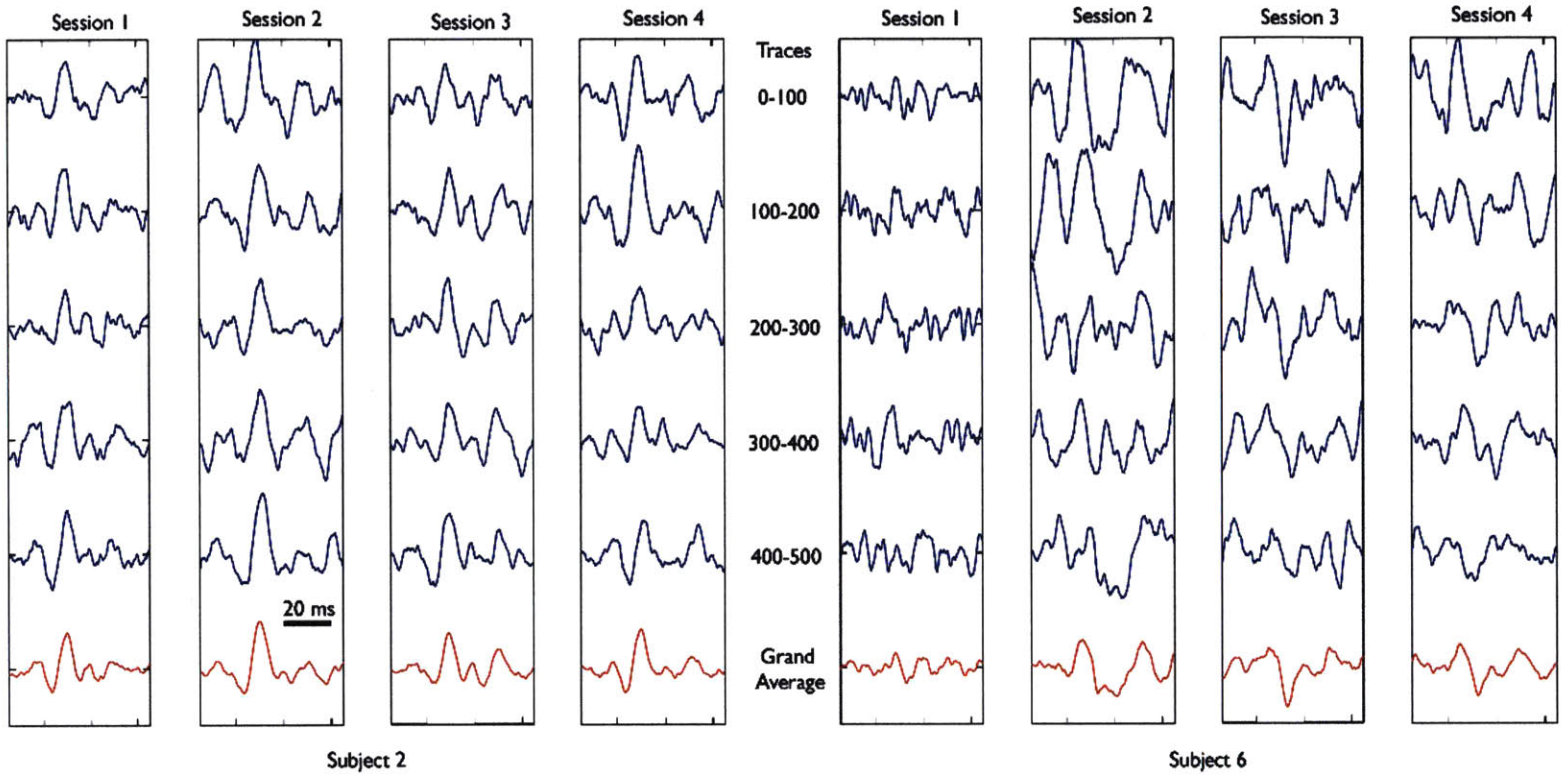

Figure 3.5 Comparison of 100-trace sub-averages for 2 subjects

This figure examines intra-session variability by computing averages of groups of 100 traces within ensembles recorded at a 90 dB stimulus level for two subjects with different degrees of inter-session variability.

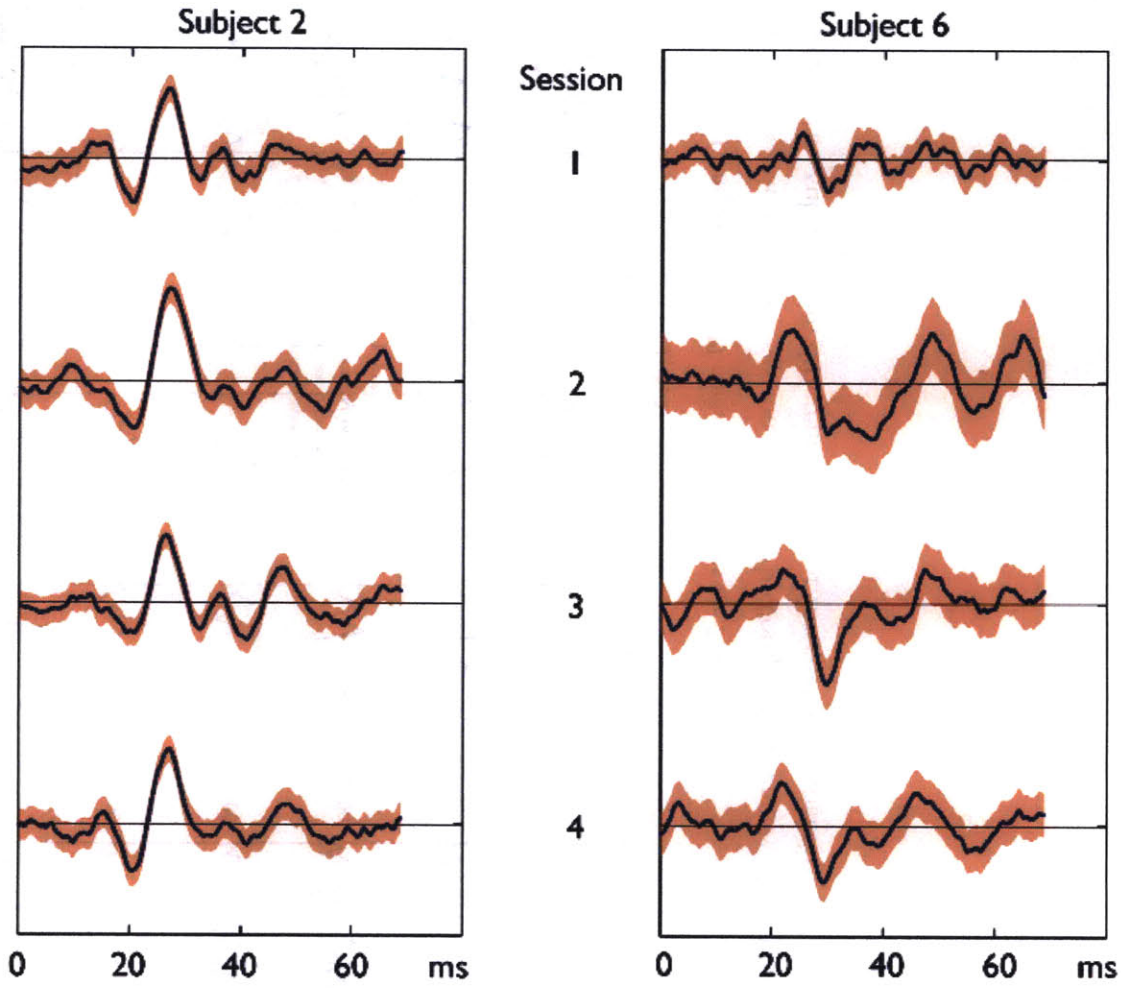

Figure 3.6 Comparison of the mean and error in mean across sessions: Subject 2 and Subject 6

This figure demonstrates the intra- and inter-session variability for the two subjects seen in Figure 3.5. Each solid line is the average of all traces in the ensemble (90dB stimulus); the shaded area is the 95% confidence interval in the estimated mean waveform. We see that the subject with larger inter-session variability also has noisier data. The amount of noise is also not constant across sessions. The standard error band also helps identify the regions of the waveform that constitute a reliable stimulus-evoked response.

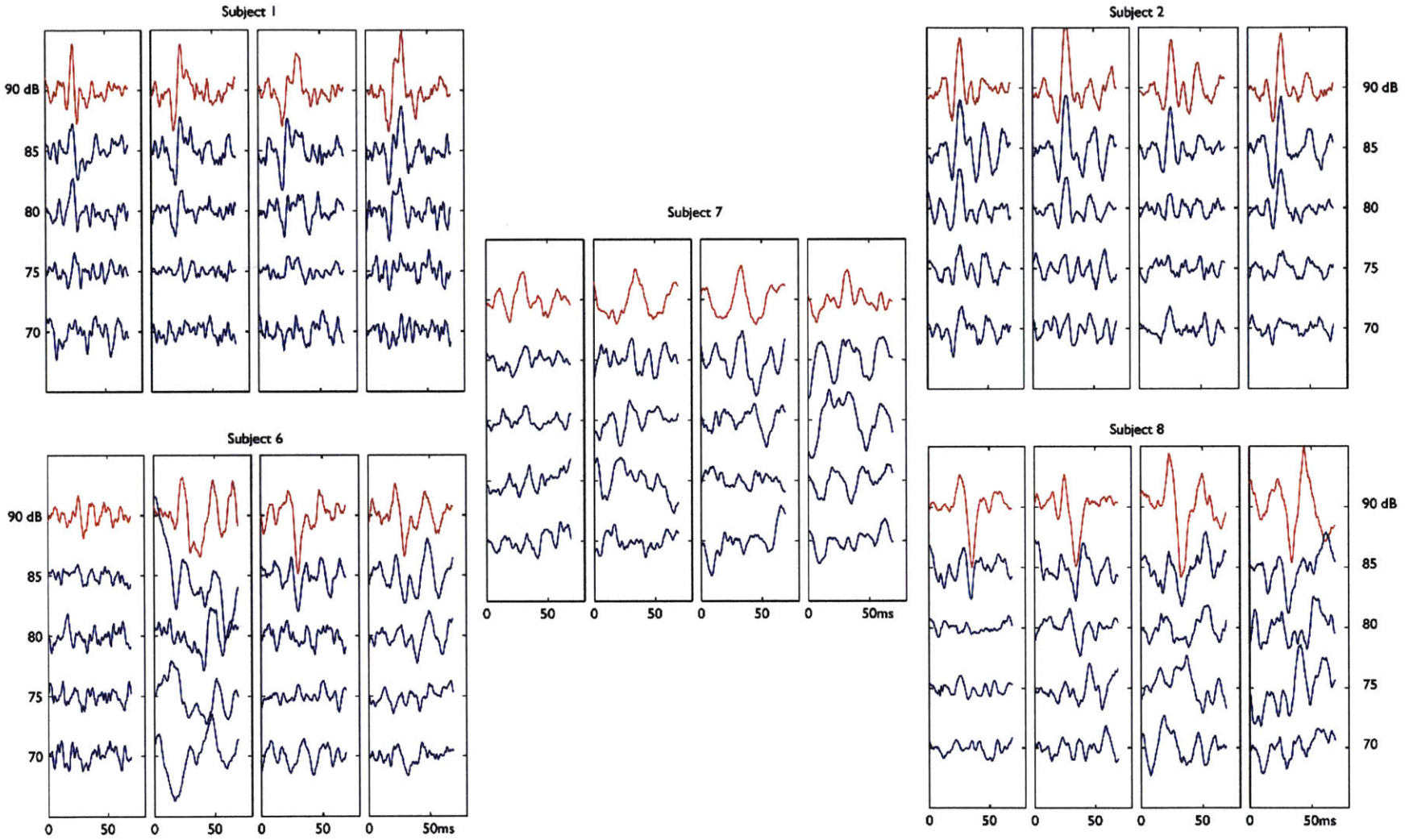

Figure 3.7 VEMP averages as a function of stimulus intensity

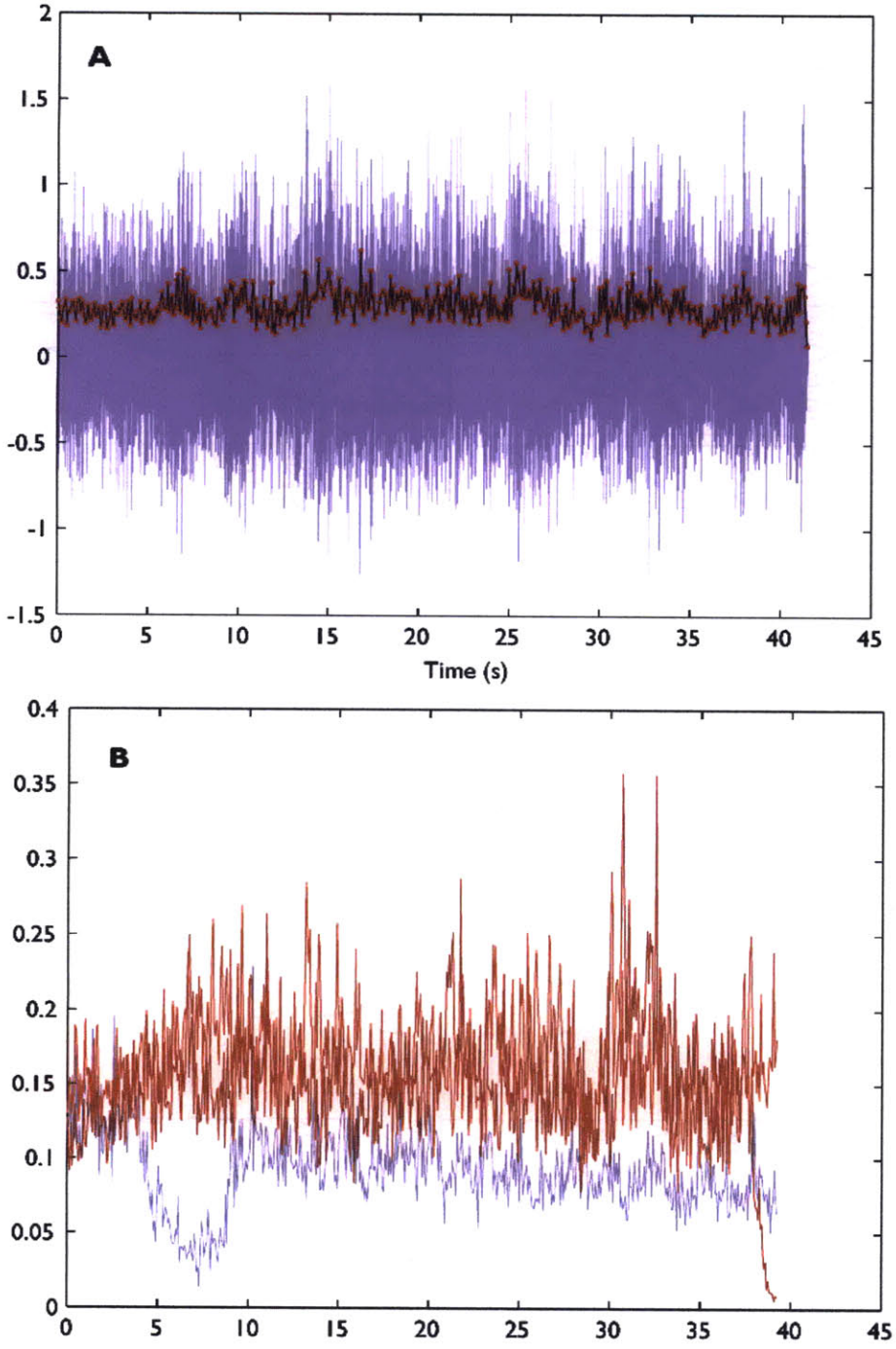

Figure 3.8 Raw EMG and the rms EMG over one contraction

A: The raw EMG signal over the course of one recording (40 s), along with the rms EMG of the sequence of traces. **B**: The trace rms EMG for two "maximum effort" and one "moderate effort" contraction, for the same subject and session. (Note: The scale for the

ordinate in the top panel is the instrument voltage: In order to convert to actual signal level in mV as used in the bottom panel, the values should be multiplied by 0.4)

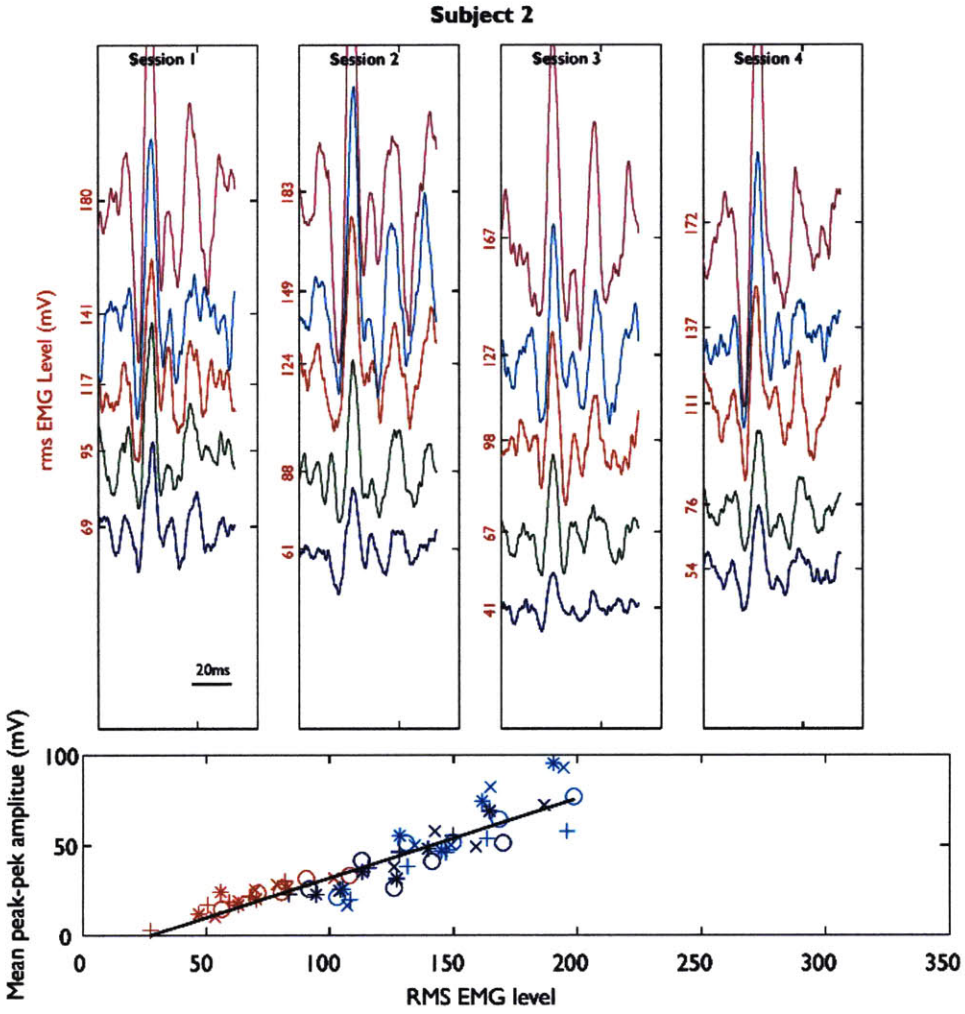

Figure 3.9 Variation of VEMP averages with the rms EMG level of the ensemble (Subject 2)

The top panel shows VEMP averages from 5 ensembles of traces each with a different average value of the rms EMG level (shown in red). The position of each curve indicates the EMG level of the ensemble. The bottom panel summarizes the data showing the peak-to-peak value of each curve as a function of rms EMG (The red symbols are the "moderate effort" contractions, while the rest correspond to "maximum effort".

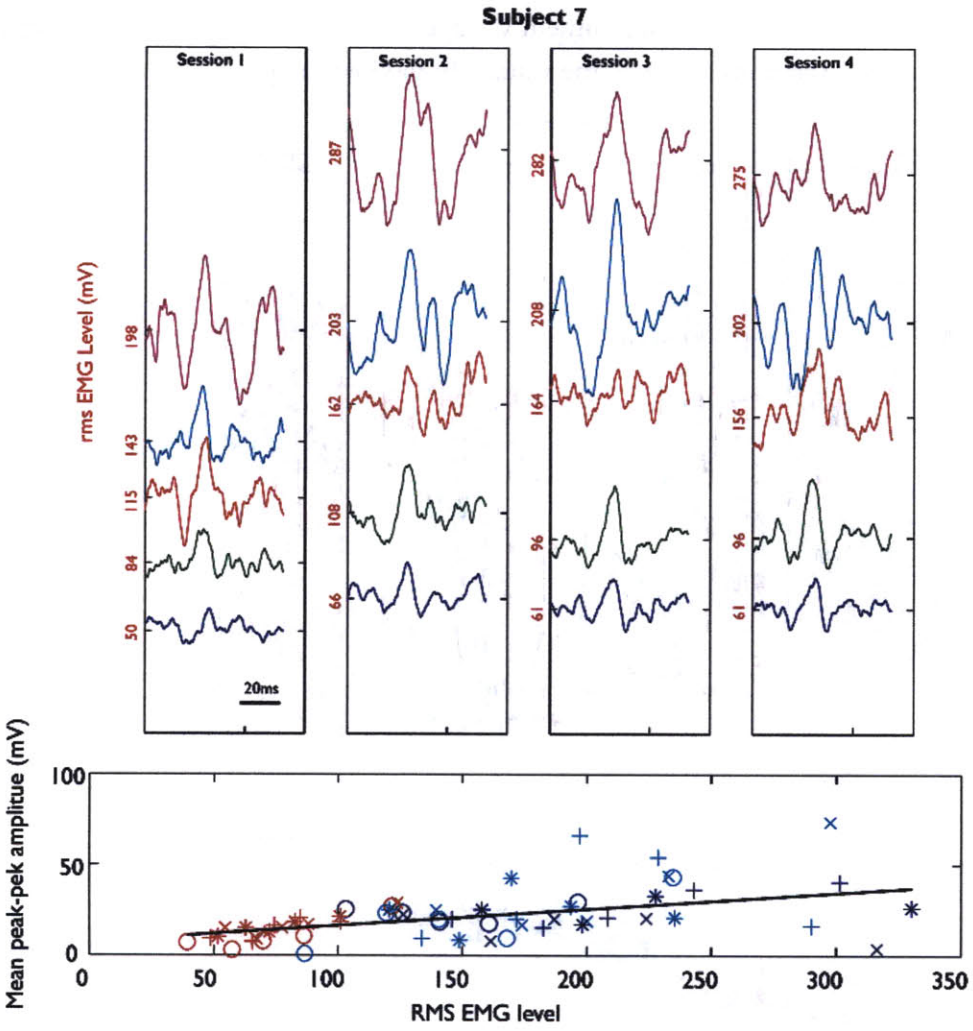

Figure 3.10 Variation of VEMP averages with the rms EMG level of the ensemble (Subject 7)

This is the same data as the previous figure, but for Subject 7.

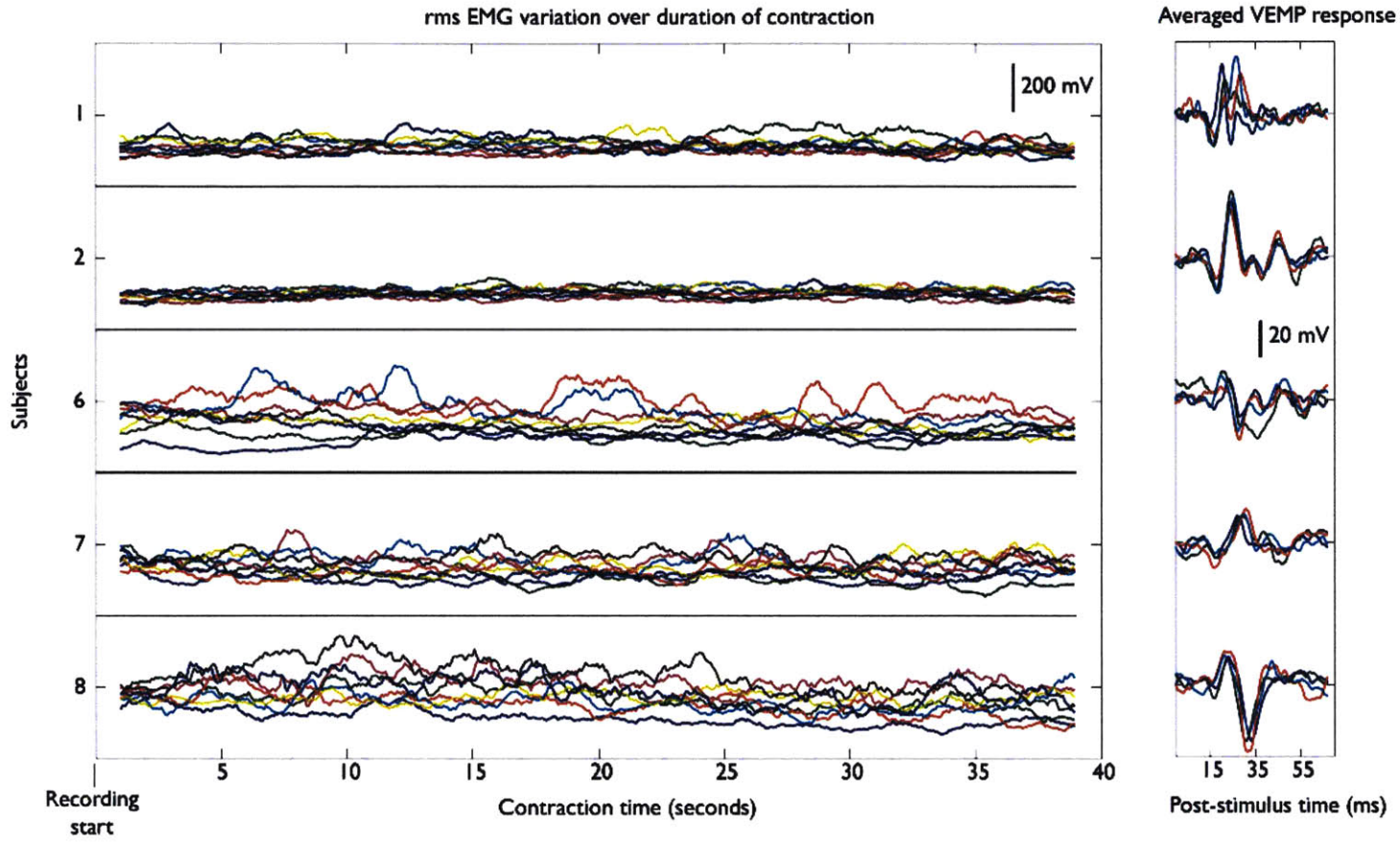

Figure 3.11 Relationship between rms EMG variability and VEMP variability for different subjects

The left panel shows the rms EMG as a function of time into the contraction for each of 8 recordings at 90dB stimulus intensity for each subject. The right panel shows the VEMP averages produced by these recordings.

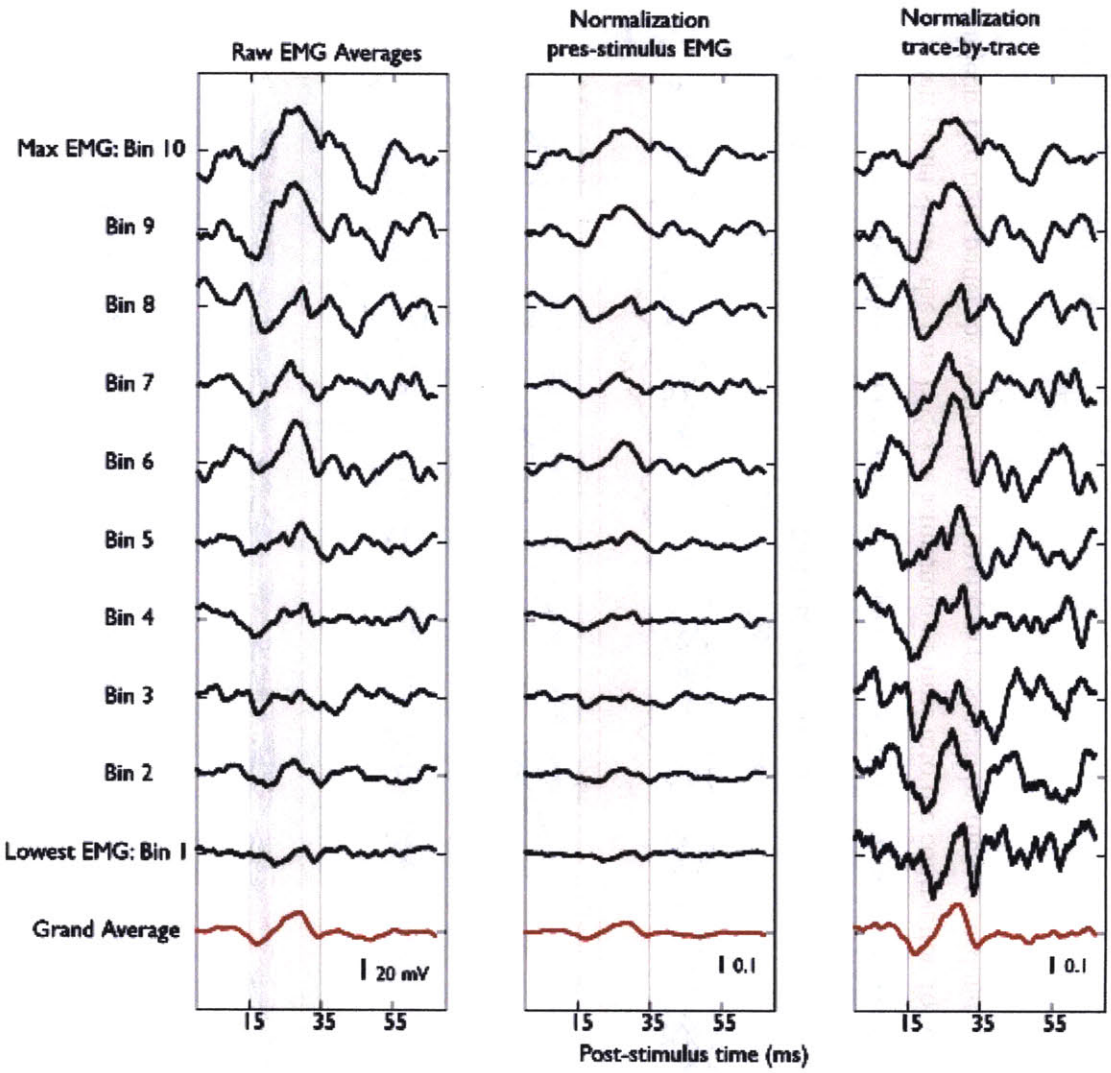

Figure 3.12 VEMP averages for different EMG bins: comparison of normalization

The ~1500 traces from a single session of Subject 7 recorded at 90 dB are divided into 10 bins by the rms EMG level. We compute the average for each bin, and obtain the curves on the left, illustrating the growth of the response with rms EMG. If each of the three recordings is scaled by the rms value of a 100ms segment of the EMG prior to the stimulus being applied (conventional normalization), we obtain the middle column. Note that the units are no longer mV, since normalization makes the data dimensionless. If we normalize each trace by its rms value, and then compute the average in each bin, we obtain the curves on the right (trace-by-trace normalization).

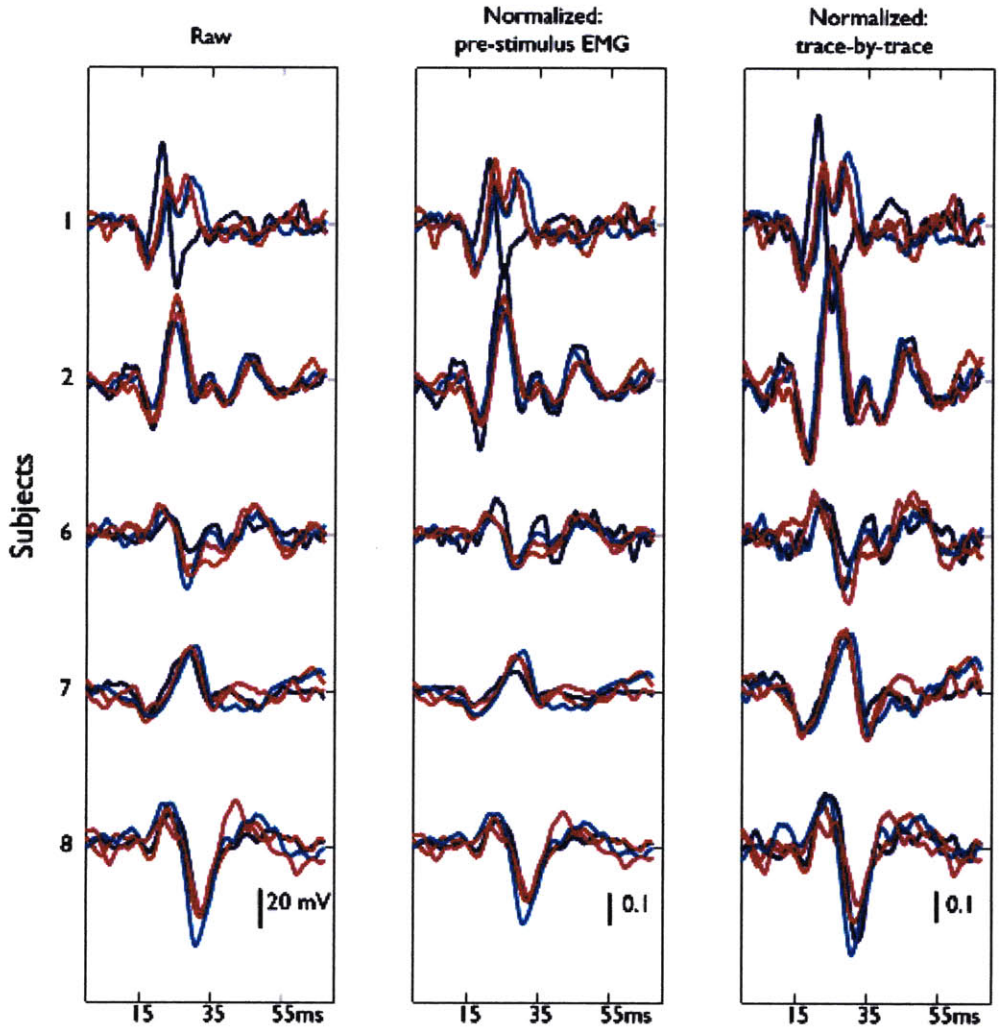

Figure 3.13 Effect of normalization on inter-subject and intra-session variability.

We get slightly different VEMP averages when we apply conventional and trace-by-trace normalization schemes. The averages for all subjects and sessions are compared with and without normalization. The effect of the normalization on inter-session and inter-subject variability is seen to be negligible.

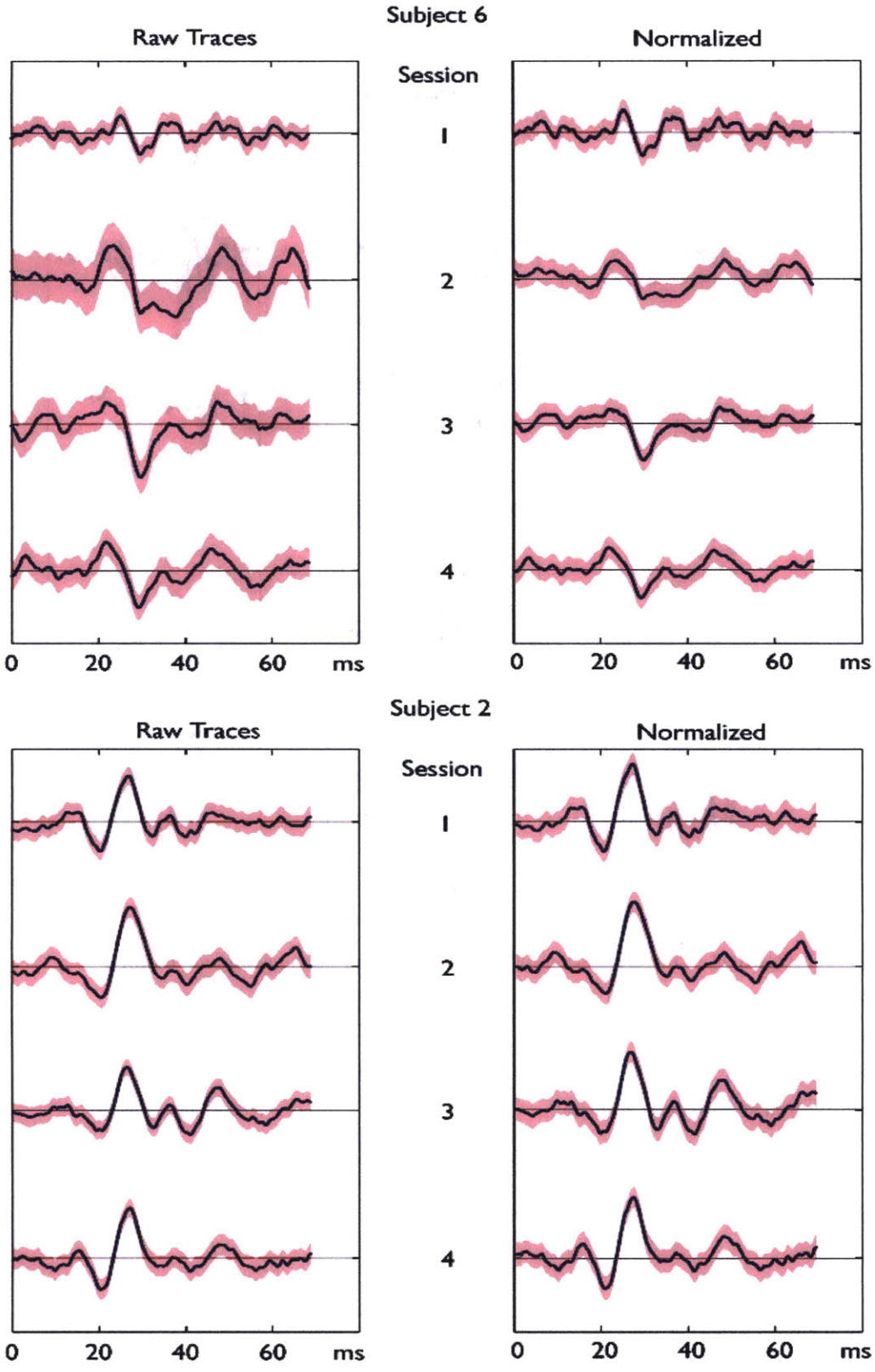

Figure 3.14 Effect of normalization on the confidence intervals of VEMP average (Cf. Figure 3.6)

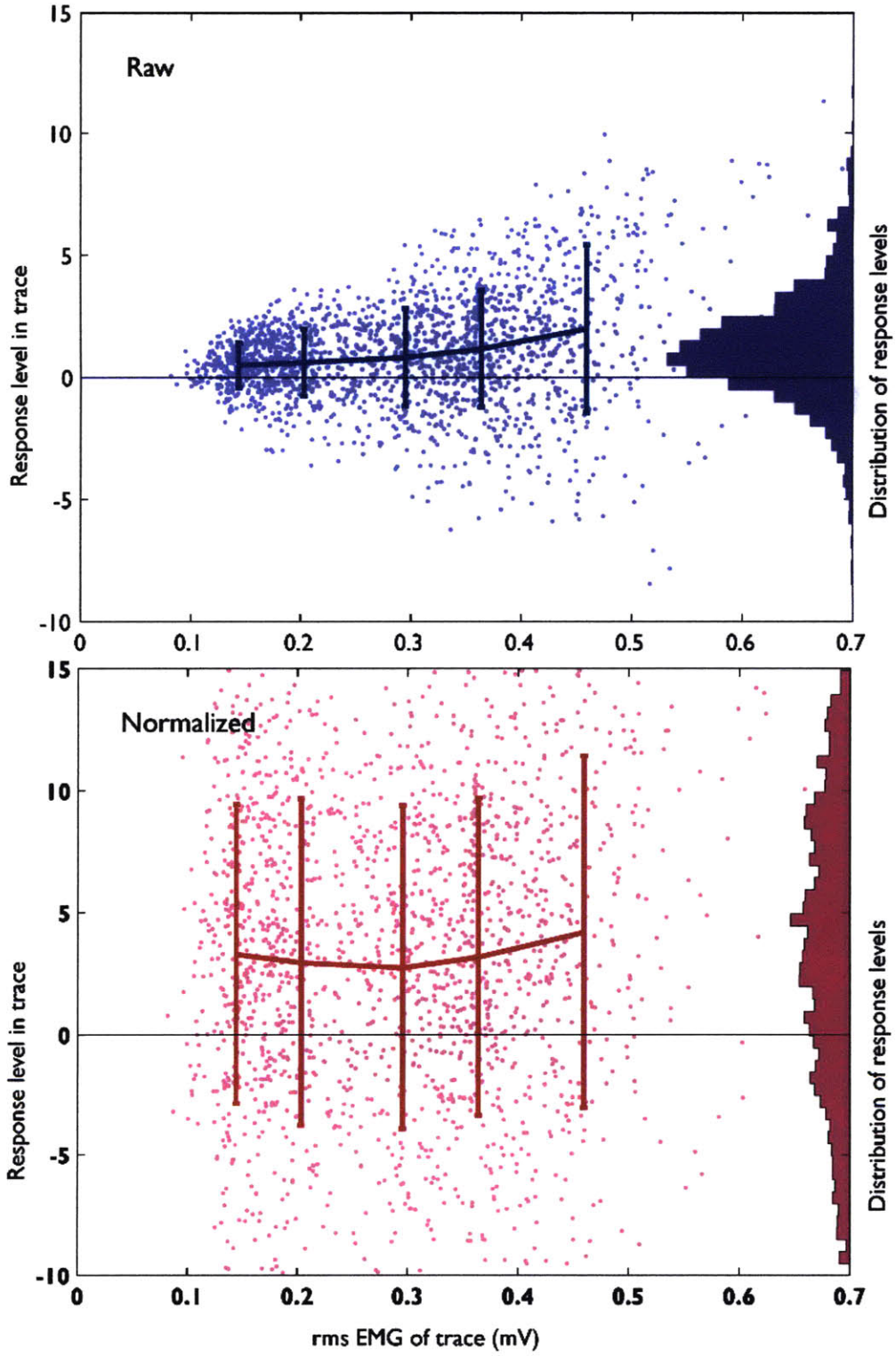

Figure 3.15 Distribution of response levels with rms EMG, and effect of normalization

The top panel shows a scatter plot of the response level in each trace as a function of the rms EMG level. The solid line shows the mean and variance of the response level in 5 bins of traces with increasing EMG level. The non-zero mean of the distribution indicates the

presence of a VEMP response. The difference among the mean values of different bins contributes to the dispersion of the response level in the ensemble average due to variation in contraction effort. Note the increase in variance along with the increase in the mean response level as the EMG level increases.

The bottom panel shows the effect of normalization on the response level in each trace. The mean of the responses no longer depends on the EMG level of the trace, but the dispersion is larger in every bin.

3.5 References

1. Rauch, S.D., et al., Vestibular evoked myogenic potentials show altered tuning in patients with Meniere's disease. Otology & neurotology 2004; **25**(3):333.

2. Welgampola, M.S. and J.G. Colebatch, Characteristics and clinical applications of vestibular-evoked myogenic potentials. Neurology 2005; **64**(10):1682.

Chapter 4. A Computational Model of VEMP

No more fiction for us: we calculate; but that we may calculate, we had to make fiction first.
~Friedrich Nietzsche

The surface EMG, like most physiological signals, is a random process. By this we mean that successive measurements, even when made under identical conditions, yield different waveforms. Of course, ensuring identical conditions is not a trivial task, especially in physiological systems; if differences in measurement conditions are not controlled or compensated for, they can result in significant differences between measurements. As we have seen, the conventional VEMP waveform is the result of averaging an ensemble of surface EMG traces, and is therefore a random process subject to the same influences as the EMG.

Thus, two VEMP averages computed using independent ensembles of traces measured from members of a normal population will necessarily be different. While some of this difference is due to the noise inherent in the signal, there are also contributions from differences in contraction effort, electrode placement, physiological differences between subjects and other inter-session and intra-session variables. This study is concerned with teasing apart the relative contributions of different factors to the response variability, with the goal of reliably measuring those factors that are clinically meaningful.

In Chapter 3, we examined this question phenomenologically by studying the variation in the experimentally measured EMG and VEMP in response to changes in factors such as stimulus intensity and contraction effort. We found that although the population we studied consisted of clinically normal subjects, there were differences in the VEMP response between subjects, between sessions, and between groups of measurements with different rms EMG levels. We also found that these differences were greater than could be explained by the randomness of individual measurements. While some of the factors (e.g. stimulus intensity) could be controlled, other factors such as contraction effort could not be completely controlled, measured or compensated for. Thus the goal of identifying the clinically relevant sources of differences in VEMP response could not be achieved by experiment alone.

In this chapter, we seek to better understand the experimental results by constructing a physiologically based model of the muscle, the voluntary motor drive, the measurement system, and the vestibular reflex pathway. We will use the computational implementation of this model to generate ensembles of simulated EMG traces similar to the experimental data. In the computational model, random and systematic sources of variability can be controlled and manipulated, and the effects of these changes on the output statistics can be studied.

We are interested in the sensitivity of the response statistics to different simulation parameters, and the values of the parameters that yield responses similar to those recorded experimentally.

It should be emphasized that we seek to compare the statistical properties, and not exact waveforms, of the model outputs and experimental data. This comparison corresponds to testing the following sequence of hypotheses:

(i) With the appropriate choice of physiologically realistic parameters, the model can produce synthetic EMGs with the same single-point statistics (i.e. distribution) and time-series statistics (e.g. autocorrelation) as the experimental surface EMG from a given subject/session.

(ii) With the model parameters chosen as above, modulating the motor unit spike rate on every trace results in a surface EMG ensemble which, when averaged, yields a recognizable VEMP-like waveform.

(iii) The synthetic VEMP trace ensemble is *statistically* similar to the experimental VEMP from the same subject/session. Specifically, VEMP subaverages computed from both experimental and synthetic ensembles of traces show a similar degree of variability. At the same time, if experimental data from two subjects/sessions are statistically dissimilar, the corresponding synthetic data ensembles are also statistically dissimilar.

(iv) The synthetic VEMP amplitude and latency parameters show a dependence on stimulus intensity and contraction effort that is similar to experimental data.

Some of terms used in stating the above hypotheses need to be clarified. For example, what do we mean by *statistical similarity* and *degree of variability* especially for high-dimensional data such as waveforms? These are questions we will address as the model is developed. Nevertheless, we aim to show that we can model the VEMP generation process in each subject/session so that it captures the broad similarities and differences in VEMP statistics observed within the small pool of normal subjects.

If we are successful in affirming the above hypotheses, we can use the computational model as a tool to find VEMP statistics that are most informative of the model's internal parameters. These same statistics can then be applied to experimental data to make useful inferences about physiological parameters of the subject from whom the data was obtained.

Similar studies comparing experimental data with muscle simulations have been performed in order to model the statistical properties of the force produced by muscle [30-33], and the statistics of the EMG [34-37] (reviewed in [38]). In terms of methodology, these studies largely follow the approach described by Agarwal and Gottlieb [39], and in forming the physiological model, they follow the approach established by Fuglevand et al., [40]. The studies differ in the level of detail used to model the volume conductor and tissue geometry,

the physiological details of the muscle fiber organization, and in the statistical parameters that are measured; these specifics are determined by the role of the model in each study. Our study follows a similar path for EMG simulation, but our goal is to understand, not the EMG itself, but the statistics of a response resulting from the modulation of the motor activity underlying the EMG.

4.1 Physiological foundations of the model

In Figure 4.1, we detail the motor and vestibular pathways, and show a conceptual model of the signal interactions that underlie the VEMP reflex. This conceptual model forms the basis for a computational model (illustrated in Figure 4.2) that is at the core of this portion of the study.

In going from the conceptual model to the computational model, we introduce a number of simplifying assumptions. These arise in part from gaps in our knowledge of physiological details and partly in order to make the computation tractable. In a later section, we discuss the basis of some of these assumptions, and the impact of these assumptions on the model outputs.

The interaction between the vestibular and motor pathways occurs at the pool of motor neurons of the spinal nucleus of the accessory nerve (CN XI) located in segments C1-C3 of the cervical spinal cord. As we have seen, each motor neuron defines a collection of muscle fibers that it innervates (the motor unit) and each action potential on the motor neuron results in the coordinated firing of action potentials that propagates along each muscle fiber from the innervation zone in the belly of the muscle towards the tendons where the muscle inserts into the bone.

When no acoustic stimulus is applied and the subject performs a constant-tension isometric contraction of the muscle, and there are no fatigue effects, the motor neuron pool is driven by a constant net motor drive which is the resultant of the cortico-spinal drive and various muscle reflexes [41]. The recruitment model maps this net drive into the firing of each motor neuron in the pool.

In response to the firing of an action potential on a spinal accessory motor neuron, the simultaneous depolarization of the muscle fibers of the corresponding motor unit causes a stereotyped pattern of surface potential changes that are recorded with the two electrodes over the belly and tendon of the muscle. We will call this unit surface response the motor unit action potential response (MUAPr) of that motor unit. The MUAPr is a single waveform that reflects the combined effect of the time-course of the transmembrane current of the muscle fibers, the properties of the motor unit (number of fibers, the mean

distance of the fibers from the electrode, the fiber diameter and conduction velocity) and the measurement system (electrode geometry, electrode position and amplifier bandwidth).

With the details of the action potential shape included within the MUAPr, the spiking activity of each motor neuron can be represented simply as a sequence of impulses (Dirac delta functions) at delays corresponding to the position of each motor unit spike [42]. The contribution to the surface EMG from a given motor unit is therefore the convolution of the MUAPr with the spike sequence of the motor neuron, and the surface EMG is the summed contribution from all the units. Equivalently, the surface EMG can be treated as the summed output of a set of filters driven by impulse trains, where the impulse response of each filter is the MUAPr of a particular motor unit.

As we have seen in the Background sections, when an acoustic stimulus is applied, part of the energy of the stimulus couples into the vestibular system (the saccule in particular), and elicits a burst of activity on the afferent nerve fibers that project on the vestibular nucleus [10]. This in turn activates reflex pathways that descend along the vestibulospinal tracts to form inhibitory projections on the motor neurons of the accessory nerve ipsilateral to the stimulated ear. As a result, if we examine the activity of a motor unit in a tonically contracted SCM muscle, each punctate stimulus applied at the ear is followed by a brief period of inhibition of the spiking activity of the unit. The time-course of this inhibition is determined by the mechanics of the vestibular periphery and the fidelity of neural encoding on the afferent and the descending pathways. The effect of inhibition on the motor unit spike sequences, and the resulting changes in surface response are determined by the neurophysiology of the motor neuron, and the MUAPr of the motor unit.

Our design of the computational model uses the following assumptions which are based, in part on current understanding of the physiology, and partly on considerations of model simplicity:

i. We assume that the inhibitory input seen by a motor unit has an invariant deterministic waveform, i.e., that the neural encoding of the vestibular response can be treated as noise-free relative to the other sources of noise in the system.

ii. We will assume that the inhibitory signal is only sensitive to the envelope of the stimulus. Measurements by Murofushi and Curthoys [43] of single vestibular afferent units in response to rarefaction and condensation click stimuli find two populations of units based upon the type of stimulus that evokes the earliest response. This was consistent with the findings of McCue and Guinan [10] on the phase locking of acoustic-responsive saccular units to tone-burst stimuli. It is not clear how these different populations of afferent units converge in the vestibular nuclei to evoke activity on the descending pathways: none of the studies that examined acoustic responses in the spinal accessory motor neurons or in SCM

motor units appear to have examined the dependence of these responses on stimulus polarity.

As we have described earlier, our experimental data are gathered using tone-burst stimuli with alternating polarity. A preliminary examination of the waveforms resulting from averaging VEMP responses tone-bursts of either polarity revealed no systematic differences between the two. Although the evidence is not conclusive, we will assume that the inhibitory signal from the vestibulocollic reflex is derived from both afferent populations, and does not show a preference for either polarity, and does not phase lock at the stimulus frequencies we use.

iii. We also assume that the processes that transform the stimulus envelope into the inhibitory signal are linear. Note that this does not refer to the nonlinearity involved in the extracting the envelope, but the neural coding and transformations that occur in the afferent signals on the vestibular nerve, the networks in the vestibular nuclei and the descending vestibulospinal and vestibulocollic pathways. This assumption is not based on measured properties of these systems, but from considerations of simplicity. All departures from linearity found in experimental data are ascribed to processes in the vestibular periphery.

iv. The spiking activity of a motor neuron can be described using a rate parameter: this is the parameter that changes as the motor drive to the muscle is varied. Depending on the statistical model of the motor unit firing (which we will describe in section 4.2.3), there may be additional parameters required to completely describe the spiking activity. The manner in which the spike statistics are changed following inhibition depends on the motor neuron membrane properties. For simplicity, we will assume that the effect of the inhibition on the spiking activity of a motor neuron is to modulate the rate parameter as a deterministic function of post-stimulus time.

v. The inhibitory modulation of the spike rate can be further idealized as a rectangular waveform defined by an inhibition duration and inhibition depth. Combined with the linearity assumption (iii), this means that changes in the stimulus intensity are reflected as changes in the inhibition depth only, while the inhibition duration remains unchanged. This assumption is central to the interpretation of both the computational and analytical model results.

vi. The duration of the inhibition can be estimated from measurements of extracellular compound potentials in SCM motor neurons measured in cats in response to galvanic and click stimuli [26, 44] . More directly, Colebatch and Rothwell [27] showed inhibition of SCM motor neurons in humans with click stimuli. The stimuli used in our study are not clicks but tone bursts, and there are no corresponding studies of inhibition duration for these stimuli. However, the above studies help

specify a lower bound on the duration.
Additional clues can be found from studies of VEMP averages in response to tonebursts with different rise/fall times and stimulus durations [45, 46].

vii. Since the muscle is modeled as a collection of motor units, each of which produces a surface response (MUAPr), we need to determine how the amplitude and duration of the MUAPr relate to motor unit properties, e.g. the number of fibers in the unit and the mean fiber-to-electrode distance of the unit. This question has been examined in a number of studies, usually by modeling the propagation of electrical signals in a volume conductor[25, 36, 38, 47, 48]. Rather than a detailed description of the MUAPr, we are interested in how the shape and the amplitude of the MUAPr vary with the depth and size of the motor unit. Based on a survey of modeling studies, and from the studies by Fuglevand et al. [49] and Monster and Chan [50] , we have made the following assumptions:

- The amplitude of the MUAPr is directly proportional to the number of fibers in the unit.
- The amplitude is inversely proportional to the mean distance of the motor unit fibers to the electrodes

viii. All units evoke the same response waveform across the surface electrodes (i.e. the MUAPr shape is the same). We accommodate some differences in the response shape between subpopulations of units in the manner in which the response shape prototype is constructed. By allowing the MUAPr prototype to be described as a sum of three basis functions with different widths and amplitudes, we implicitly permit sub-populations of motor units which evoke different surface responses. However, individual motor units are not assigned to these populations and the proportion of units in these populations does not change with motor drive. This invariance of the unit response waveform is supported by empirical data from studies such as Hughes and Colebatch [51], albeit in smaller muscles.

The above assumptions represent a compromise between highly detailed electrical models of the muscle [25], and highly idealized models where all the units in the muscle are treated as a single entity [52]. Based on these assumptions, we assign a single MUAPr prototype waveform to all the motor units. Each unit is assigned an amplitude value based on the size and depth of the unit. The MUAPr prototype waveform is specific to each subject and session, under the assumption that it is strongly influenced by the electrode and tissue geometry. We describe the process of designing this waveform in Section 4.3

The spiking activity of each motor unit is described in our model by a quasi-periodic spike train, where the inter-spike interval (ISI) is a renewal process with a Gaussian distribution about a fixed mean value. Negative ISI values are dropped, although given the low

coefficient of variation, the frequency of such censoring is small. The mean inter-spike interval is the inverse of the spike-rate assigned to the unit by the recruitment model. The Gaussian ISI is a fairly common assumption in many analyses of motor unit spiking [53], although other distributions, such as Weibull [54] and Gamma [55] distribution have been also been proposed.

The standard deviation of the ISI distribution is varied along with the mean ISI, so that the coefficient of variation is maintained at a constant value. We have chosen a coefficient of variation of 0.2 (i.e. standard deviation = mean/5) based on experimental data from Clamann [53]. While a majority of modeling studies have used a constant coefficient of variation (e.g. [56]), others have used more complicated relationships between the mean and standard deviations (e.g.[39]).

We assume that the surface EMG can be treated as the output of a linear filter driven by white noise. This allows us to design the MUAPr waveform as the impulse response of a filter whose spectral characteristics match the experimental data. We justify the whiteness assumption by treating the motor unit ensemble as a single filter driven by a spiking process that is the superposition of the activity of all the individual motor units. In Sections 4.2.3 we discuss the validity of this assumption and its implications.

4.2 Components of the computational model

The above assumptions allow us to transform the physiological model of Figure 4.1 to the computational block diagram of Figure 4.2. The computational model is a set of Matlab routines that are called in sequence and simulate individual blocks in the figure. The output of the model is an ensemble of waveforms representing synthetic surface EMG or VEMP traces recorded over a period of about 40 seconds. The inputs to the model are (i) the motor drive over the course of the recording period, (ii) the depth (D) and duration (T) of the inhibitory response to the acoustic stimulus, and (iii) the motor unit action potential response (MUAPr) waveform.

The MUAPr parameter may be an idealized waveform derived from theoretical considerations alone, or it could be specific to the subject and session we wish to model. In the latter case, we use the statistics of experimentally recorded surface EMG traces (*not VEMPs*) of the subject/session to compute the MUAPr. This process is described in Section Figure 4.3 The experimental data are used to compute the statistics of the EMG from which to design the MUAPr waveform for the specific subject and session. The process of designing the waveform is described in Section 4.3.

In the following sections, we outline the properties of each component of the computational model.

4.2.1 Muscle model

The muscle is an array of 250 motor units. This number is estimated from the EMG-based motor unit number estimates of human skeletal muscles[57, 58], and counts of spinal accessory motor neurons [14]. The units differ from each other in their size (number of muscle fibers in the unit), and the distance to the electrodes of the electrical center of the unit.

The total number of fibers is derived from the muscle dimensions and the average cross-sectional area of a muscle fiber. The data on the dimensions of SCM differ widely, probably reflecting the anatomical differences in the population, as well as differences in methodology. Based on sectional anatomy [59] and dissection studies[16], we estimated the effective cross sectional area of the SCM at 3.7 cm^2. We also assume that the proximal margin of the muscle lies 4 mm below the skin surface. The average fiber diameter is assumed to be 100 μm, yielding a count of approximately 50,000 fibers in the muscle.

These fibers are distributed among the 250 motor units in a non-uniform manner. The number of fibers in each motor unit (the unit's innervation ratio) is known to be proportional to the twitch force produce by the unit [60]. It is also known that the twitch forces of the motor unit pool are exponentially distributed [40], with the largest twitch force approximately 100 times larger than the force from the smallest units [2, 40]. From these two findings, we define an exponential distribution of 250 twitch values between 1 and 100, and allocate the muscle fibers based on each unit's twitch force. Figure 4.3 shows the resulting innervation ratio distribution.

With some exceptions, the motor units of most muscles are distributed randomly over the cross-sectional area of the muscle [21]. The cross sectional area covered by the fibers of each unit (the motor unit territory) depends on the number of fibers in the muscle and on the number of other units that share a given area (the "interdigitation factor" [2, 61]). We assume an interdigitation of 25 in computing the motor unit territory, and assume that large units cover the entire thickness of the muscle. This allows us to compute the depth of the electrical center of each unit, as shown in Figure 4.4.

The number of fibers and the mean distance to of each unit electrodes contribute to the relative size of the surface potential generated by the unit. The surface response amplitude is assumed to be proportional to the number of units and inversely proportional to the unit depth [62]. In order to account for the unequal contributions from the proximal and distal fibers within a unit, we apply a correction of $1/3^{rd}$ of the motor unit size to its depth. The resulting distribution of response amplitudes is shown in Figure 4.5.

The size and depth of the motor unit specifies the *relative* amplitude of the motor unit response. The absolute amplitude (in μV) depends on the amplitude A of the surface

response of a single action potential. We have no direct measurements of A, and our choice of this parameter will determine the amplitude of the resulting surface EMG.

4.2.2 Recruitment model

The recruitment model translates the motor drive parameter into the firing rate of each unit. The motor drive K is a number between 0 and 100, representing the range of voluntary contraction effort, i.e., it corresponds to the percentage of the maximum voluntary contraction (%MVC). At $K = 0$, the firing rates of all units are zero, and at $K = 70$, all the units have been recruited.

Motor unit recruitment follows Henneman's size principle [21]. At the start of the simulation, each unit is assigned a threshold motor drive and the slope of the relationship between rate and the motor drive. The resulting pattern of motor unit firing rates at different motor drives is shown in Figure 4.6.

4.2.3 Motor unit spiking model

A recruited motor unit fires in a quasi-periodic fashion, where the inter-spike interval (ISI) is Gaussian distributed about a mean value determined by the firing rate assigned to the unit. In Figure 4.7, we show the distribution of all the inter-spike intervals among all the motor units over the course of a 200 ms EMG simulation.

The firing probability (or firing rate) of a unit at a given time is computed by simulating the spike sequence of the unit over multiple independent trials and estimating the mean number of spikes in a sequence of narrow time bins. This estimate is a random process, and can be characterized by the mean rate at each time-bin and the correlations between the rates at different bins.

When the time axis is defined as the time duration following a given motor unit spike, we measure the post-spike firing probability (or a spike triggered average), which is shown in Figure 4.8 for two units at two different values of motor drive. We see that the mean rate is quasi periodic with a periodicity equal to the mean ISI of the unit. The periodicity gets weaker with time, and disappears after roughly 5 cycles. The duration needed for the spike rate to become uniform is dependent on the standard deviation of the ISI distribution; in this simulation, the standard deviation is $1/5^{th}$ the mean ISI.

When the time axis is defined independently of the spiking activity, as is the case for a stimulus-triggered average in our experimental data, the averaged rate becomes independent of the post-stimulus time, so that the firing probability becomes uniform, as illustrated in Figure 4.9. Despite the uniform rate, the correlations between the spike counts persist, and result in shaping the spectra of the spiking process (Figure 4.10). The non-white nature of

this process has important implications to the estimation of the motor unit surface response in Section 4.3

The surface EMG measures the response to the combined activity of all the units in the pool. These units fire independently of each other, and span a range of mean firing rates as shown in Figure 4.6. As a result, the composite spiking process can be expected to be decorrelated to an extent depending upon the variance in the ISI and the range of motor unit spike rates; in the limiting case, where the units have very similar firing rates and their firing is almost periodic, the composite spike process remains correlated over long intervals. For the choice of parameters in our model, we show the power spectrum and autocorrelation of the composite spike process at different motor drives in Figure 4.11 and Figure 4.12. We see that the spike rate at stimulus presentation is significantly correlated with the rate at preceding time instants over a 50-70 ms duration.

In the rest of the study, we do not consider the above behavior: we treat the spike rate as a white process driving the volume conductor filter. Although the spectral shape of the spike rate process has important consequences on the validity of the unit surface response (MUAPr) calculated in Section 4.2.4, the actual waveform shape is not critical to our conclusions about the statistics of the surface EMG and VEMP.

More important is the relationship between the variance and mean of the rate at a given instant. We see in Figure 4.9, that the variance of the rate estimates is larger for the units whose mean rate is higher. We verify this property by computing a number of trials of the motor unit pool at different motor drives, thus simulating units over wide range of mean firing rates. We compute the mean and variance of the spike counts over 1 ms bins, and show the relationship in Figure 4.13. The ratio of variance to mean is close to 1 for most motor units and over a wide range of mean firing rates, a property that is characteristic of a Poisson process.

For each trace, the spiking model produces spike sequences for each of the active motor units. The spike positions are encoded at a precision much greater than the sampling rate of the experimental and simulated surface EMG signals, to avoid introducing artificial correlations between spikes and spike trains.

4.2.4 Surface response model

The motor unit action potential response is the surface response generated by a single motor unit action potential on the muscle. In our model it corresponds to the filter impulse response $h(t)$. Although in reality the waveform depends on the depth, size and other characteristics of each motor unit, this model assumes that the same waveform can be used to describe all the units, and that it is invariant with time and motor drive.

There is no direct means of measuring the surface response to a single action potential when the motor unit activity is driven by voluntary contraction effort. We then have two choices: we can estimate $h(t)$ from first principles, by modeling the volume conductor and a moving current dipole. Alternatively, we could design $h(t)$ based on experimental data from the subject/session. With the modeling approach, we may lack sufficient detail to capture differences in response due to differences in anatomy and electrode geometry between subjects and sessions, whereas with the experiment-based approach, the problem may be ill-posed and yield physiologically unrealistic solutions. Our solution, described in detail in Section 4.3 is a compromise between these two approaches. We design $h(t)$ as the sum of component waveforms derived from physiological models, but tailored to the characteristics of the surface EMG from individual subjects and sessions. In Figure 4.14, we show $h(t)$ waveforms used in the simulation which have been derived from the autocorrelation of the experimental surface EMG signal from normal subjects.

It should be pointed out that the $h(t)$ found here are not unique: a given autocorrelation can arise from any of a number of transfer functions. Therefore, two subjects or sessions whose EMGs have very similar spectra could have transfer functions that are significantly different. We are not interested in the specific $h(t)$ shapes, but in reflecting the diversity of the transfer function waveforms that can arise from differences in EMG spectra. We search for $h(t)$ in a constrained solution space using an iterative algorithm starting from the same initial state in each case. The resulting waveforms are different from subject to subject and session to session, but the constraints inherent in the estimation procedure mean that these differences are smaller than might exist in the actual $h(t)$'s.

For each motor unit, each surface EMG trace is computed as the summation of individual spike responses $\sum A a_i h(t-\tau_i)$, where each $h(t)$ is offset by a delay τ_i determined by the position of each motor unit spike, and is scaled by the response amplitude a_i of the unit. The summation is taken over the (variable) number of spikes over a duration equal to the length of the trace + the length of $h(t)$. Note that the spike positions τ_i as well as the $h(t)$ waveform are computed at a time resolution that is 10 times the sampling rate of the surface EMG. A set of 500 such simulated traces forms an ensemble, which corresponds to experimental traces recorded over a 40 second contraction. .

From the model components described thus far, we are able to simulate the surface EMG produced by the muscle for a given motor drive, and with the response characteristics

specific to a particular subject and session. We now consider the modulation of motor unit spike rates that results in the VEMP.

4.2.5 Inhibition model

The inhibition model describes the influence of the tone-burst stimulus on the spiking activity of the motor neurons. The stimulus is assumed to result in a fixed "internal response" that modulates the spike rate of the active motor units. This presumed internal response signal represents the response of the saccule, the neural coding and transformations that occur in the vestibular nuclei. We assume that each motor unit receives inhibitory projections of equal strength.

The modulation function is characterized by a duration T, which is fixed at 6ms, and an inhibition depth D that takes values between 0 and 1. Once the spike positions for a particular motor unit are determined based on the spike's firing rate, the inhibition model deletes the spikes that fall within the interval T with a probability of deletion determined by the inhibition depth D. The thinned spike sequence is then passed to the surface response model to generate the motor unit's contribution to the surface EMG trace.

The inhibition depth is thus a measure of the size of the internal response to the stimulus. It reflects the stimulus intensity, as well as physiological characteristics of the peripheral vestibular system being modeled. We therefore expect that the relationship between the stimulus intensity and the inhibition depth is a key feature that is informative of the physiological state of the vestibular system. The primary use of the model is therefore to investigate ways to estimate the inhibition depth from experimentally recorded data.

Our choice of the inhibition model is driven in part by a desire for simplicity and analytical tractability: the effect of changes in stimulus intensity translates into simple scaling of the modulation function. Since the duration and the waveform do not change, the VEMP waveform recorded at maximum intensity can serve as a template for estimating the response size at other stimulus levels. The value of the duration T is based on measurements of inhibitory potentials [26] and of spike rate changes [27] following click stimuli, and the fact that the tone-burst stimulus is 8 ms in duration with its energy concentrated at the center of the pulse. Alternative approaches to estimating the actual inhibition time-course with fewer rigid constraints are briefly discussed Chapter 6, but do not form part of this study.

4.2.6 Additive noise

The signal measured by the electrodes includes additive noise due to instrument sources as well as the electrical activity of muscles and nerves unrelated to the SCM that is being measured. This noise component is modeled in the simulation as zero-mean white Gaussian noise that is low-passed to a bandwidth of 1250Hz with a 6^{th} order Butterworth filter. The filter parameters are based on the noise signal recorded with no head turning and no acoustic stimulus. The filter bandwidth and the amplitude of the noise signal are set so that the spectrum of the simulated noise matches that of the experimental noise. We find that even at small amounts of head-turning, the EMG from the muscle (presumably from the SCM, since it is directly under the electrodes) quickly dominates the contribution of the additive noise. Therefore, we do not attempt to match the noise generator parameters to data from every subject and session, but use one set for all simulations.

4.2.7 Model Inputs/Outputs

The inputs to the model include the inhibition depth D, motor drive K and the MUAPr waveform $h(t)$ computed for the particular subject and session we wish to simulate. Each run of the model yields a set of 500 synthetic EMG traces, corresponding to a recording duration of approximately 38.5 seconds. Each trace is an array of 1723 samples corresponding to the trace length of 77ms sampled at 25 kHz, the same rate as the experimental recordings.

4.3 Fitting the model parameters

The three input parameters of the model are designed so that the statistical properties of the output traces match those of the experimentally recorded trace ensemble. The motor drive and the MUAPr waveform are designed to match the properties of the surface EMG only, leaving one parameter, inhibition depth, which we can use to fit the properties of the VEMP. *If we are successful in simulating the VEMP properties, this would provide a validation for the model as well as a means of estimating the inhibition depth, a property of the vestibular system that can not directly be observed.*

We cannot directly estimate the amplitude A of the single fiber surface response. This is a scale factor that converts the simulated signal values into actual voltage measurements. The amplitude of the output signal is affected by the scale factor A as well as the motor drive K, and this ambiguity would be directly resolved if a parameter can be computed from the model output that shows a different dependence on the motor drive than on the scale factor

A. We do not observe such a difference in the distribution of EMG samples between scaling and the motor drive, so the ambiguity remains. For most clinical applications, resolving this ambiguity is not important, since we are generally concerned with *relative* changes in signal amplitude.

4.3.1 Estimating the MUAPr waveform

A central assumption of our parameter estimation method is that the experimental surface EMG is the result of a white noise spiking process driving a linear filter with impulse response $h(t)$. We can therefore estimate $h(t)$ for a particular subject/session from the power spectrum or the autocorrelation of the experimental data. This estimation is difficult because: (i) the waveform is a virtually infinite-dimensional parameter, and (ii) estimation of the transfer function of the filter from the output spectrum is often an ill-posed problem, especially when the filter has a low bandwidth and/or spectral nulls. We note that the frequency response of the electrode montage and instrumentation has a null at DC, making $\int h(t)\,dt = 0$.

We make the estimation problem more tractable by reducing the dimensionality of $h(t)$. It is now constrained to be a weighted sum of three "basis" functions, where each function is a Gaussian pulse that is scaled along the time axis, scaled in amplitude, and shifted in position. Estimating $h(t)$ therefore reduces to choosing the amplitude, width and position of the three pulses so that the autocorrelation of the summed waveform matches the autocorrelation of the surface EMG. We fix the amplitude and position of one of the pulses at nominal values of 1 and 0 respectively, leaving a total of 7 parameters to describe $h(t)$. In Figure 4.15, we see how these pulses are combined to form a single response function.

The parameter values are computed using a simple iterative search algorithm, where the goal is to match the autocorrelation function of the experimentally recorded surface EMG signal from a given subject/session, subject to the constraint that the $h(t)$ integrates to zero.

- The autocorrelation function is computed from the ensemble of recorded traces. If the EMG-only (i.e., stimulus-free) recordings are unavailable, data recorded at the lowest stimulus intensity are used.
- An initial parameter set and the step size are selected, generally based on the parameters previously computed for a different subject/session.

- The $h(t)$ is assembled using these parameters, and the autocorrelation of $h(t)$ is computed.
- The fitting error is defined as the sum of the squared difference between the data autocorrelation and the autocorrelation of the model response. This difference is weighted so that the autocorrelation at small lags (< 20ms) is more closely fit than the large lag values.
- The fitting error is computed for each of 3 parameter vectors, where one single element of the parameter vector is varied between the current estimate p, and $p(1 \pm \Delta)$ where Δ is the step size. The parameter vector is updated with the element p that yields a lowest error. After sequentially optimizing each of the 7 parameters, we return to the first parameter and repeat the process, decreasing the step-size at each iteration. In this way, we search for a local stable point of the error surface in the 7-dimensional parameter space. We illustrate this process in Figure 4.16 where we evaluate $h(t)$ for one ensemble: Subject 8/ Session 3.

We find that the algorithm converges rapidly in each case, and yields a response waveform whose autocorrelation matches that of the data from the given subject/session.

There is no guarantee that the response computed above corresponds to a globally optimal solution. Indeed, it is clear that the solution is not unique, since time-reversed and inverted responses $-h(t)$ and $h(-t)$ yield the same autocorrelation function as $h(t)$. This non-optimality does not cause concern since we are interested in modeling mainly the statistical behavior of the EMG and VEMP, not exact waveforms. The solution we find is viewed simply as a *plausible* MUAPr that describes the volume conductor and only one of an infinite number of similar solutions. In Figure 4.17, we show the results of the estimation process for all subjects and sessions.

4.3.2 Estimating the motor drive

The motor drive parameter K controls the rate of the motor unit spiking process that drives the linear filter described by $h(t)$. An accurate simulation of the EMG incorporating the effort variations requires an estimate of the motor drive for each trace of the ensemble.

Measures of contraction effort used in prior studies of muscle force and EMG include the variance, the root-mean-square (rms) value and the mean absolute value (mav) of the surface EMG [63]. We discuss the choice of measure in detail in Section 4.4.1.

Estimating the variance or the rms level of the signal requires averaging over a certain time interval. A longer interval provides a more accurate estimate of the level (i.e., with a smaller mean square error), but also assumes that the signal is stationary over the averaging interval. One of the central problems of VEMP is the non-stationarity of the motor drive, and we need to understand the time over which the motor drive may be considered stationary.

Our approach to estimating K thus uses two parameters established by examining the synthetic EMG produced by the model at different values of motor drive:

- The relationship between the variance or rms value of the EMG and the motor drive for different subjects/sessions
- The time interval over which the motor drive can be assumed to be stationary is estimated by comparing the low-frequency components of the synthetic and the experimental EMG.

These procedures are discussed in detail in Section 4.4; here we only note that these observations allow us to estimate the level of the surface EMG, smooth it appropriately, and translate this level into a motor drive value. We set the numerical scale for K by assuming that the largest observed value of the EMG variance (filtered) corresponds to $K = 100\%$ of maximum voluntary contraction (%MVC).

4.4 Synthetic EMG: Properties

With the parameters determined as in Section 4.3, we can examine the model outputs and compare the results with the experimental data. Figure 4.18 shows a qualitative comparison of a selection of traces, and illustrates the similarity of signal characteristics. The following sections examine the relationships between the simulation parameters and surface EMG statistics in model outputs, in comparison with similar measures on experimental data.

4.4.1 The rms EMG is a measure of motor drive.

We have seen earlier (Figure 4.13) that for individual motor units, an increase in motor drive translates into increases in the firing rate and in the variance of the spiking process. In our model, the surface EMG is the output of a filter with a zero DC response, driven by the spiking process which is assumed to be white and stationary.

It is well known (e.g. [64]) that for a linear system driven by a stationary white input process $x(t)$ with mean μ_X and variance σ_X^2, the mean and variance of the output $x(t)$ are given by

$$\mu_Y = \mu_X \int h(\alpha)\, d\alpha \quad \text{and}$$

$$\sigma_Y^2 = \sigma_X^2 \iint |h(\alpha)|^2 d\alpha \quad \text{respectively.}$$

In case of the EMG, this means $\int h(t) = 0$, making the mean of the EMG is zero, and the EMG variance is expected to be proportional to the variance of the spiking process, (through $\iint |h(t)|^2$). The spike rate variance is equal to the mean spiking rate, which in turn is proportional to the motor drive.

Examining the model outputs, we find that the simulated composite *spiking* activity of all units exhibits this behavior (Figure 4.19, A and B). However, when we examine the behavior of the synthetic *EMG*, (Figure 4.19, C and D), we find that the expected relationship does not hold: the *standard deviation*, rather than the variance of the synthetic EMG, is seen to be proportional to the spike rate variance. As a result, for the synthetic EMG produced by our muscle model, the standard deviation or root mean square (rms) value is a better estimator of the motor drive than the variance. This relationship is illustrated in Figure 4.20 for each subject and session.

While this behavior is surprising for the output of a linear filter, the result is consistent with a majority of EMG and muscle force modeling studies which use the rms EMG as a measure of voluntary contraction effort. The use of rms EMG in these studies is based on a multiplicative model of the EMG signal [23, 63] shown in Figure 4.21.

The reason for the difference between the expected relationship of input and output filter statistics, and the relationship found in our computational model is not obvious. This discrepancy has, however, been observed in an earlier study [65] which examined the mean-to-standard deviation relationship of the spike rate for motor cortex neurons and motor neurons. It was found that the mean and the variance of the firing rate were linearly related. In contrast, measurements of muscle force found that the standard deviation was proportional to the mean force, consistent with theoretical models of optimal motor control [66]. The authors in [65] attributed this discrepancy to the orderly recruitment of units under Henneman's size principle.

In this study, we will estimate the motor drive as a linear function of the rms EMG level. This translation is done by assigning the largest measured value of the rms EMG (over all the available ensembles from a particular subject/session) and to a motor drive of 95 %MVC. Assuming that a zero motor drive results in zero rms EMG (i.e., neglecting the

additive noise), we find a single scale factor that, when multiplied by the measured EMG level, gives the motor drive.

In the rest of this discussion we will use the term *trace EMG level* to refer to the rms value of the EMG samples (synthetic or experimental) over the course of a single inter-stimulus interval (trace). Thus an ensemble of consecutive traces corresponding to a single recording or simulation trial will yield a sequence of trace EMG levels that reflect the contraction effort or motor drive.

4.4.2 RMS EMG estimates are highly variable

The trace EMG level is a random variable. It has an intrinsic variability superposed over variations due to changes in motor drive. Trace EMG levels from simulations at constant motor drive will only display statistical variations. Therefore, by comparing these trace EMGs with of trace EMGs from experimental data, we can isolate the component of the variation that is due to actual changes in effort (Section 4.4.3), and use this component to drive a new set of simulations that incorporate realistic changes in motor drive (Section 4.4.4).

The time-course of the synthetic trace EMG level (Figure 4.22 A) over a single simulation run, and the distribution of these levels (Figure 4.22 B), indicate that a large proportion of the trace-to-trace variability of the rms EMG is present even when the motor drive is held constant. Changes in contraction effort can therefore account for only a small proportion of the variability of the trace EMG level. The figure shows the experimental and simulated EMG only for Subject 1/ Session 1, but the same behavior is found across subjects and sessions.

4.4.3 Filtered RMS EMG estimates are a measure of effort

Since any changes in motor effort are expected to occur slowly relative to the trace duration, we can smooth out the statistical variation of the measured trace EMG level in order to use it as a measure of true variation in motor effort. To do this, we must first define the cutoff frequency of the low-pass smoothing filter

The next set of figures (Figure 4.23) shows the low-frequency range of the spectra for the measured trace EMGs superposed over the spectra of the trace EMGs of simulated traces. The goal is to identify the frequency and the relative magnitude of the low-frequency components that presumably reflect changes in contraction effort.

The spectrum of the trace EMG sequence is found to be specific to each subject: the cutoff frequency is the same for all the sessions from a given subject. By filtering the experimental trace EMG sequence with a low-pass filter with the subject's cutoff frequency,

we can obtain smoothed estimates of the rms EMG, as shown in Figure 4.24. We treat this filtered EMG signal as reflecting changes in motor drive. From the figure, we see that the subjects differ widely in how stable the motor drive remains over the course of the contraction: some subjects maintain the motor drive in a narrow range, but with rapid changes within the range, whereas the motor drive of other subjects shows large, slow excursions.

4.4.4 EMG simulation with variable motor drive

We now have the MUAP surface response $h(t)$ for each subject and session, as well as an estimate of the motor drive for each experimentally recorded trace. We should be able to generate realistic EMG simulations corresponding to each ensemble of recorded traces.

In order to avoid the computational load running the entire simulation including the recruitment model for each simulated trace, we pre-compute sets of synthetic EMGs for a number of distinct motor drive values for each subject/session. When we wish to generate an ensemble of EMG traces with variable drive to match that of an experimental recording, we compute the rms EMG level of each trace, map it to a motor drive value, choose a synthetic trace at random from the appropriate pre-computed set and assemble the ensemble. The resulting rms EMG profile and its histogram are shown in Figure 4.25, which shows the contrast with Figure 4.22.

4.4.5 Distribution of EMG samples

The distribution of single EMG samples (as opposed to the distribution of the trace EMG levels discussed in the previous section) has been a topic of study in the EMG community, particularly as it influences the design of optimal EMG processors (e.g. [67]). Different studies have suggested different standard densities (e.g. Gaussian, Laplacian) to fit EMG distribution, without a clear consensus on the reason for differing observations. Our modeling results shed new light on this question by allowing a comparison between synthetic and experimental EMG, but they also raise new questions with implications for muscle physiology. This problem is peripheral to the VEMP question, so we only note here that the non-Gaussian nature of the EMG distribution observed in our experimental data is adequately explained by modeling the EMG with variable effort. This is illustrated in Figure 4.26.

4.4.6 Time-series statistics of EMG

Our simulations have used $h(t)$ that are derived from the autocorrelation of experimental data from each subject/session. We therefore expect that the time-series statistics of the simulated EMG with constant as well as variable motor drive match the statistics of the experimental data. We show this in Figure 4.27.

Figure 4.26 and Figure 4.27 support the first of the hypotheses stated at the start of the chapter: "With the appropriate choice of physiologically realistic parameters, the model can produce synthetic EMGs with the same single-point statistics (i.e. distribution) and time-series statistics (e.g. autocorrelation) as the experimental surface EMG from a given subject/session." In the next section, we examine simulations with spike inhibition, which produces the VEMP response.

4.5 Synthetic VEMP: Properties

When the computational model is run with a non-zero value of inhibition depth, the resulting synthetic EMG waveforms show a systematic shift in the mean value over the post-stimulus interval. This modulation, which can be observed when the traces in the ensemble are averaged, is the VEMP signal.

For our simplified conceptual model, each post stimulus EMG trace $x(t)$ is the convolution of the composite spiking process $r(t)$ and the unit surface response (the MUAPr).

$$x(t) = r(t) \otimes h(t)$$

The mean EMG is found by taking the expectation of $x(t)$:

$$\mathbb{E}(x(t)) = \mathbb{E}(r(t)) \otimes h(t)$$

The mean $\mathbb{E}(r(t))$ of the spike process is the mean post-stimulus spike rate. In the absence of a stimulus, the mean spike rate is constant, and $\mathbb{E}(x(t))$ becomes proportional to $\int h(t)$, which is zero by design. When a stimulus is present, we model the mean spike rate to follow a stereotyped timecourse $r_s(t)$ where the spike rate diminished by a fixed fraction for 6 ms following the stimulus. The theoretical post-stimulus mean EMG expected from

this model is then $r_s(t) \otimes h(t)$. In the limit of an infinite number of traces, we expect the VEMP average from our model to converge to this value.

Figure 4.28 shows the VEMP average resulting from the outputs of the model operated with an inhibition depth of 0.12. At this stage, we do not have an estimate of the scaling factor A required to produce synthetic EMG with a realistic amplitude. Therefore, we calibrate the model outputs by comparing the amplitude of the VEMP with the amplitude of the "noise" signal outside the expected range of post-stimulus response time. We choose the inhibition depth such that the resulting VEMP average displays similar relative amplitudes. We find that for Subject1, at least, an inhibition of only 12% of the spikes in the motor unit pool is sufficient to produce a realistic VEMP response. We have thus verified the second hypothesis: "With the model parameters chosen as above, modulating the motor unit spike rate on every trace results in a surface EMG ensemble which, when averaged, yields a recognizable VEMP waveform".

The informal method use used to pick the inhibition depth in Figure 4.28 illustrates an important idea which is central to later analysis of the VEMP, namely that the response strength can be quantified using the noise level as a metric. When the properties of the underlying noise process are not known (as in experimental VEMP data), we rely on the signal to noise ratio at the output as a measure of the size of the response. In a conventional VEMP test, the signal to noise ratio is used implicitly by the tester when attempting to detect a response at low signal levels, e.g. for threshold measurements. Presence of a response is declared when the measured signal in the region of the "expected response" exceeds the surrounding noise floor by a certain percentage.

In VEMP, the principal source of noise is the EMG from the muscle under test. As we have seen in our study of EMG simulations (Section 4.4), estimates of this EMG noise level are highly variable from trace to trace due to statistical variations as well as changes in motor drive, making the VEMP amplitude estimation and the VEMP detection problem much more challenging. In this study, we use a slightly different measure of signal to noise ratio, based on the definitions of signal level and signal variability developed in Chapter 3. In Section4.7, we apply this measure to the problem of estimating the internal response amplitude (i.e. estimating the inhibition depth) as it varies with stimulus intensity.

Figure 4.29 shows the experimental and simulated VEMP waveforms for all subjects and sessions. For reference, we also show the computed single spike responses (MUAPr) derived from the EMG-only data for each subject and session. We see that the simulated VEMPs are very similar across subjects and sessions. This is due to the similarity of the MUAPr waveforms used in the simulation. Recall that the MUAPr was selected to match the autocorrelation function of the EMG-only data. Since the autocorrelation function does not retain the phase information, the MUAPr represents only one possible choice out of a

large solution space; other equally valid waveforms can exist. Our particular choice of MUAPr is a result of the iterative algorithm used to derive it, and the choice of initial conditions on the algorithm. Since EMG data from each subject/session were processed in a similar manner, the similarity of the time-series statistics of the EMG of different subjects/session means that the algorithm converges to similar-looking MUAPr solutions. Nevertheless, small differences in the spectral properties of the EMG are seen to produce corresponding differences in the VEMP (see, for example, the differences in autocorrelation and MUAPr between the sessions of Subject 6 in Figure 4.17).

In Figure 4.30, we examine a selection of the MUAPr waveforms and the synthetic VEMPs from each subject. We also show the theoretical mean VEMP waveform; the departure of the synthetic VEMP averages from this mean represents the residual effects of the random fluctuations in the spike rate after averaging over 500 traces. We see that the size of this noise amplitude is large relative to the size of the VEMP even under the controlled conditions of the simulation.

4.5.1 Growth of simulated VEMP amplitude with inhibition depth

Figure 4.31 shows experimental VEMP responses at different stimulus intensities and compares them with synthetic VEMPs at different values of the inhibition depth. This figure allows a number of comparisons: between simulated VEMPs at different inhibition depths, between recorded VEMPs at different stimulus levels, between VEMPs at different sessions for the same subject, and between simulated and experimental VEMPs. A careful examination shows several interesting features of the response:

(i) The MUAPr shape has a strong influence on the VEMP response especially for small amounts of inhibition. For example, comparing the synthetic VEMP from Sessions 1 and 2 of Subject 1 at the smallest inhibition depth (4%), we see that the responses are very different even though the motor drive, the inhibition, and the muscle architecture are identical in both instances.

(ii) The amplitude of the simulated VEMP appears to increase systematically with the inhibition depth for all subjects/sessions, whereas the amplitude of the experimental VEMP as a function of stimulus intensity is very different: in many instances (e.g. Subjects 7 and 8), we find that the VEMP amplitude is unchanged for all but the highest stimulus intensity. This nonlinear relationship is not surprising – the stimulus is measured on a logarithmic dB scale, and the transformation from the stimulus to the inhibitory signal on the CN-XI motor neurons is likely nonlinear as well.

The key point of feature (ii) is that the relationship that we find between the inhibition depth and the amplitude of the simulated VEMP could allow us to associate a putative "inhibition depth" with the amplitude of an experimental VEMP average as well. We will

then have associated an observed response feature with an un-observable, but physiologically meaningful parameter. The strength and reliability of this association can be assessed by processing sets of independent experimental measurements within and across sessions, and measuring the dispersion of the estimated inhibition depth. Our assumption is that each subject is physiologically identical across observations and sessions, and should therefore have the same inhibition depth. Since the data are inherently random, we expect a certain amount of dispersion in our inhibition depth estimates. The simulation results can help establish the amount of this inherent variability and provide a metric to assess the quality of the inhibition depth estimates. As we will see, the simulation results can also help identify alternatives to the VEMP amplitude as the statistic from which to estimate the inhibition depth.

It is not sufficient for the estimates of the presumed inhibition depth to be reliable; indeed, a function that simply maps all the observations onto a single number would be found to be perfectly reliable, and also completely meaningless. One test of whether the estimates are meaningful is whether the estimates change with physiological changes in the vestibular periphery. Such a study in humans would call for measurements across a number of clearly identified pathological populations, and is outside the scope of this study, even if it were possible. Instead, as we have discussed earlier, we use changes in stimulus intensity as a surrogate for pathophysiological changes in vestibular sensitivity to a fixed stimulus. Our question then becomes: are the inhibition depth estimates at different intensities statistically different and do these estimates vary systematically (if nonlinearly) with stimulus intensity? It is then very interesting to find out whether different subjects in our "normal" population show the same pattern of inhibition depth variation with stimulus intensity. These are questions we will address in the later sections of this chapter.

4.5.2 Growth of simulated VEMP amplitude with motor drive

The simulated VEMP average grows with the motor drive. As the drive increases, although the probability of inhibition of a particular spike is unchanged, the number of inhibited spikes increases, and the contribution at the surface of the "missing" spikes is larger. In Figure 4.32 we show the growth of response with motor drive (for simulations) and with stimulus intensity (for experimental data), for a selection of subjects and sessions. The simulated trace ensemble consists of the same number of traces as the experimental session, with variable motor drive as described in Section 4.4.4. The range of experimental filtered rms EMG values is determined, and the motor drive parameters are chosen to map 95% MVC to the largest value, and 15% MVC to the smallest value of the filtered EMG.

In order to plot each panel of the figure, we compute the filtered rms EMG level of the traces (synthetic or experimental), arrange the ensemble of traces in order of increasing EMG level, then group the traces into 5 bins with equal numbers of traces. With each bin

thus corresponding to a different range of EMG levels, we compute the average of the traces in each bin. It is important to realize that the EMG ranges associated with each bin are different in different panels, but are the same for the synthetic and experimental data in each case.

4.5.3 VEMP amplitude growth (quantitative)

In this section, we will examine the VEMP amplitude growth quantitatively, and in later sections, we will develop the inhibition depth estimator. But first we must contend with the fact (seen in Figure 4.31 and Figure 4.32) that the response shape can vary widely from subject to subject and session to session for simulation and experimental data. We address this problem in our discussion of experimental data in Chapter 3. Here, we use the same approach: the response waveform at maximum stimulus intensity (or inhibition depth) and contraction strength (or motor drive) is used to create a prototype waveform for the particular session/subject; and the inner product of a trace with this prototype is treated as the response level of the trace. Thus each ensemble of simulated or recorded traces is transformed into a set of scalar numbers whose statistics can be studied as a function of different experimental parameters. We will refer to these scalars as the "response levels".

In Figure 4.33, we show the mean and the standard deviation of the response level of simulated data as a function of inhibition depth at a fixed motor drive. The upper panels show that for all subjects and sessions, the response level increases almost linearly with inhibition depth. The slopes of this relationship vary considerably, indicating that differences in MUAPr shape between subjects and sessions can influence the response growth function, even though the underlying vestibular response is identical.

The standard deviation of the response level, shown in the bottom panel is seen to not change with increase in stimulus intensity (and therefore is independent of changes in response level). In this respect, the system's behavior is similar to an independent additive noise model.

For both the mean level and the standard deviation, the units and the y-axis scale are arbitrary, because the ambiguity in the unit spike response scale factor A has not been resolved. As a result, we do not show a scale for the ordinate in these graphs and focus on relative values of the statistics at each stimulus intensity.

This figure compactly characterizes the inter-subject, inter-session variability (top panel) and the intra-session variability (bottom panel) of the stimulus growth function for simulations with carefully controlled parameters. The intra-session variability, in particular, represents a lower limit to the variability one can expect in response level measurements. In experimental

data, where a larger number of external factors can influence the response, one would expect a larger standard deviation of the response for the same mean response level.

One of these extraneous factors is the variation in motor drive. As we have seen, this factor can be estimated in experimental data using the appropriately filtered rms EMG level, allowing for the possibility of compensating for such variations in effort during clinical measurements. This is a refinement of the trace-by-trace normalization approach described in Chapter 3. In order to find out whether normalization is useful, we need to measure how much increased variability is contributed by variations in effort. To do this, we first systematically assess the effect of motor drive on simulated VEMPs in Figure 4.34. We find, as expected, that the mean response level increases with motor drive, and the relationship is close to linear. We also find that the response level becomes increasingly variable as the motor drive increases, again in an almost linear fashion over most of the motor drive values used.

The co-variation of response mean and standard deviation represents a significant departure from an additive Gaussian model of the signal, and reiterates the need for a different type of signal processing than traditional evoked potentials.

4.6 Time-varying EMG and Normalization

We have seen that we can simulate the effect of variable effort by changing the motor drive in concert with variations of the rms EMG of the experimental signal. We can repeat the process generate synthetic VEMP traces corresponding to an ensemble of experimental VEMP traces. In order to compute the motor drive parameter, we need the filtered trace EMG level with the cut-off frequency specific to the subject. We compute the trace EMG level for the experimental VEMP data in the same manner as for the EMG data: by taking the root mean square value of the samples of the trace. This method assumes that although the stimulus causes a change in the statistics of the trace samples (including the rms value), this change is negligible in comparison to the rms value of the background EMG.

A comparison of the response growth functions with fixed and variable motor drive is shown in Figure 4.35. We see that although the motor drive variations break up the neat linear growth of the response, the overall effect is minor, as emphasized by a comparison of the standard deviations (Figure 4.36). This suggests that even if the filtered trace EMG levels were to yield perfect information about the motor drive, normalizing each trace would have a minimal impact on the variability of the resulting response.

4.7 VEMP growth functions: model and experiment

We are now in a position to compare the amplitude growth function of the simulated VEMP responses with that of the experimental data. Some of the properties of the experimental VEMP have been described in Chapter 3.

Figure 4.38 is the experimental counterpart of Figure 4.37 which showed the signal mean and standard deviation for simulated data. Note that while the simulated VEMP could be studied as a function of the inhibition depth, in reality we do not have access to the putative "inhibition depth" for the subject under study. The control variable is therefore the stimulus intensity in dB, and the response growth curves (top panel) reflect not only the growth of the size of the response with the amount of inhibition, but also the presumably nonlinear relationship between stimulus level and the inhibition depth.

An examination of the growth curves in the top panel shows considerable differences between subjects and sessions. Possible sources of these differences include:

(i) Intrinsic differences in vestibular response between subjects (we assume that for a normal subject, the vestibular system remains stable across sessions, therefore this is unlikely to contribute to the inter-session differences.

(ii) Differences in the muscle-to-electrode transfer function,

(iii) Differences in the extent and rate of changes in the motor drive over the recording

(iv) Statistical noise that remains after averaging.

The bottom panel quantifies the statistical noise in response level: it shows the standard deviation in the response level across the ensemble of traces. We see that the standard deviation is independent of the stimulus intensity, but like the mean level, it varies considerably from session to session and from subject to subject. Taken together the mean and standard deviation growth curves illustrate the large differences among subjects and sessions in the size of the response, the variability of the responses and the response growth characteristics.

As we have seen, the computational model can model influences of statistical noise and motor drive variation, and to a limited extent, differences in transfer function. A comparison of simulation with variable drive (Figure 4.37) and experimental data (Figure 4.38) shows that the size of the *relative* differences in response magnitude between sessions and subjects is reflected in the simulation outputs as well.

To summarize:

- We see from simulated VEMP response levels (Figure 4.33) that there exists an almost linear relationship between the mean response level and the inhibition depth.
- This could allow us to translate an observed signal parameter (the mean response level) into a physiologically meaningful model parameter (the inhibition depth). Presumably, the inhibition depth at a given stimulus intensity is invariant from session to session and within a session, for a given subject.
- However, there are several problems:
    - The slope of the response level – inhibition depth curve changes from session to session and subject to subject, so the mapping is not universal.
    - Two ensembles recorded at different motor drive produce different mean response levels, and therefore yield different inhibition depth estimates.
    - An arbitrary and unknown scale factor A enters into the simulated traces and into the response levels. This also enters into the slope of the response level – inhibition depth relationship, and makes it difficult to translate experimentally measured response level into inhibition depth.
- We thus see that the growth curve of the measured response levels (Figure 4.38) simply reflects the variability of the experimental VEMP that we observed in Chapter 3 (Figure 3.7).
- Can we do any better?

4.8 Growth function of inverse coefficient of variation

For an ensemble of synthetic VEMP traces, we have seen in Figure 4.33 that there is considerable variation in the slope of the mean response level growth function across sessions and subjects (the growth function, for simulated data, is with respect to inhibition depth). In the same figure, we find that the growth curves with the larger slopes also appear to have larger standard deviations in the response level. This suggests that for each ensemble of traces, if the mean response level were scaled by the standard deviation, the resulting parameter would show a consistent growth with inhibition depth. This dimensionless parameter, which we call inverse coefficient of variation (iCOV), is explored in Figure 4.39.

We find the iCOV, like the mean response level, grows linearly with inhibition depth (Figure 4.39 A), but its slope is more consistent across subjects and sessions than the mean response level (Figure 4.39 B).

4.8.1 Growth of iCOV: simulation and experiment

We are naturally led to ask whether the improved consistency of iCOV over response level holds in the case of experimental data as well. Before we make this comparison, we will recapitulate the steps up to this point:

- We have been able to generate ensembles of synthetic traces using the unit surface responses for each subject and session computed from the experimentally determined autocorrelation function *of the EMG alone.*
- Each trace in the ensemble is computed using a fixed **inhibition depth**, which is a measure of the magnitude of the internal vestibular response to the stimulus
- For each subject, we have calculated the cutoff frequency that separates statistical noise and effort variation effects in the rms EMG. We use this cutoff to filter the EMG and compute the motor drive profile for each experimental recording.
- Each trace in the synthetic ensemble is simulated using a **motor drive** value computed from the filtered EMG of corresponding experimental data.
- Thus, for each ensemble of experimental traces, we can create an ensemble of synthetic traces with a specified inhibition depth. All the simulated ensembles have the same muscle model (i.e. identical numbers of motor units, with identically distributed properties), and the same inhibition profile. The simulated ensembles differ from each other in the **MUAPr waveform shape** (which is designed to be

specific to the subject and session, but is not uniquely determined), and in the time-course of the motor drive (which is derived from the rms **trace EMG level** of the particular experimental recording).

- For a simulated or experimental ensemble, we can calculate the match-filter signal amplitude for each trace, and obtain the sequence of scalar **response levels**. In order to do this, we compute the inner product with a prototype response waveform obtained at maximum stimulus intensity or maximum inhibition depth.
- We can compute the mean and standard deviation of the response levels for each ensemble. The ratio of the mean to standard deviation is the dimensionless **inverse coefficient of variation (iCOV)**. Since the iCOV is dimensionless, we can compare the experimental and simulated ensembles without concern for the ambiguity due to the unit response size A.

Figure 4.40 A shows the growth function of the response level with stimulus level (for the experimental data, top panel), and with inhibition depth (for simulation data, in the bottom panel). The experimental data in each instance is recorded with "maximum" contraction effort. After scaling these response level measurements by the standard deviations, we obtain the iCOV plots in Figure 4.40 B.

For simulated data, we find, as before, that the linear relationship between the iCOV and inhibition depth is much more consistent. For experimental data, the iCOV values and the relationship between iCOV and stimulus intensity are seen to be dramatically different for different subjects. It also appears that the inter-session differences are smaller for iCOV than for the response level – this is a point we will explore further in the next section.

Finally, we see that the y-axis for both the plots in Figure 4.40 B represents the same dimensionless quantity. Therefore, the relationship between iCOV and inhibition depth found for the simulated data can be applied directly to the iCOV computed for experimental data.

We are thus in a position to address the question posed at the end of Section 4.7: From each experimental measurement, can we find a parameter that is better than the mean response level in computing the (presumed) inhibition depth? The iCOV promises to be such a parameter.

4.9 Estimating inhibition depth

In order to translate the iCOV into inhibition depth, we use the simulation results to relate the two quantities. This is shown in Figure 4.41, where all the pairs of iCOV and D values

are indicated. A linear regression between the iCOV and inhibition depth yields a slope of 5.397 with a 95% confidence interval of +/- 0.1.

We can apply this relationship to experimental data, and associate an inhibition depth value to each ensemble of recorded traces. It should be remembered that this value is a parameter of the conceptual model of VEMP generation, and not an independently measurable physiological entity; nevertheless, we will continue to refer to it in the context of experimental measurements as the "inhibition depth", and omit the qualifiers "putative" or "presumed".

Our procedure for processing an ensemble of traces therefore becomes:

- Compute the prototype response from the average of traces obtained at maximum voluntary contraction and maximum stimulus intensity.
- For every trace in the current ensemble, compute the inner product with the prototype. The ensemble of traces is now reduced to a sequence of real numbers.
- Find the ratio of the mean and standard deviation of each sequence. This is the iCOV.
- Convert the iCOV into inhibition depth using the fixed slope (~5.4) of the straight-line fit to the iCOV vs. inhibition depth found from the simulated data.

When we apply this procedure to ensembles of traces recorded at different stimulus intensities, we obtain the growth characteristic of the inhibition depth.

Although our experimental pool consists of "normal" subjects, we are not guaranteed that their growth characteristics are identical – there is little normative data on the variability of saccular sensitivity, and its growth characteristic outside of VEMP literature. Therefore we should not be surprised at inter-subject differences in the inhibition depth.

However, there is no evidence that a non-pathological vestibular system is particularly labile over intervals of weeks or months. Therefore our experiment design, with reproducible recording procedures and small inter-session intervals leads us to expect that the inhibition depth remains stable across sessions. Along similar lines, we also expect that repeated recordings within a session, and sub-ensembles of traces within a recording, correspond to identical inhibition depths. Finally, we should expect that if the estimation procedure is sufficiently robust, recordings made with different degrees of contraction effort produce similar inhibition depth estimates.

These are properties that traditional measures of VEMP response magnitude such as peak-to-peak amplitude do not possess: in many instances, the inter -session and intra-session variability of these measures overwhelm the systematic differences that might exist between different stimulus levels, and therefore obscure any differences in growth characteristic

between subjects. We have also seen the dependence of the response size on contraction effort variations.

We are now in a position to test whether our inhibition depth estimation procedure offers an improvement over traditional response size estimates. Our metric for the comparison is the ability of the measures to distinguish VEMP responses to different stimulus intensities. We do this by measuring the mean and the dispersion (standard deviation) of the two estimates on the body of experimental data we have obtained.

4.10 Inhibition depth growth characteristics

We measure the reproducibility of inhibition depth estimates for experimental data as follows:

For each stimulus level, we have recorded ensembles of approximately 500 consecutive traces. We break these into 3 sub-ensembles containing about 160 traces each.

We have performed three recordings at each stimulus intensity, two recordings with the subject maintaining maximum contraction effort, and one at a "moderate" effort.

The above recordings are repeated over 4 independent sessions for each subject.

Therefore, for each subject we have 36 ensembles of 160 traces each, at every stimulus intensity. As we have discussed earlier, these 36 ensembles are presumed to correspond to the same underlying inhibition depth. We can therefore examine the spread of the 36 inhibition depth estimates.

For comparison, we choose a traditional response level estimate (in the form of the peak-to-peak value within the region of expected response) for each of the 36 VEMP averages.

Figure 4.42 through Figure 4.46 show the VEMP average waveforms and a comparison of the resulting growth characteristics using both measures[1]. Figure 4.47 shows the growth curves from all subjects along with the 1-sd error bars.

4.11 Discussion

The goal in this study was to characterize the variability of the VEMP and find ways to derive from conventional VEMP measurements a reliable and clinically meaningful measure

[1] The peak-to-peak amplitude is computed as the difference between the largest and smallest values of the VEMP average within the region of expected response (which is determined for each session/subject from the response at maximum intensity). This introduces a positive bias in the p-p amplitude values, but reduces their standard deviation.

of vestibular function. We approached this question by developing a model of the physiological basis for the response. We expected that if a model could be found, whose outputs reflected the observed features of experimental VEMP, one could perform tests on the model that reveal details of the relationship between internal variables (which would be unobservable in experiment) and output parameters. This is analogous to experiments using animal models, where controlled manipulations, ordinarily not possible on human subjects, are used to reveal relationships that can then be used in developing clinical tests.

4.11.1 Model limitations

Like all models, the computational model used in this study is necessarily simplified, and captures only some of the features of the human subject. These simplifications are necessary to make the model tractable, and the model design represents a compromise between physiological realism and analytical simplicity.

Since the VEMP arises from the interaction of the motor and vestibular systems, models of both systems are necessary in our study. An important feature of our model development was the decoupling of the VEMP and EMG components. By designing the motor component of the model to fit the EMG data, and the vestibular component to fit the VEMP, the modeling was greatly simplified.

The degree of detail with which the motor and vestibular systems are modeled (i.e. the number of free parameters assigned to each system) is different, and this design choice reflects certain "informed biases" that should be borne in mind when examining the results.

One bias comes from the question being addressed: Since the vestibular system in each subject was "normal", we assumed that their internal vestibular responses were identical except for the one factor, the modulation depth. This was because the modulation depth related fairly directly to VEMP amplitude, and the amplitude is clearly known to be different between normal and pathological populations. Other mechanisms of vestibular change (changes in duration, or in timing jitter) could give rise to changes in response amplitude, but the relationship is much more complicated. It is possible that in pathological ears, changes in VEMP arise from these types of changes, so one should be cautious about over-interpreting the results of the inhibition depth estimate in pathological populations.

Another source of the bias is the obvious diversity of gross anatomy among subjects. It is easy to conceive of differences in surface signals arising from differences in muscle size, neck length and conventional models of the action potential propagation and volume conduction support this notion. For this reason, a majority of free parameters were assigned to modeling the muscle-electrode transfer function. Was this model adequate? The relatively small diversity of the estimated MUAPrs in comparison with the diversity of the VEMP responses (Figure 4.29) suggests that either our MUAP estimation was over-

constrained, or that the differences arose from complicated patterns of vestibular modulation. Further study of single MUAP surface responses or of surface responses to electrical or magnetic neurostimulation could help clarify this question.

Thirdly, we assumed that the basic architecture of the muscle (the number of motor units, the recruitment pattern) is the same between subjects. Thus, the parameters describing the muscle are not free, and are not fitted to the EMG. There are sound biomechanical reasons for assuming that muscles with identical function would have similar properties. However, effects of gender, age and body type have not been considered when assigning the parameter values. It is likely, however, that the VEMP is insensitive to changes in these parameters, a property that could be verified in the future by a sensitivity analysis of the computational model.

4.11.2 Key findings

Despite the limitations discussed above, the modeling study has a yielded a set of very interesting results. We list them briefly:

We find that the components of the EMG arising from spiking noise of the motor units can be separated from the components corresponding to variations in motor drive by filtering the sequence of root-mean-square EMGs. The filter cutoff frequency is specific to each subject, and the same for all sessions from the subject.

We find that the distribution of measured EMG values is non-Gaussian. Our simulations show that at least part of the non-Gaussian nature can be attributed to variations in effort. These variations that result in EMG amplitudes being distributed as a mixture of Gaussians.

We find that a muscle model based on well-established principles of rate-recruitment (Henneman [68]) and motor unit (Clamann [53]) , produces composite spike trains whose mean and variance are equal over a wide range of motor drives.

Despite the above finding, the motor drive used in the model is best estimated using the square root of the EMG variance rather than the variance itself. This is consistent with the convention of using the rms EMG as a measure of motor effort.

Synthetic VEMP waveforms with duration and amplitude comparable to experimentally measured VEMPs can be created by inhibiting the motor unit spiking for a brief (6ms) interval. A decrease in rate of less than 15% over this interval is sufficient to replicate the amplitude of the VEMP at the maximum (90 dB HL) stimulus level used in the study.

The inner-product of the EMG trace and the subject-and-session-specific prototype waveform is a robust measure of VEMP magnitude. It correlates well with conventional measures such as peak-to-peak amplitude, and has smaller variance.

VEMP amplitude measured using this metric increases linearly with inhibition depth.

The slope of the relationship between VEMP amplitude and inhibition depth as well as the variance of the VEMP amplitude estimates change from subject to subject and session to session. The common muscle architecture, recruitment, spike statistics and modulation waveform mean that the *only* source for this variability is in the shape of the muscle-electrode transfer function. We find that slope of the VEMP-inhibition depth relationship varied within a subject by as much as 1.7-fold, and across the subject pool, by as much as 2.7-fold.

When normalized by the standard deviation of the VEMP amplitude estimates, the simulated growth curves were much more uniform, and the slopes differed at most by a factor of 1.3 across all subjects and sessions. This ratio, (which we termed iCOV) can therefore be used to recover the inhibition depth from an ensemble of VEMP amplitude measurements, regardless of subject and session.

We use the iCOV to estimate the inhibition depth of experimental data. We find that the trial-trial variability (across sessions and within sessions) of the inhibition-depth estimates for a given subject at a given stimulus intensity is much smaller than the peak-to-peak amplitude variability over the same data.

The smaller variance of the depth estimates mean that the response amplitudes at different stimulus levels differ from each other at a greater level of significance. We can compute response growth curves for the inhibition depth with much tighter confidence intervals than possible with peak-to-peak amplitude.

Within the small subject pool we were able to observe significant differences in the response growth characteristics between subjects. This suggests that using iCOV, we may be able learn more about the physiological mechanisms that translate stimuli into motor modulation, and about normal and pathological variation in the properties of these mechanisms.

4.12 Figures

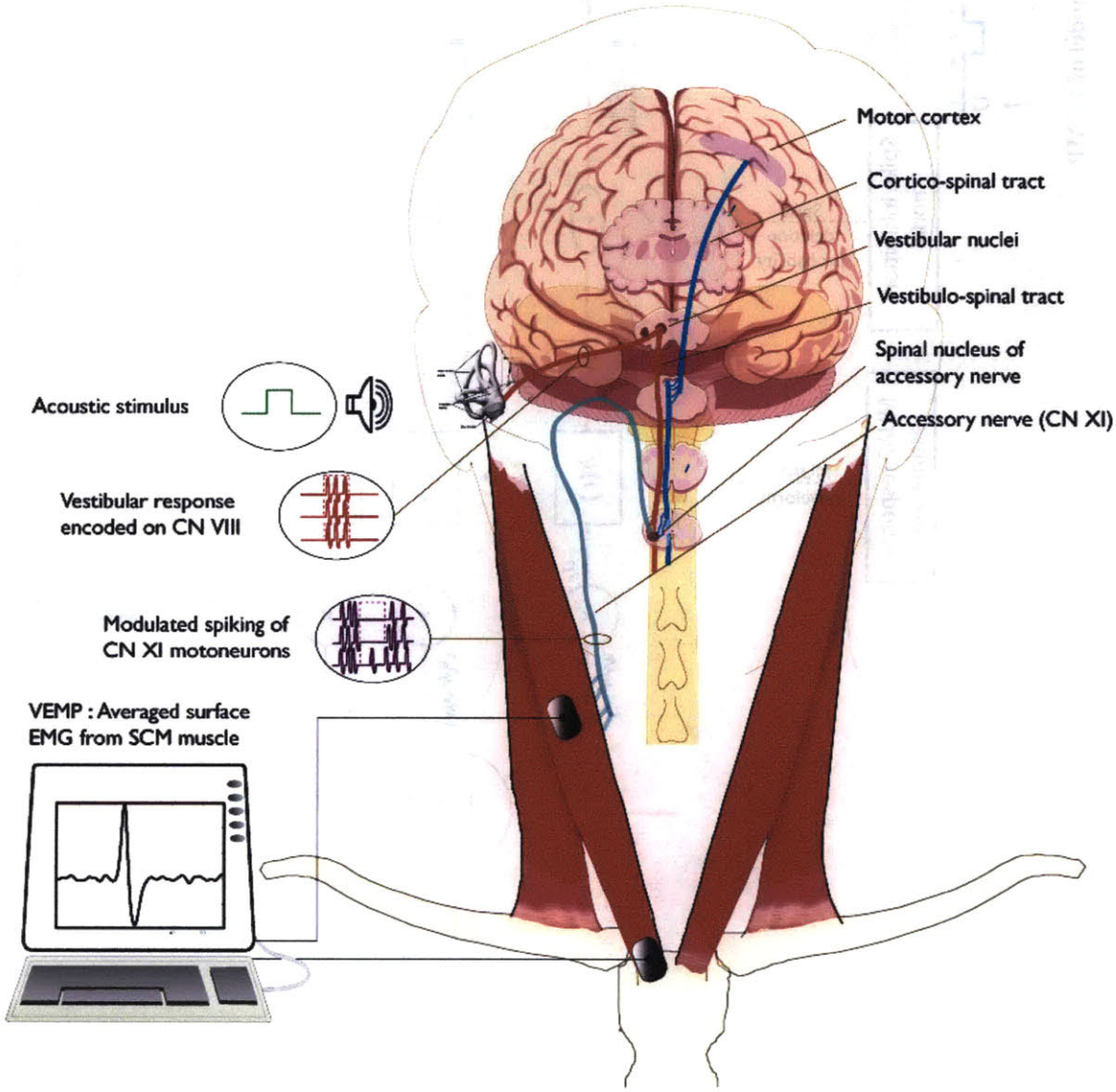

Figure 4.1 Physiological model of VEMP

Labels on the right indicate the main neuroanatomical structures underlying the VEMP reflex. Labels on the left show in schematic form some of the signals involved in generating the VEMP response

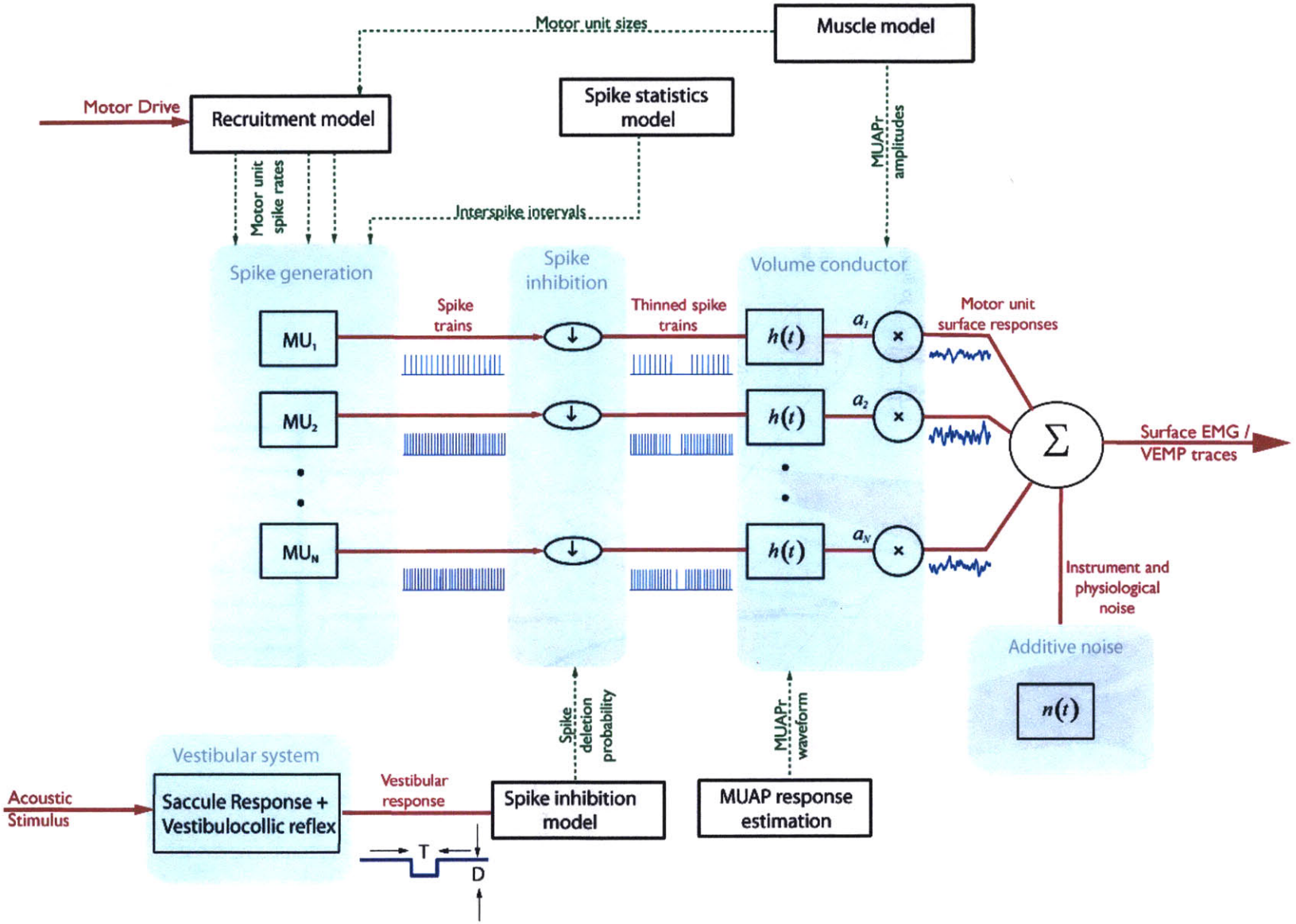

Figure 4.2 Elements of the computational model of VEMP

Fig. 4.2 (cont'd) **Elements of the computational model of VEMP** The motor drive and the vestibular response interact to form the surface EMG/VEMP output: thick red lines show the signal pathways involved. Each block in the figure is a component of the simulation program that generates the ensemble of synthetic EMG and VEMP traces. The shaded regions represent the physiological systems and processes involved in generating each surface EMG trace, while boxes outside these regions are processes that determine the parameters controlling the EMG generation; these control pathways are shown by dotted lines.

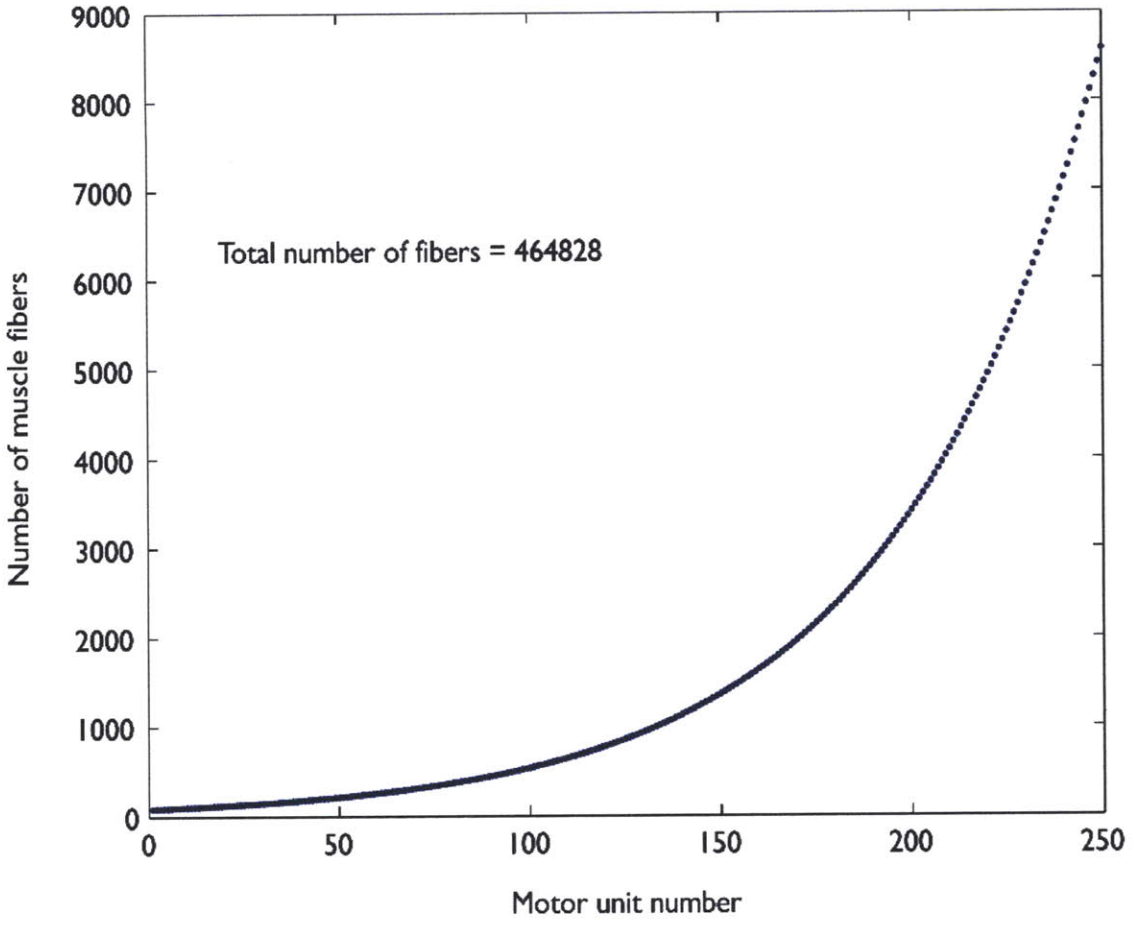

Figure 4.3 Distribution of muscle fibers among the motor units.

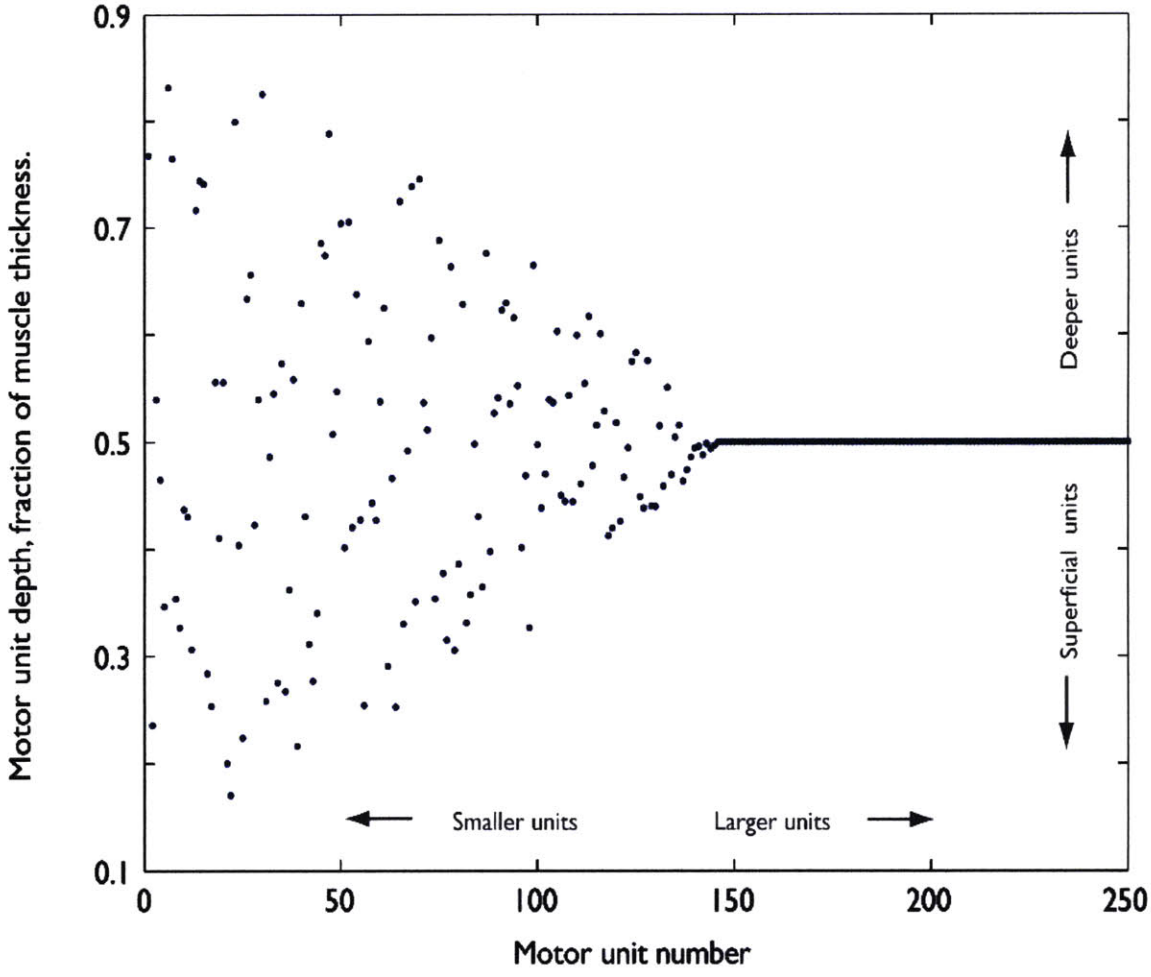

Figure 4.4 Distribution of motor unit effective depths

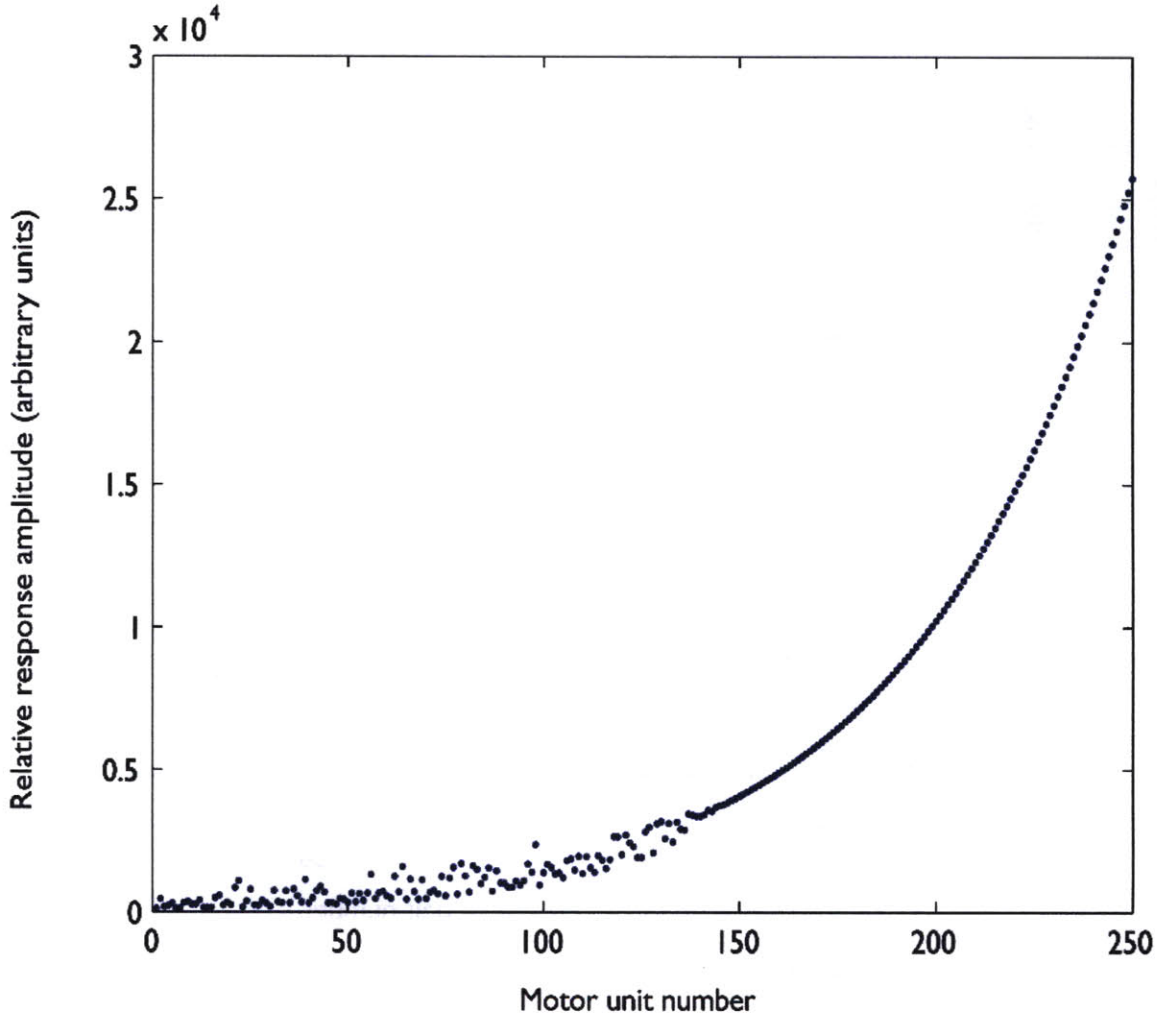

Figure 4.5 Distribution of relative sizes of the surface response from each motor unit

Based on the number of fibers in each unit and its effective depth, we can compute the size of its surface response. Since these are relative sizes, the amplitude units are arbitrary.

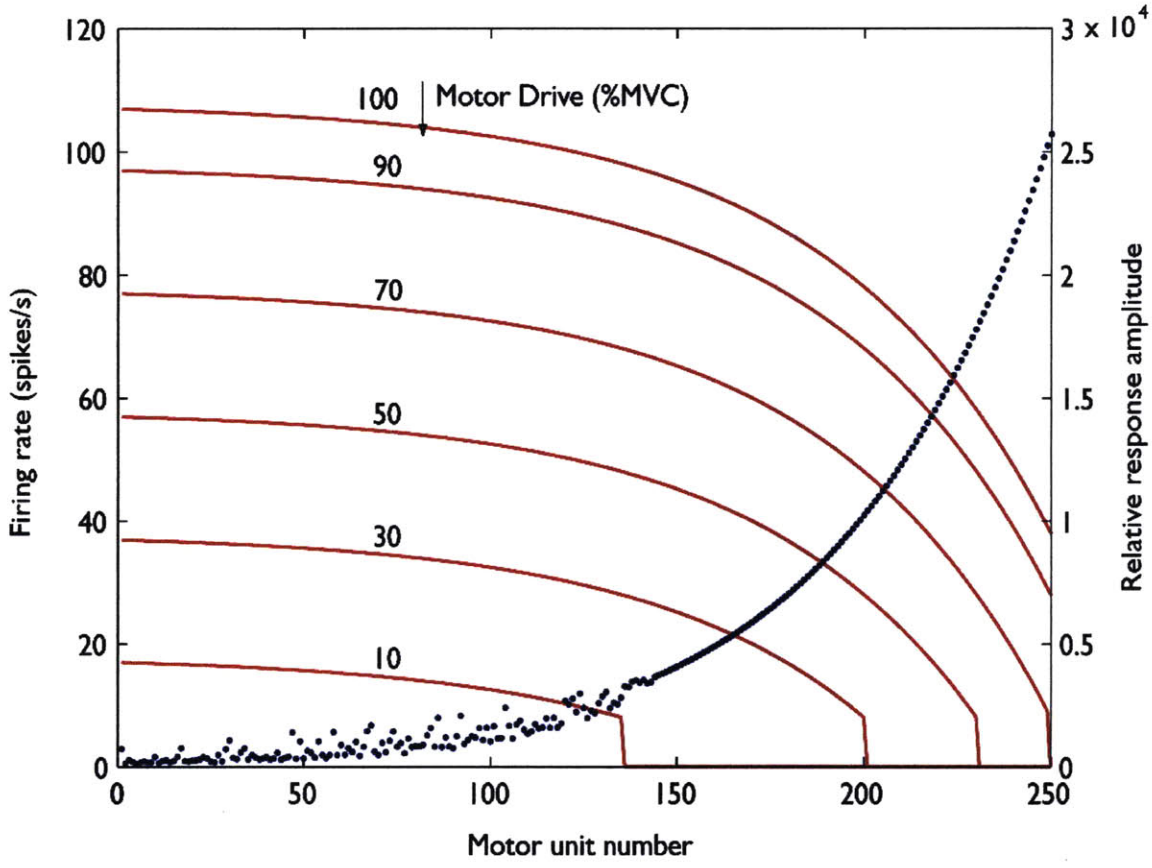

Figure 4.6 The recruitment of motor units with motor drive

This figure shows the firing rates across the motor unit pool at different amounts of motor drive (MD). The recruitment order follows Henneman's size principle: The smallest units (those with fewest fibers) are recruited first, followed by larger ones. Each unit is recruited with an initial firing rate of 8 spikes/s, and the rate increases linearly with MD. More units are progressively recruited (i.e. have a non-zero firing rate) as the motor drive increases, and at a motor drive of 70 % maximum voluntary contraction (%MVC), all units are recruited. For reference, the size of the surface response from each unit is shown in blue (the same data as Figure 4.5), showing that in our simulation, the incremental contributions to the surface EMG are recruited in a highly stereotyped order.

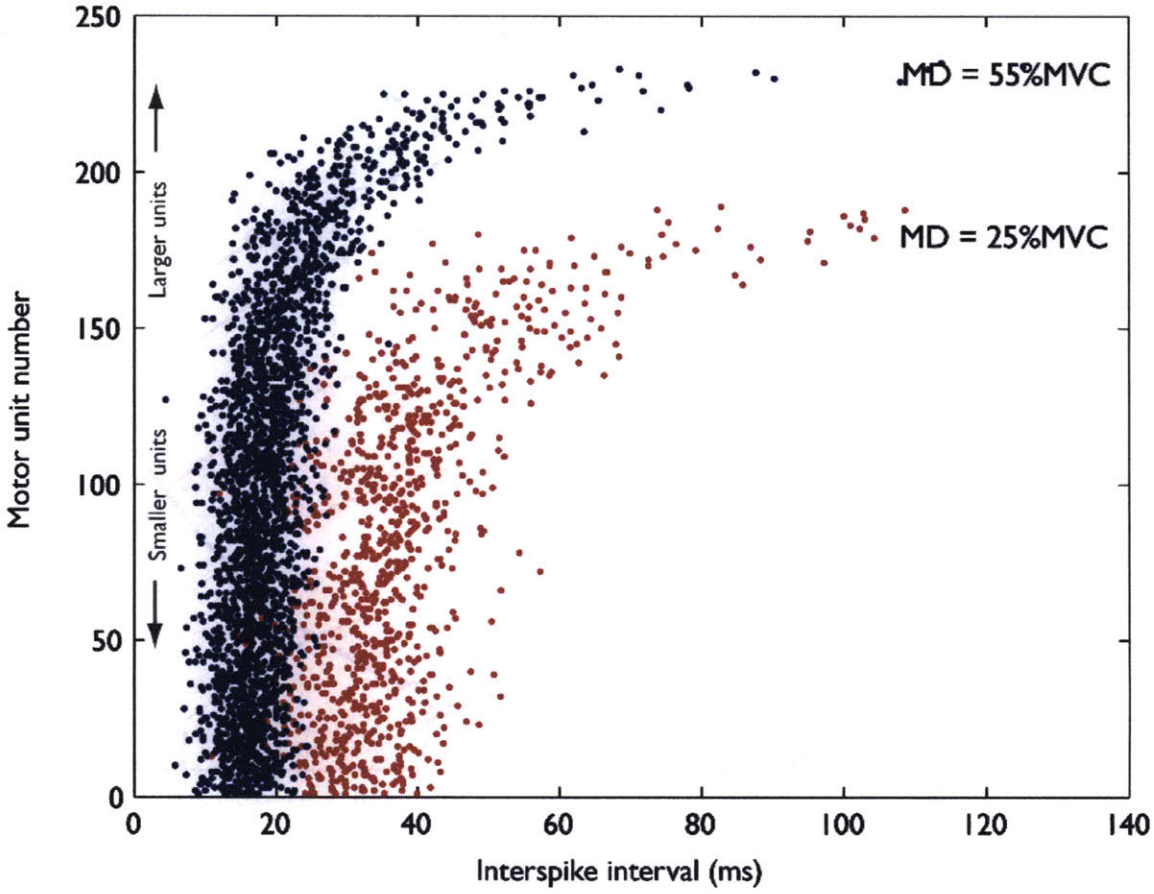

Figure 4.7 Distribution of interspike intervals

The distribution of interspike intervals (ISIs) is shown for each unit in the motor unit pool at motor drive values corresponding to two different contraction levels. Each point represents the interval between consecutive spikes, and all the intervals for a given unit constitute one row. The data are derived from one run of the model (for generating one 200ms EMG trace). Note that a lower MD results in a fewer recruited units, smaller rate (larger ISI) of each unit, and larger ISI spread.

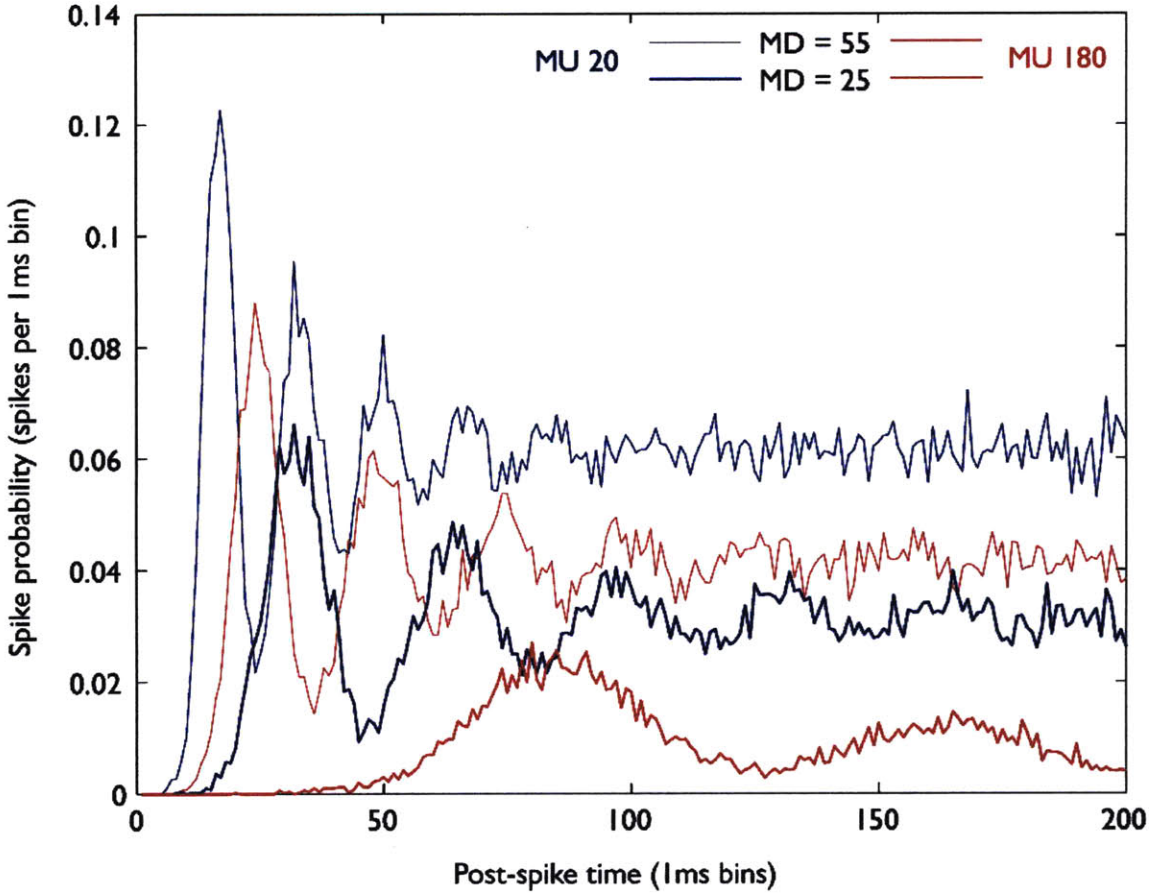

Figure 4.8 Post-spike firing probability at different motor drives

For two motor units (#20 and #180), this figure illustrates the spike-timing dependence due to the quasi-periodic nature of the motor unit firing. Each curve represents the firing probability of a given motor unit at a fixed motor drive following the occurrence of a single spike. The values are computed for 1ms bins using a spike-triggered average over 5000 independent trials. The periodicity in the spike probabilities corresponds to the mean rate of each unit at different values of the motor drive.

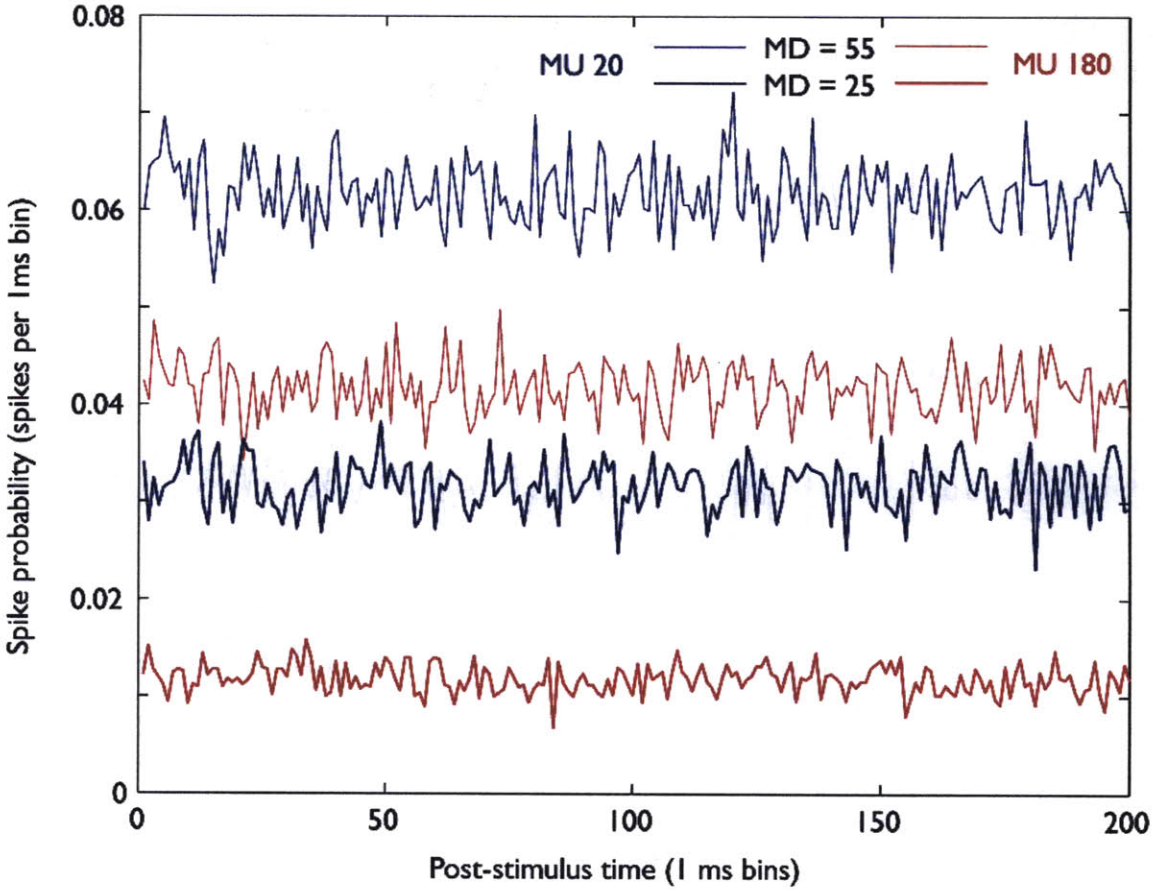

Figure 4.9 Post-stimulus firing probability vs. time

Here we look at the same data as Figure 4.8, but with the time measured from the start of the stimulus. Since the stimulus occurs independently of the spike times, the firing probability is not dependent on the time: we can see this in the absence of periodic patterns in the spike rates. This is the situation we expect in experimental data. Note that the variance in spike probability appears to increase as the mean firing rate increases.

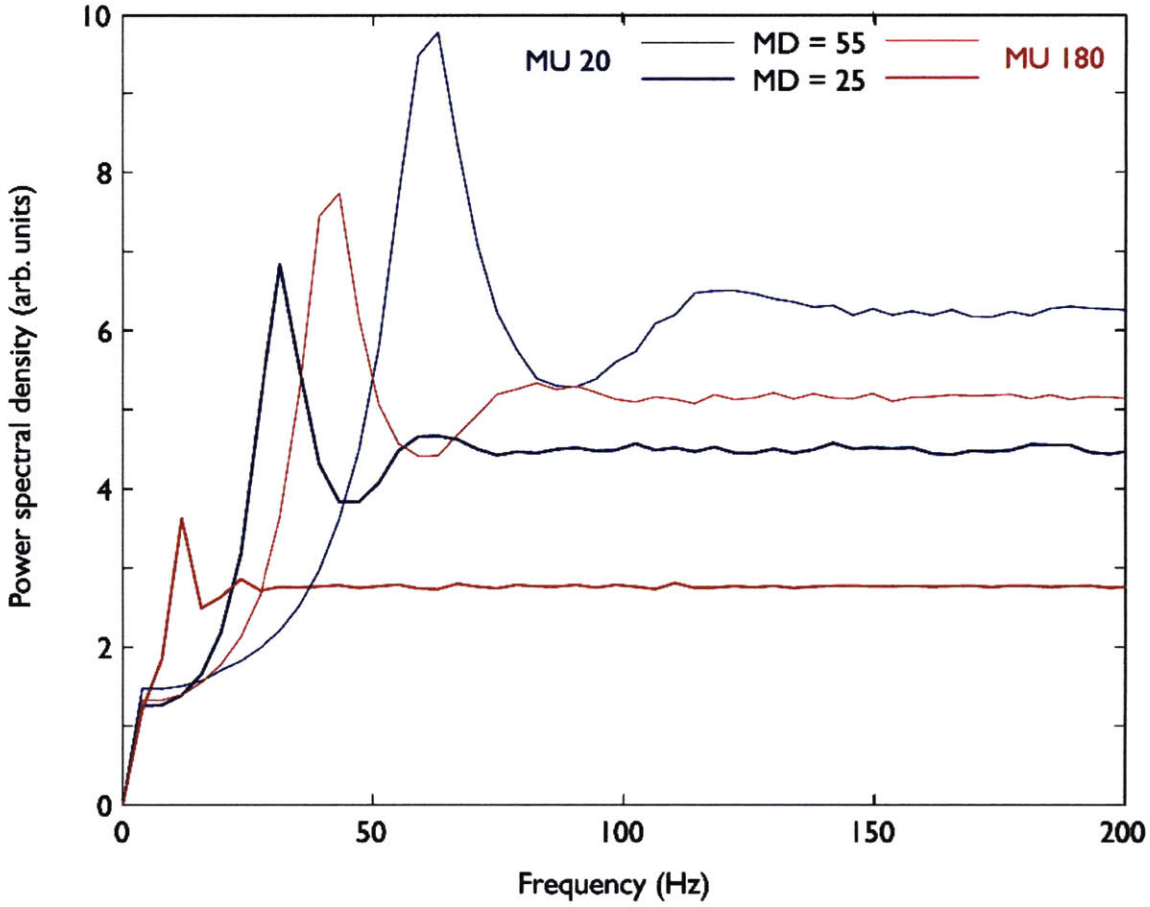

Figure 4.10 Power Spectrum of spike sequences

This figure shows the same data as Figure 4.9 in the frequency domain. We see that even though the mean post-stimulus spike rate of each unit is a constant, the correlation illustrated in Figure 4.8 is present in the spike sequences. Thus, although the spike rate is a white process at higher frequencies, it can no longer be assumed to be white at frequencies close to the mean spike rate.

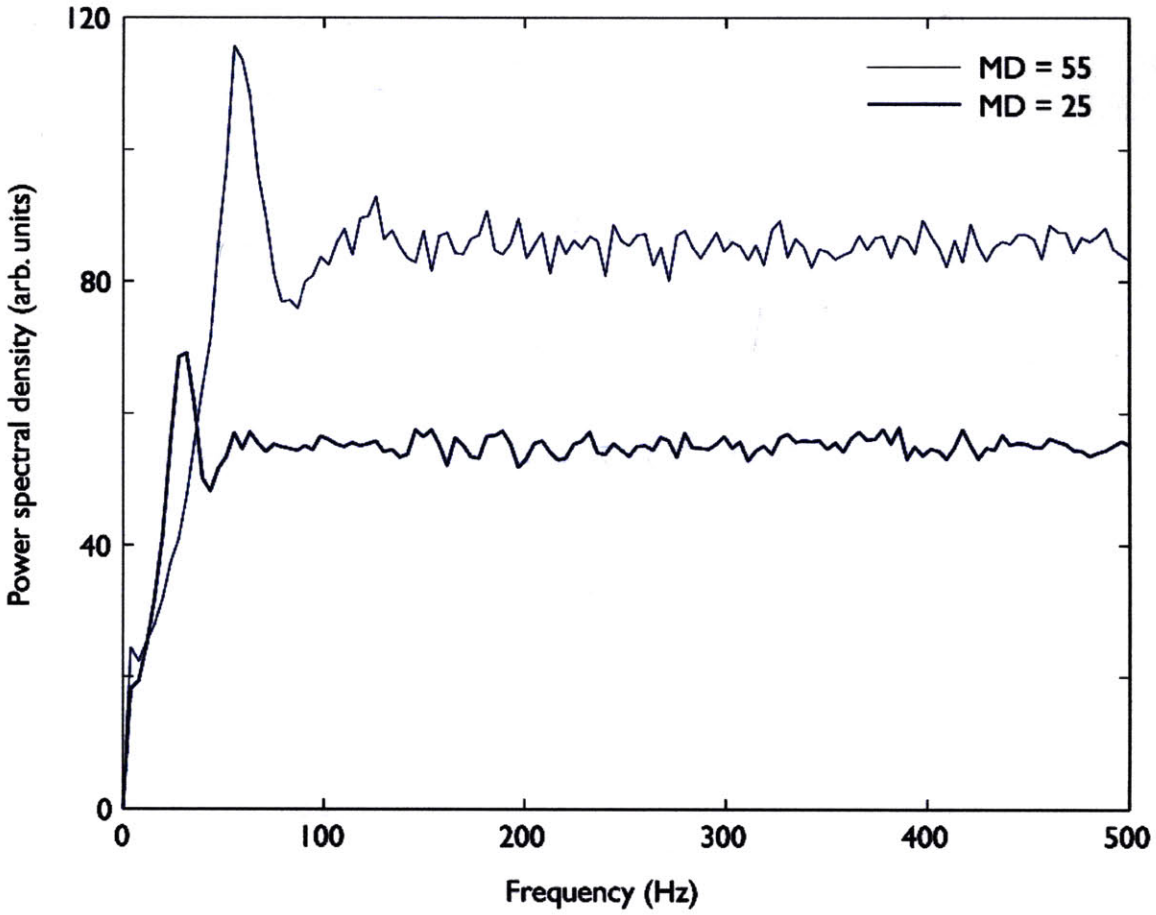

Figure 4.11 Power Spectra of the composite spiking of all 250 units

This figure shows the power spectrum of the rate sequence of the composite spiking processes from all 250 units. The units have the range of mean ISI and the ISI variance values specified by the recruitment model at motor drive MD=25 and 55 %MVC.

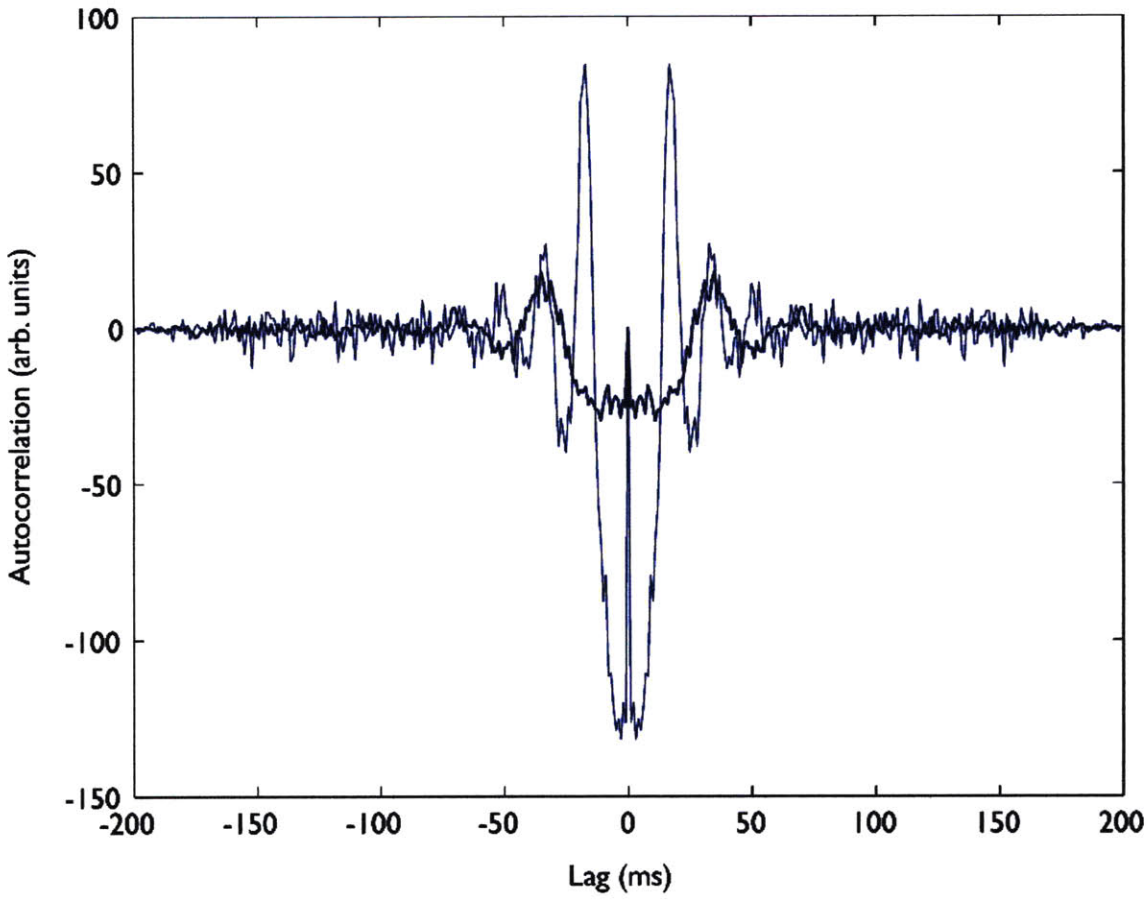

Figure 4.12 Autocorrelation sequences of the composite spike-rate processes

We show the same data as in Figure 4.11, but in the time domain, to illustrate the time range over which the spike counts are correlated. The correlation at lag 0 is set to zero for clarity.

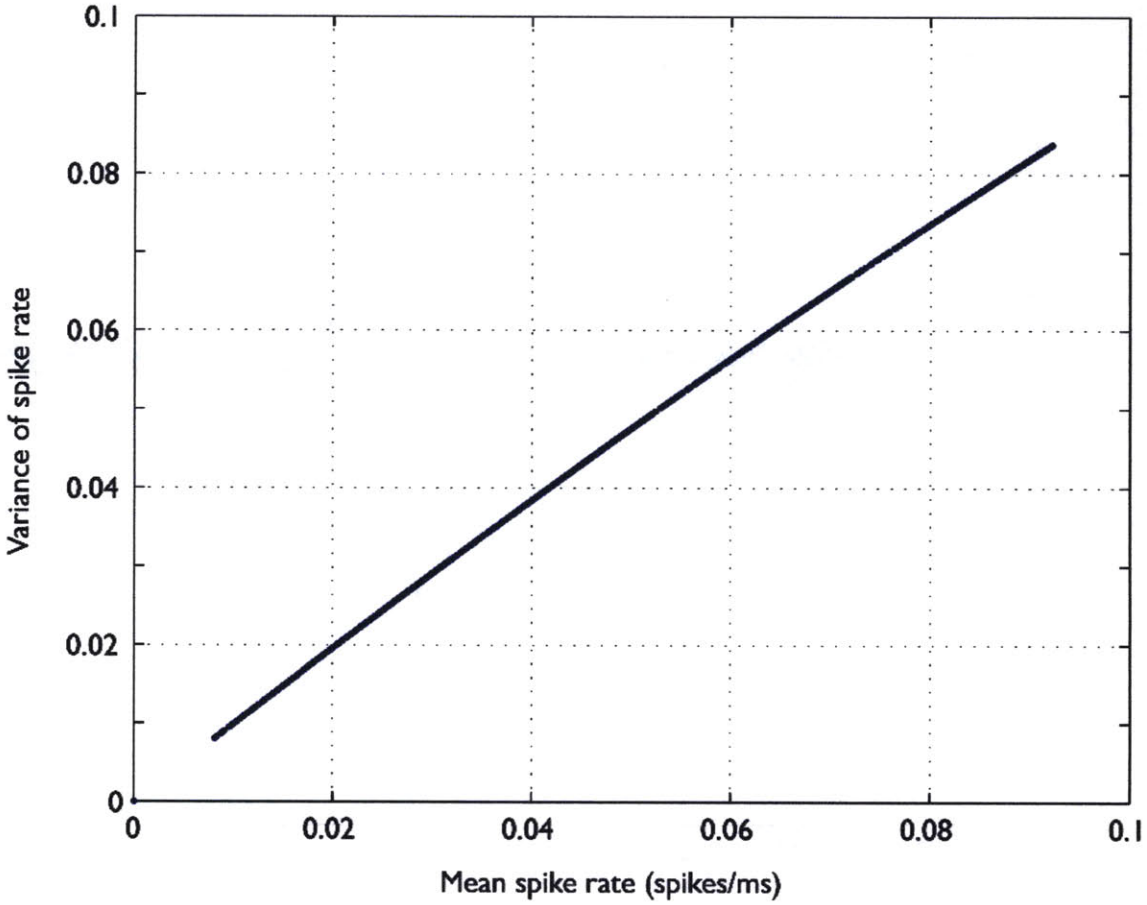

Figure 4.13 Variance vs. mean of the spike rate of different motor units

This figure shows a scatter plot of the variance and mean of the number of spikes in a 1 ms bin. The points are computed from all 250 motor units at motor drive values of 25, 45, 65 and 85 %MVC. We find a very close relationship, with the index of dispersion or Fano factor = 1 for low rates, with a small decrease at higher rates.

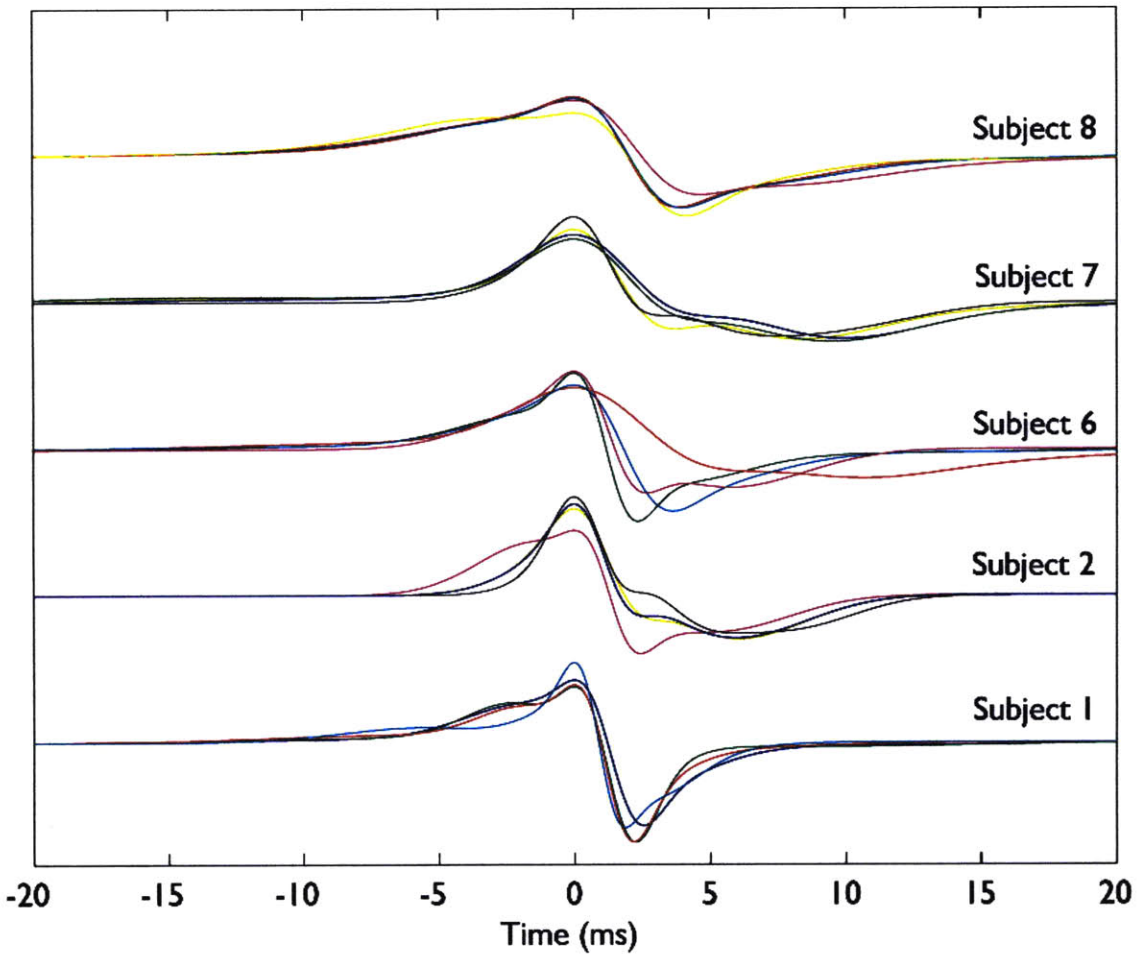

Figure 4.14 MUAPr waveforms computed for different subjects and sessions

Surface responses to single motor unit action potentials (MUAPr) waveforms are computed based on the autocorrelation of the surface EMG signals recorded from each subject/session. The figure shows the MUAPr for 4 sessions from each of 5 normal subjects.

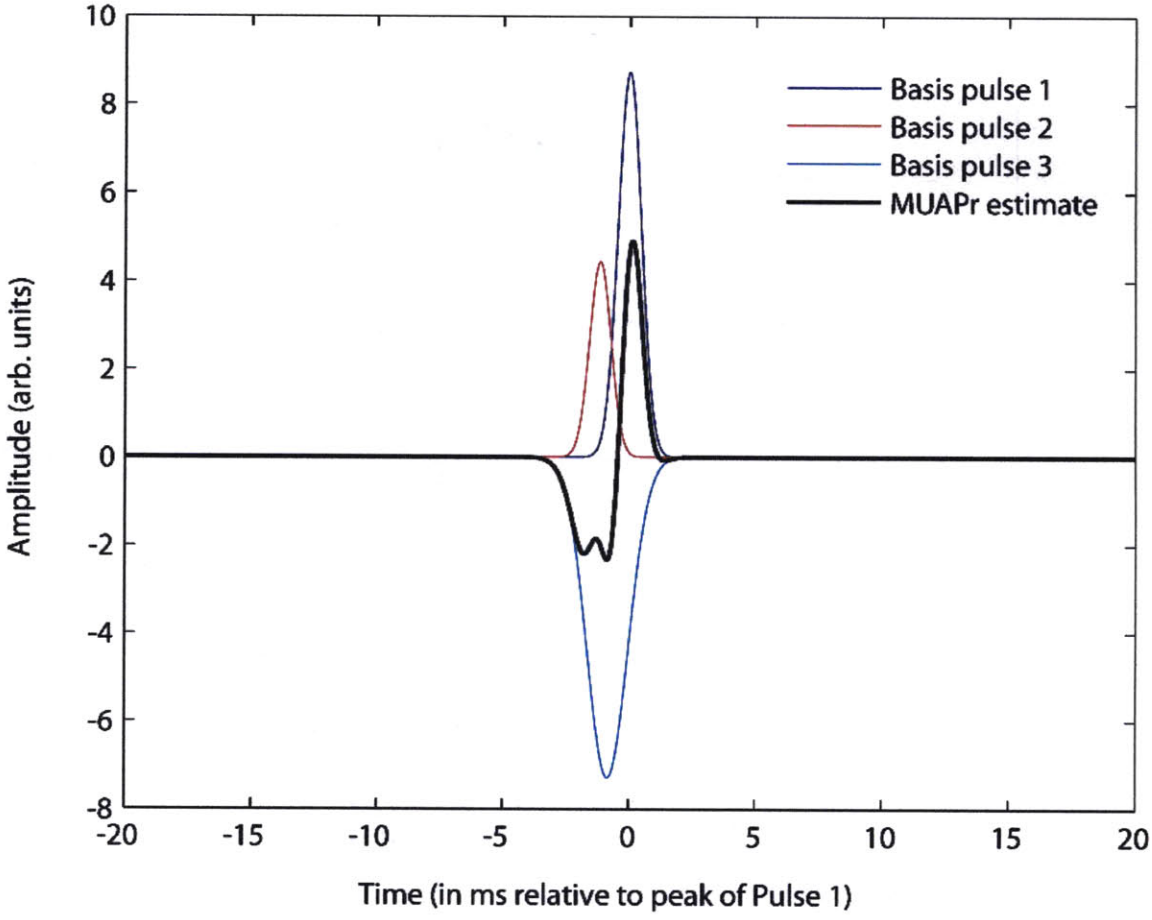

Figure 4.15 Constructing the MUAPr waveform

This figure shows the three basis functions and the unit surface response $h(t)$ constructed by adding them. The parameter values in this example are:

	Amplitude	Width	Delay
Basis 1	1	0.46	0
Basis 2	0.47	0.42	4.63 ms
Basis 3	-1.47	0.80	3.37 ms

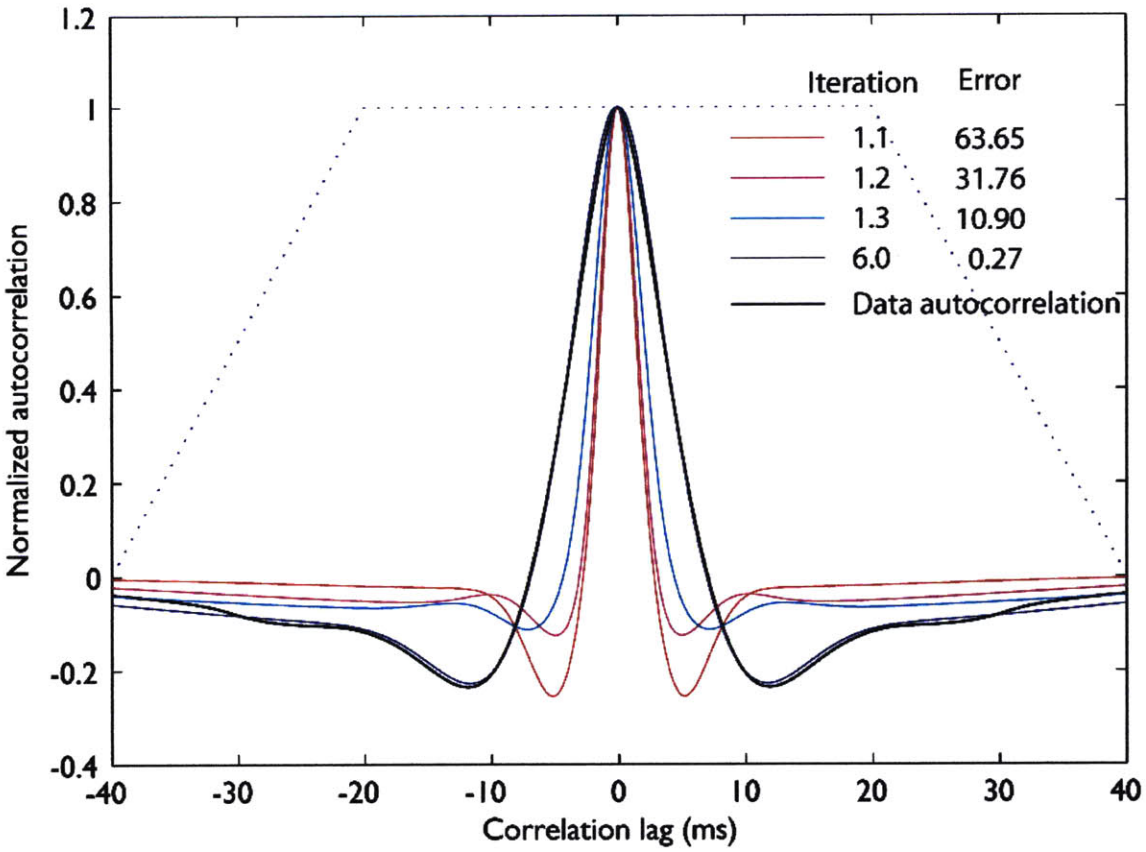

Figure 4.16 Iterative computation of the MUAPr response

This figure illustrates the iterative computation of the parameters that define the surface response $h(t)$. At each iteration, we compute the autocorrelation of the estimated $h(t)$ and measure the square error with respect to the autocorrelation of the experimental data. The error is weighted more towards smaller lags as shown by the dotted line. During each iteration, the error is minimized in 7 steps, one for each of the parameters being computed. We show the autocorrelation of the response estimate at the first 3 steps of the iteration 1 and at the end of iteration 6 to illustrate the convergence of the algorithm. This computation is shown for Subject 8 / Session 3.

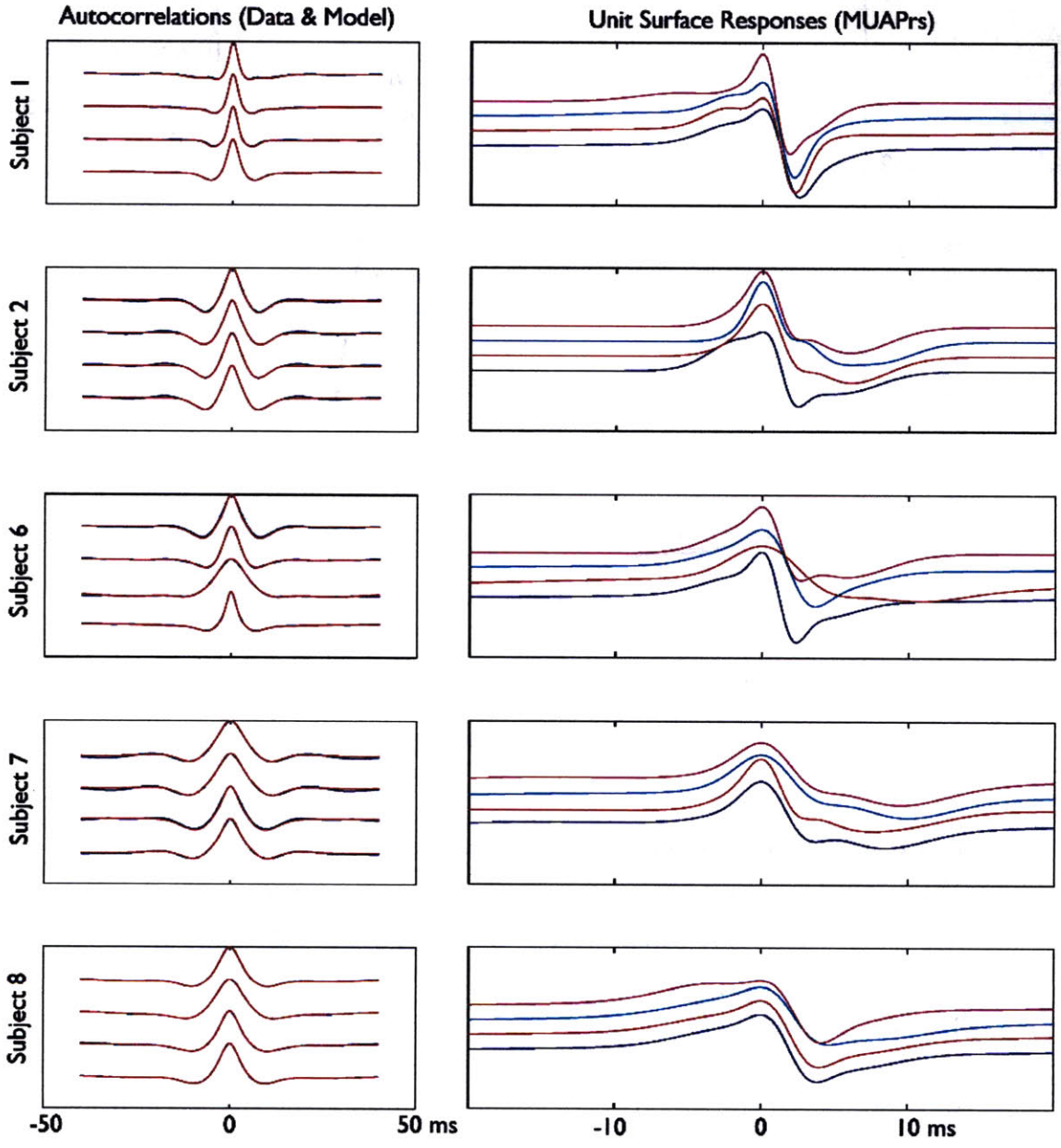

Figure 4.17 Autocorrelation functions and corresponding computed MUAPr responses, all subjects/sessions

For each subject and session, this figure shows the autocorrelation computed from the data in the left column (blue), the unit surface response $h(t)$ computed from the data autocorrelation on the right column, and the autocorrelation of $h(t)$ in red on the left column.

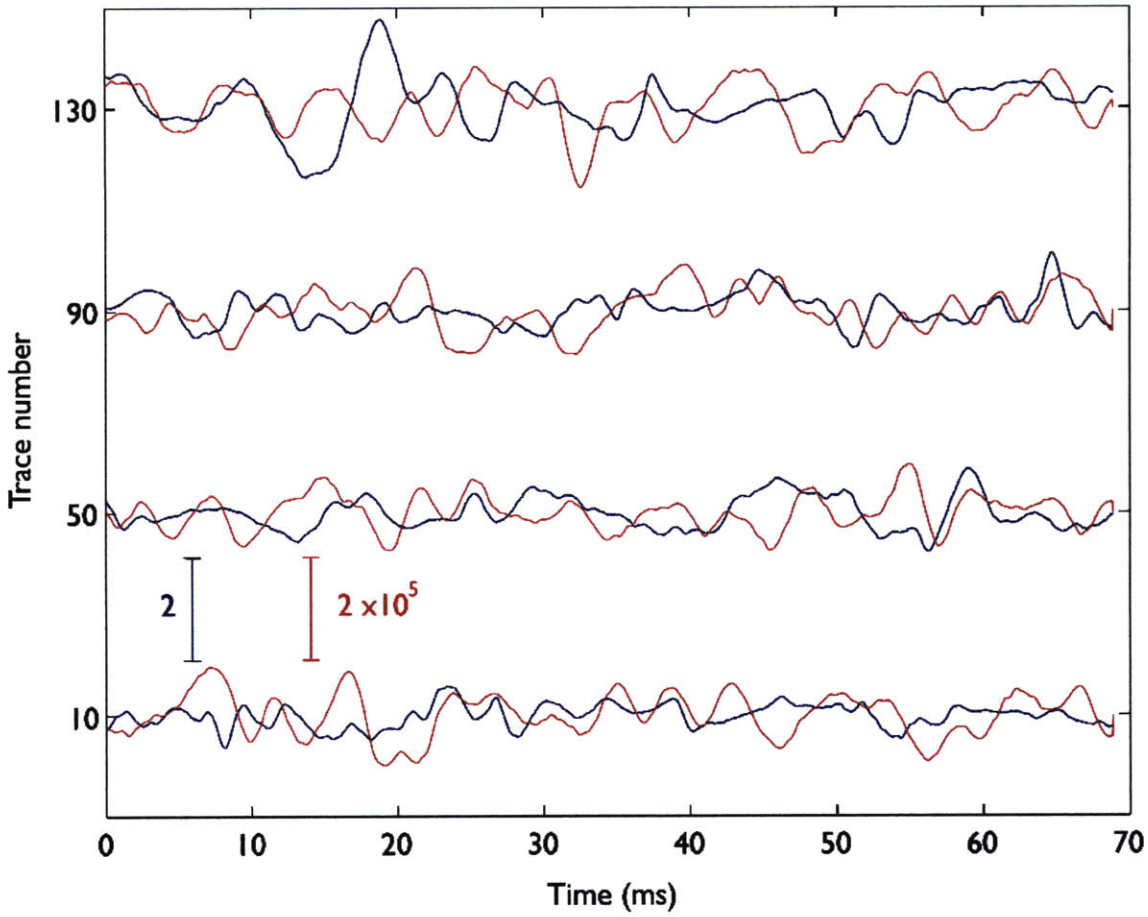

Figure 4.18 Experimental and simulated EMG traces

This figure shows a selection of 4 different experimental (blue) and simulated (red) EMG traces from Subject 1/ Session 2. The experimental data was recorded at a 70dB stimulus level in lieu of the stimulus-free condition, while the simulation was carried out at an inhibition depth of 0 and a motor drive of 55%MVC. The scale bars show the relative difference in the units between experiment and model data. When the amplitude scale factor A is established, the two sets of data should be at the same scale. This figure is chosen to visually illustrate the similarity between model and experiment.

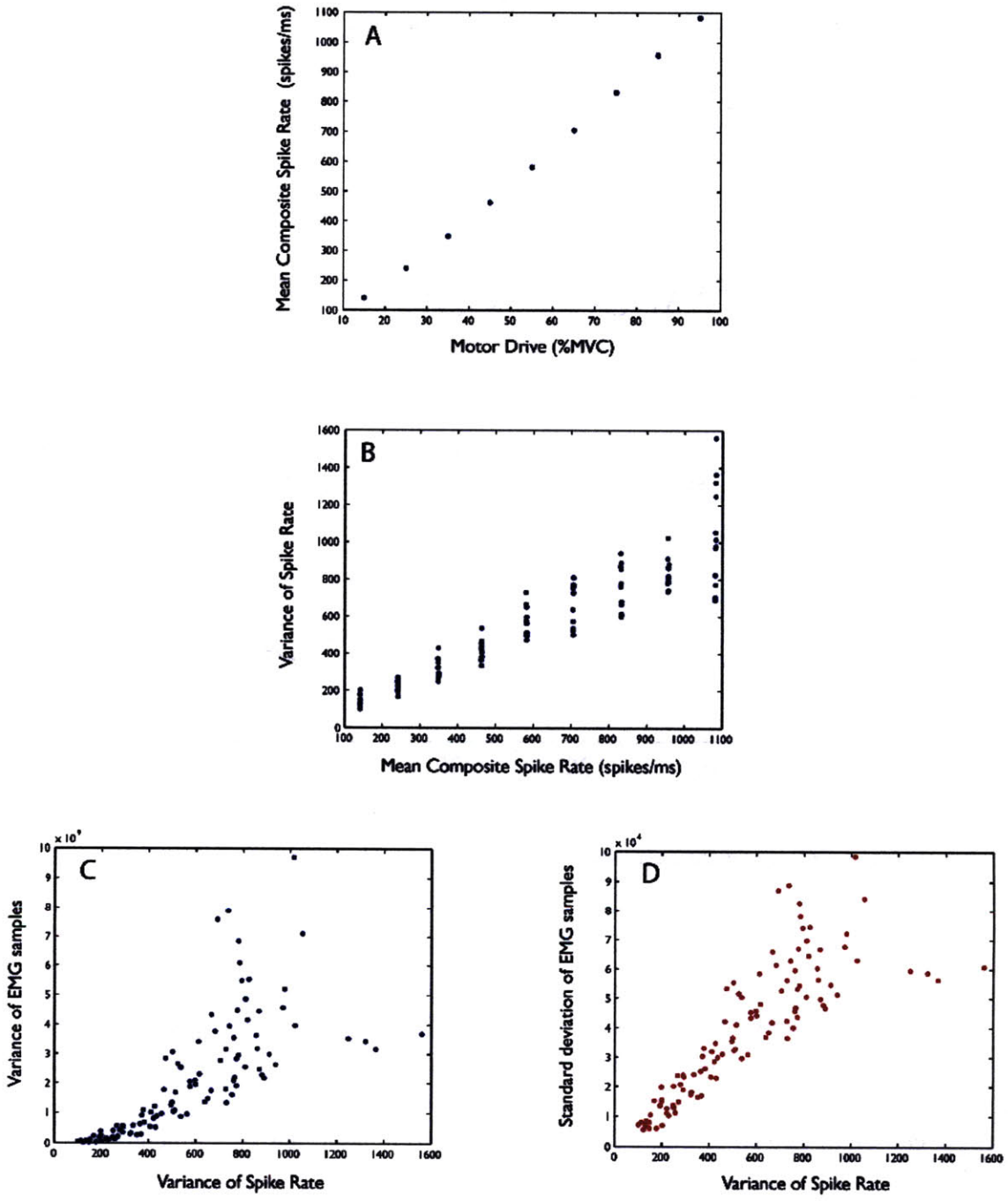

Figure 4.19 Relationships between spike statistics and EMG statistics

This sequence of scatter plots shows the relationships between statistics of simulated EMG ensembles (50 traces each) computed for different subjects/sessions at motor drive values between 15 and 95 %MVC. **A:** The mean spike rate from each ensemble is shown as a

function of the motor drive. **B**: The variance of the spike rate as a function of the mean spike rate (similar to Figure 4.13, but for the composite rate). **C**&**D**: Contrast the behavior of EMG variance and rms EMG as a function of the spike rate variance (See Section 4.4.1 for details).

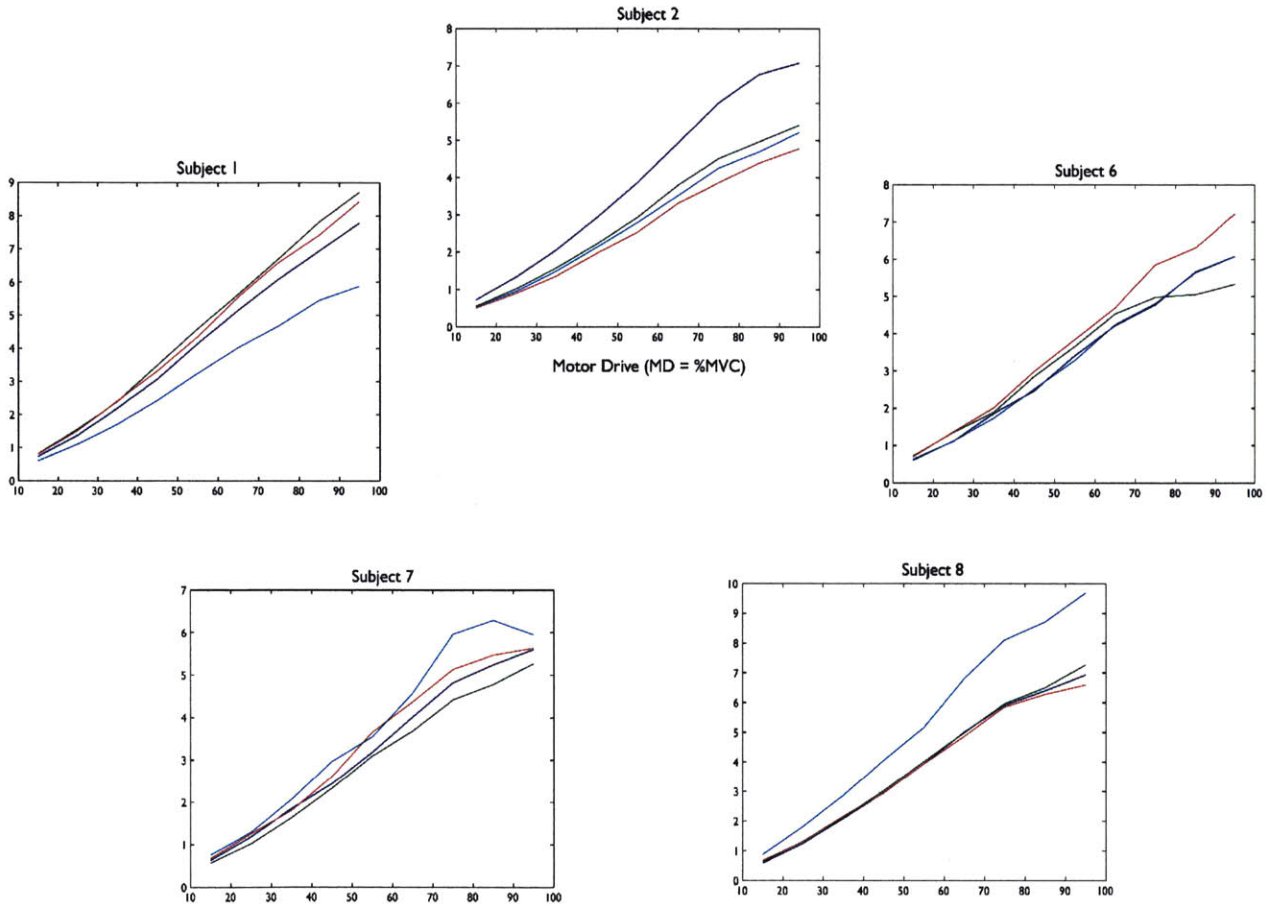

Figure 4.20 RMS EMG level of synthetic EMG as a function of motor drive

This figure shows the results of computing the rms EMG level at different values of the motor drive between 15 and 95 %MVC. Each graph shows curves for all 4 sessions of a particular subject. Note the slight differences in the y-axis scaling. The rms EMG is seen to be linearly related to the motor drive, although the slope may be different across sessions and subjects.

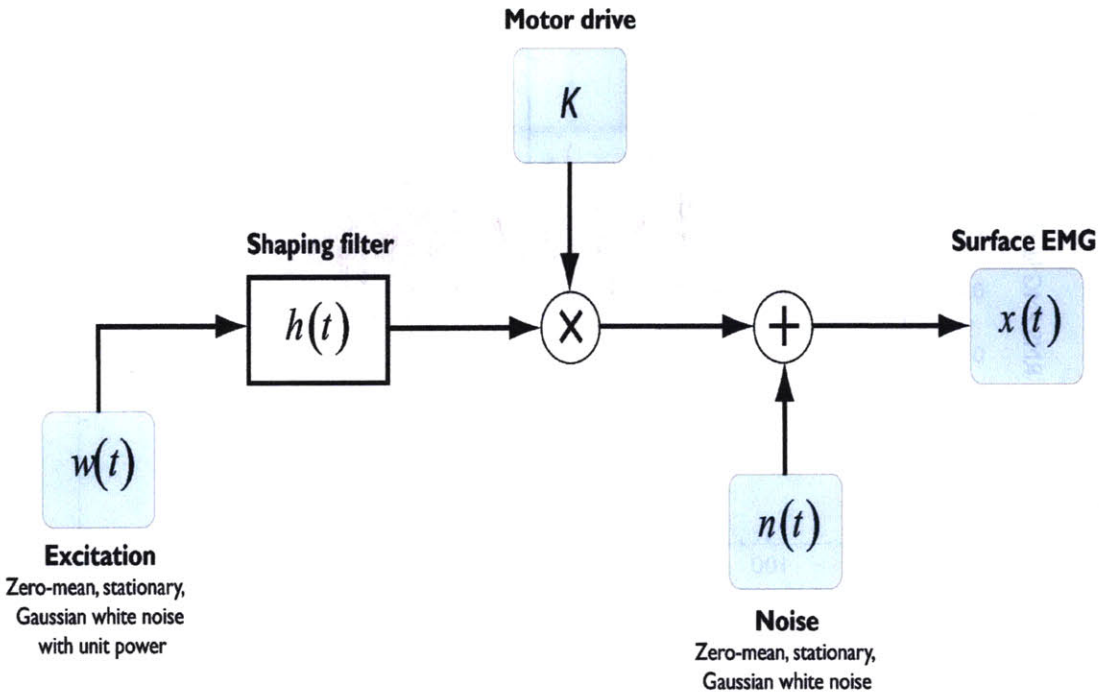

Figure 4.21 The "functional" EMG model [23, 63]: basis for rms EMG –based estimators

This figure (adapted from [63]), illustrates the signal model used in traditional motor control studies. For this model, the motor drive may be estimated from the measurements by taking the root mean square of the surface EMG.

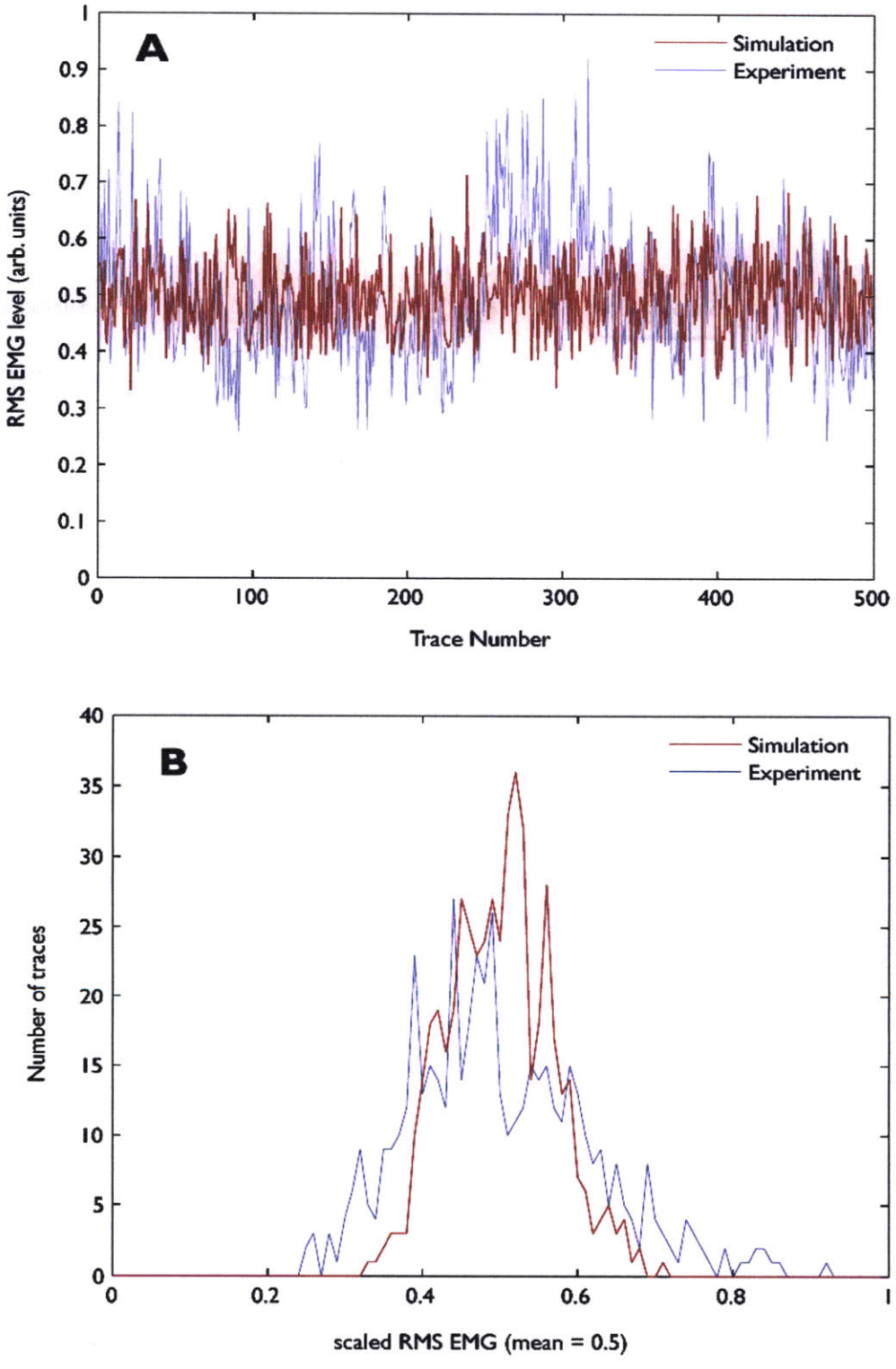

Figure 4.22 Time-course (A) and distribution (B) of the RMG EMG of 500 consecutive traces (Subject1/ Session1)

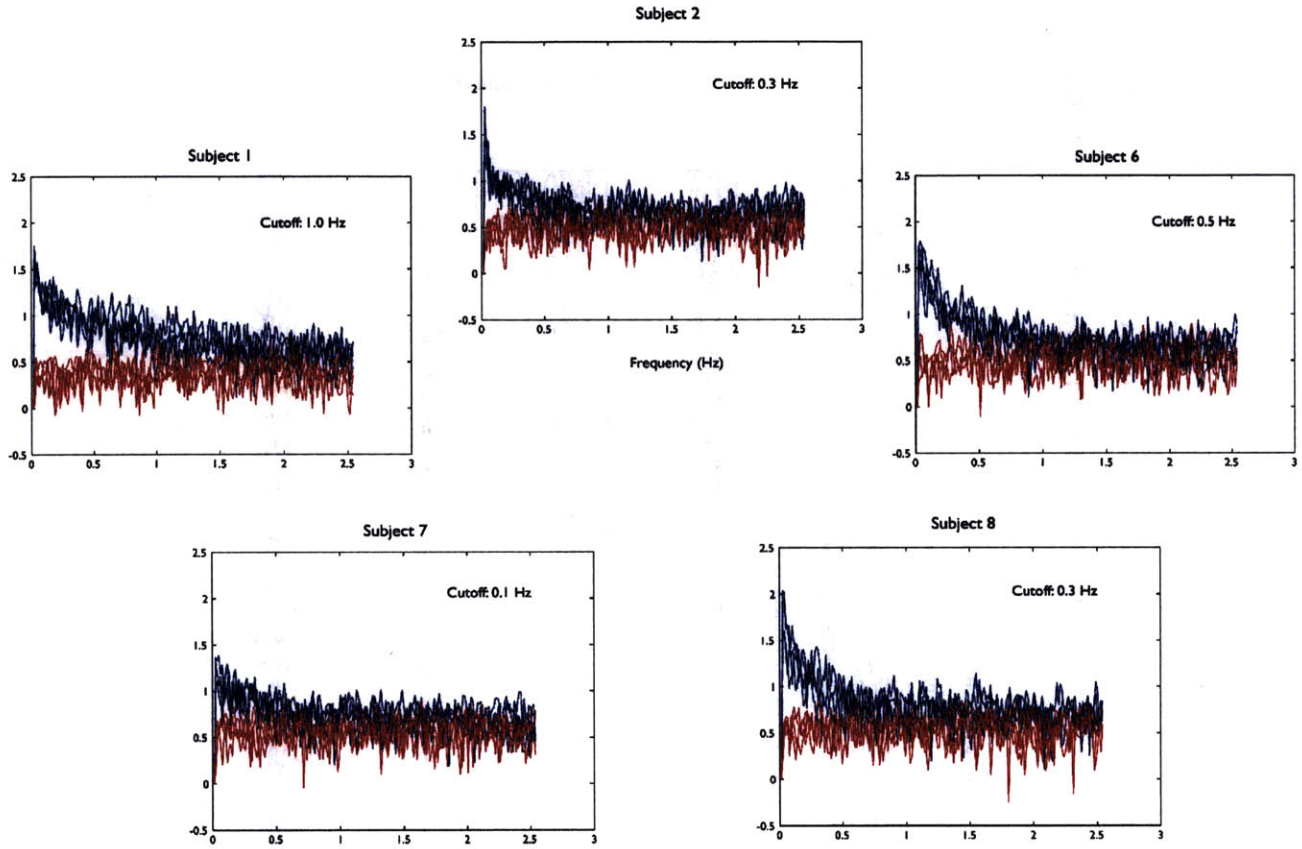

Figure 4.23 Spectra of simulated and experimental RMS EMG (low frequency region)

This figure shows the power spectra of the rms EMG sequences of all the traces for each subject. The simulated data (red) has a flat spectrum, while the experimental data (blue) shows additional components at frequencies below 1 Hz. These low-frequency components correspond to changes in motor drive, and can be extracted by low-pass filtering the rms EMG with the appropriate cutoff frequency.

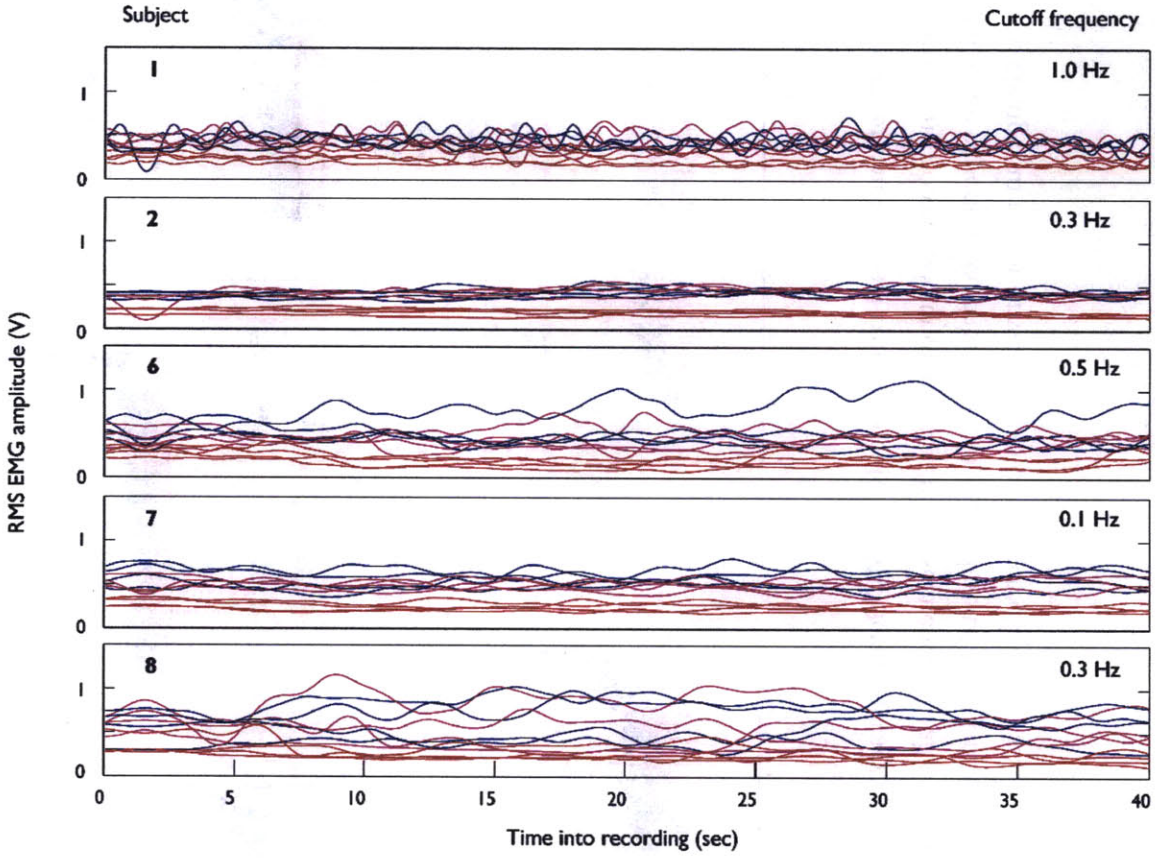

Figure 4.24 Filtered EMG levels from experimental data

Each curve shows the rms EMG level over the course of a single 40-second contraction, computed by smoothing the trace-to-trace EMGs illustrated in Figure 4.22 A. Each panel contains all the data from a particular subject recorded at a 70 dB stimulus level. The red traces show the "moderate" contraction ensemble, while the blue and cyan traces are recorded at "maximum" contraction effort. The cutoff frequency used to smooth the data is different from subject to subject, and is determined from Figure 4.23.

The fltered EMG is used as a measure of the motor drive. Note the clear differences in magnitude and variability characteristics of the motor drive across subjects.

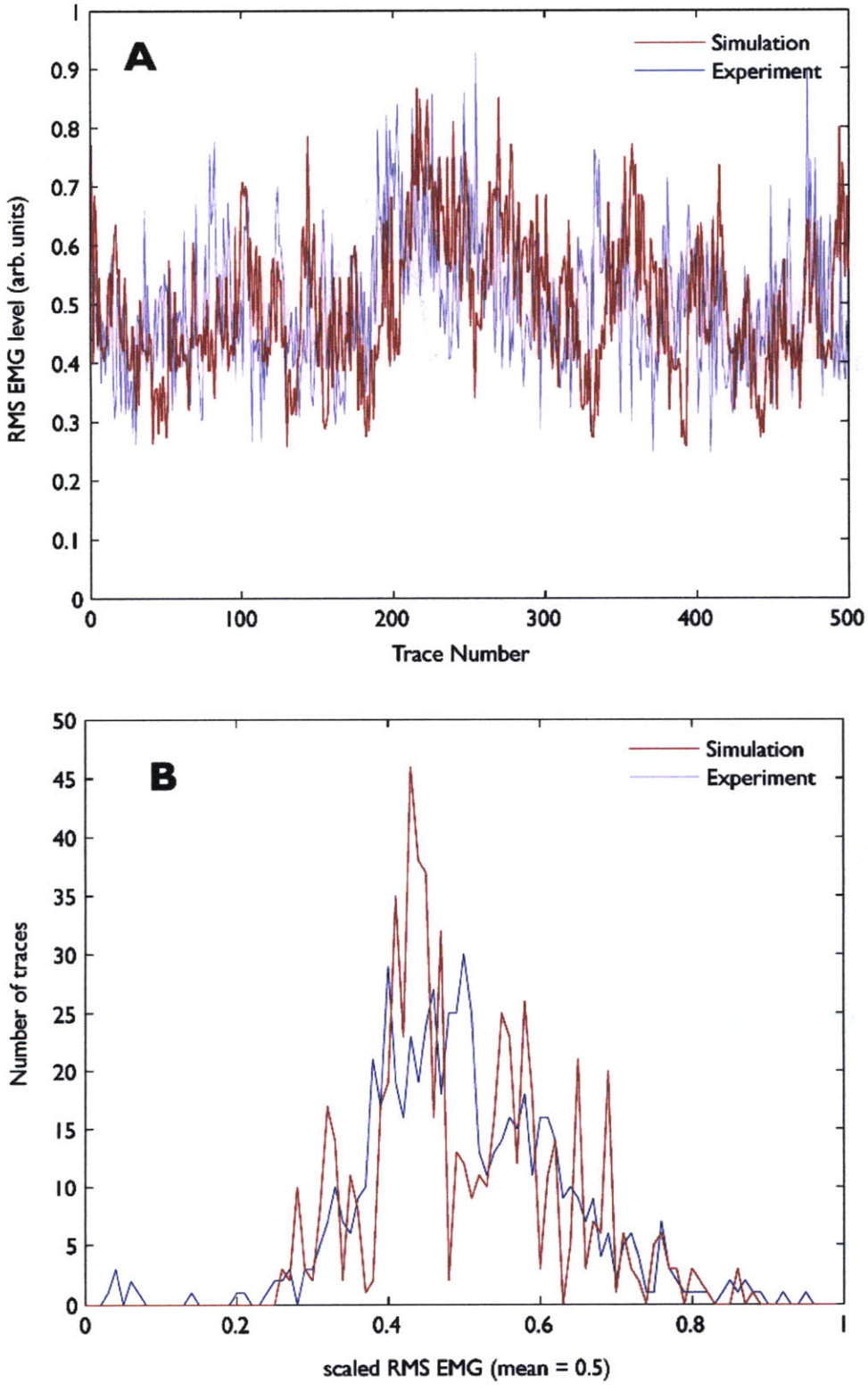

Figure 4.25 Time-course and distribution of EMG as in Figure 4.22 with variable motor drive.

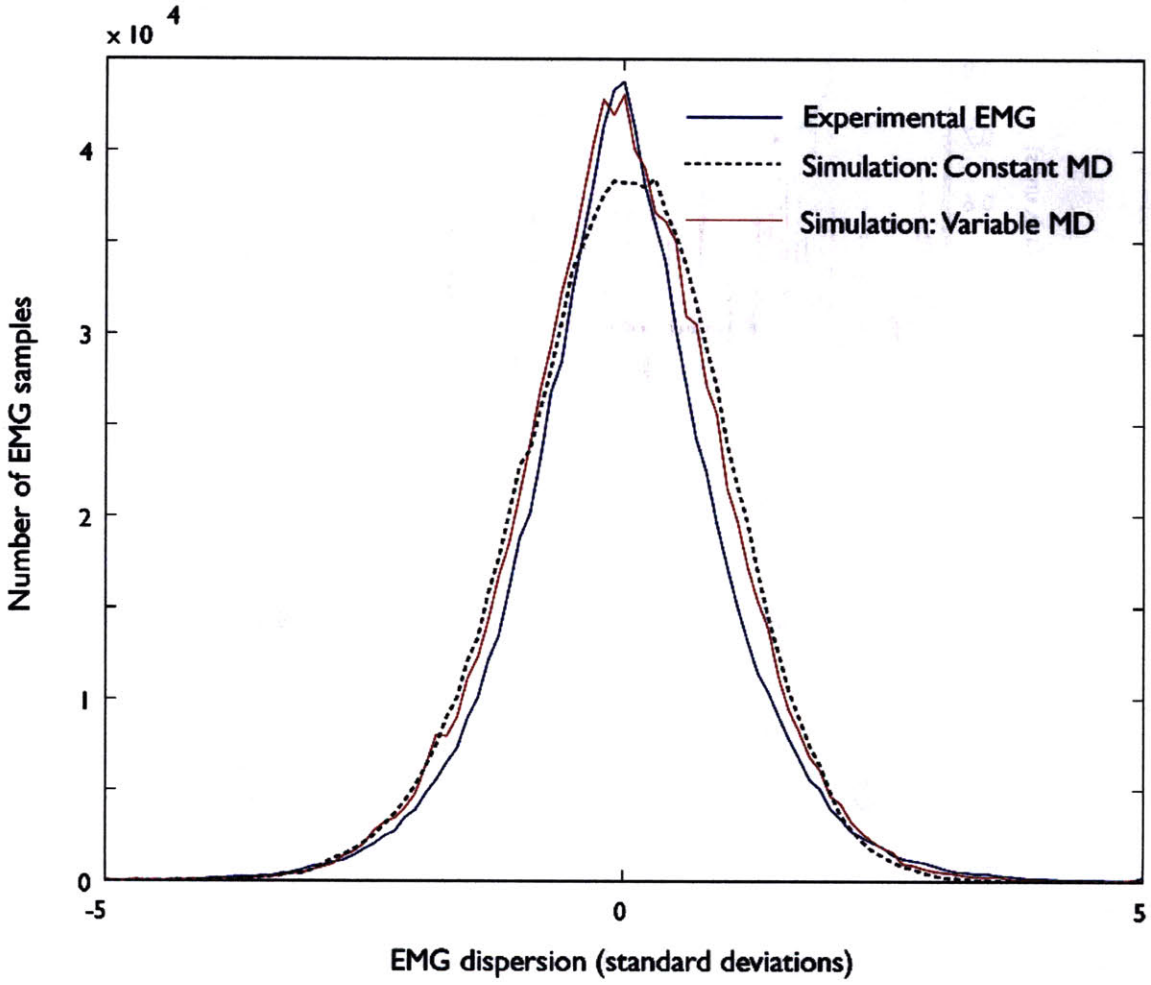

Figure 4.26 Distribution of EMG samples: Experimental + Simulated, with & without variation of motor drive.

The blue line shows the histogram of EMG samples from Subject1/Session1. The data are shifted and scaled to give zero mean and unit standard deviation. Note the sharp peak near zero. The dotted line shows the same data for simulated EMGs with constant motor drive. The distribution is seen to be more Gaussian. The red line is the simulated EMG, with motor drive varied from trace to trace as described in the text. Note the similarity of the distribution near zero to the experimental data.

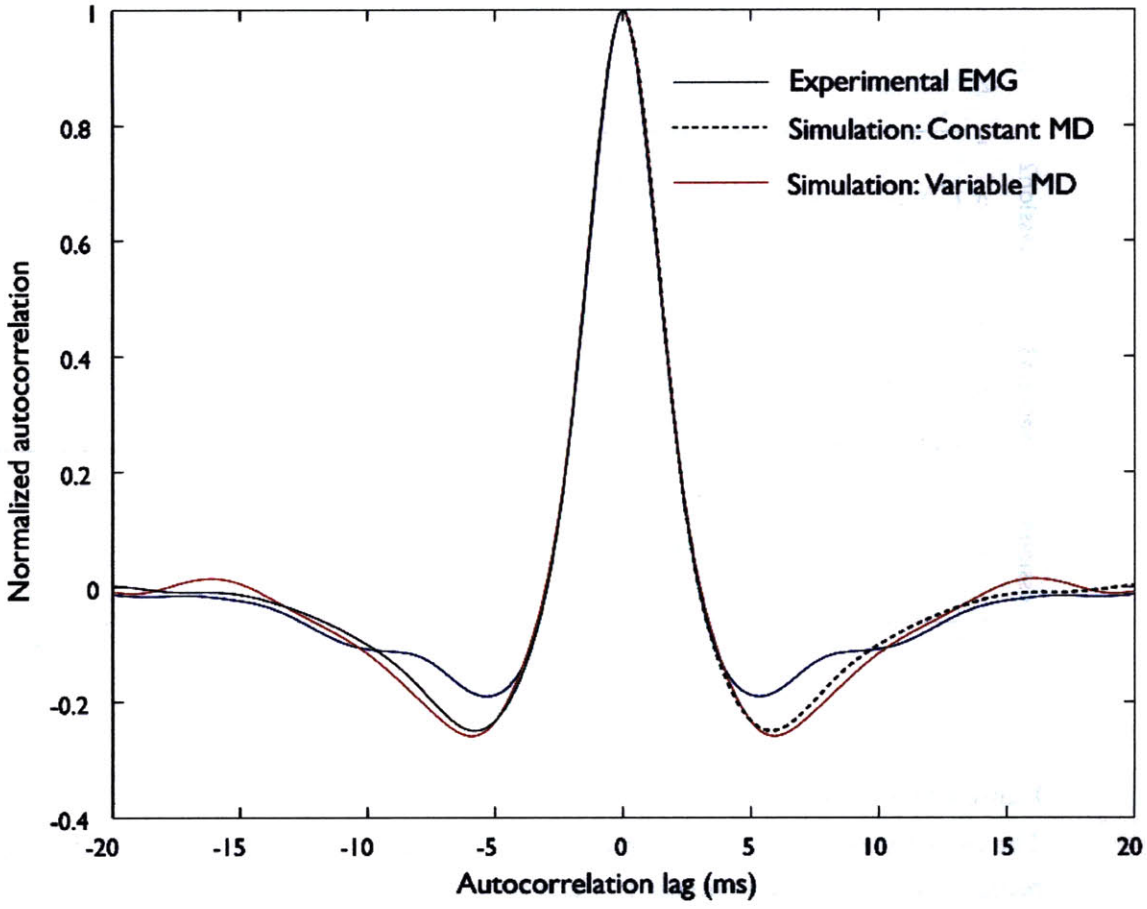

Figure 4.27 Autocorrelation of the EMG: Experimental + Simulated, with & without variation of motor drive

This figure compares the normalized autocorrelations of the experimental and simulated data. It is complementary to the comparison of distributions shown in Figure 4.26: this figure compares time-series statistics.

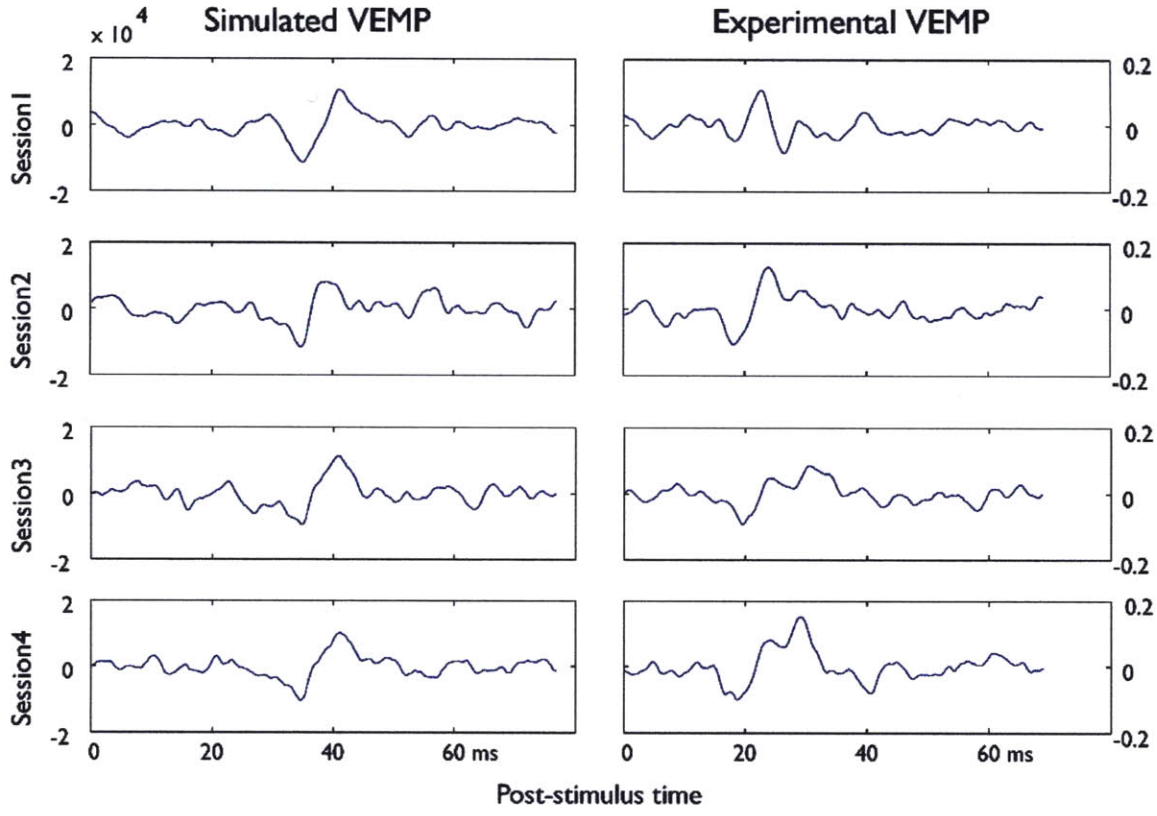

Figure 4.28 Experimental and Simulated VEMPs for Subject 1

The right panels show the experimental VEMP waveforms computed for 4 different recording sessions from Subject 1. Each trace represents the average of ~500 traces recorded under maximum voluntary contraction, with a stimulus level of 90dB HL. The left panels show corresponding simulation data: the average of 500 traces generated with a constant motor drive of 75 %MVC at an inhibition depth of 0.12. The inhibition duration is fixed at 6ms in all simulations.

We see that while the experimental and simulated waveforms are not identical, key similarities and differences can be identified. We find similarities in the relative levels of the VEMP response and the noise outside the 10-30ms response region. However, there is a dramatic difference in the scale of the waveform: we have not evaluated the unit response size parameter A required to establish a meaningful amplitude scale for the simulations.

Session-to-session differences in simulated VEMP can be attributed to statistical noise and to differences in the unit response as illustrated in Figure 4.17

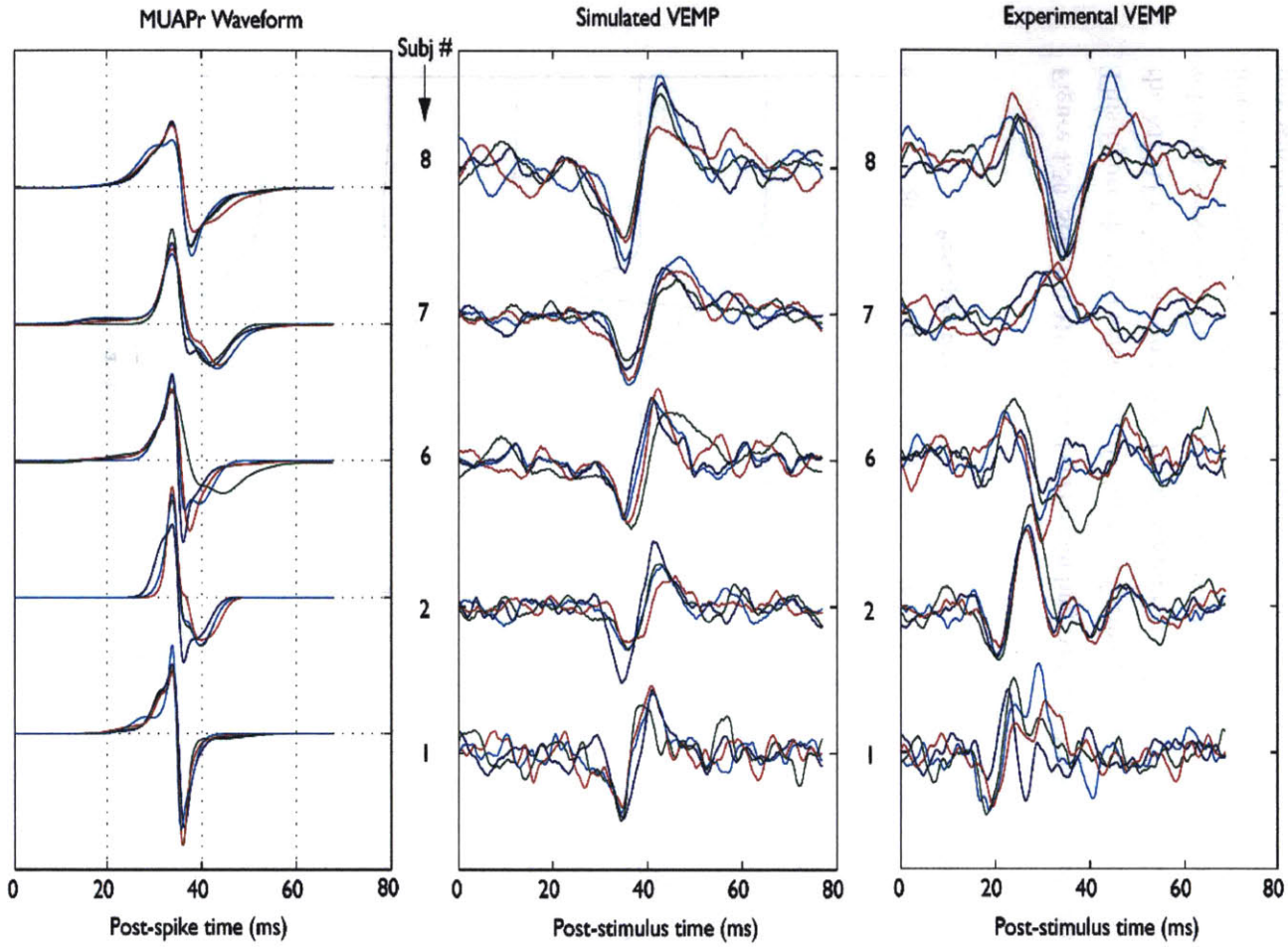

Figure 4.29 Computed surface response, simulated VEMP and experimental VEMP for all subjects and sessions

This figure extends the comparison of Figure 4.28 to all subjects and sessions. The left column shows the MUAPr waveform derived from the experimental EMG recorded under low- or zero-stimulus conditions. The middle column shows the waveform of the average of 500 simulated traces at a motor drive of 55 %MVC and an inhibition depth of 0.08. The right column shows the average of approximately 500 experimental traces recorded with the subject exerting maximum contraction effort, and a 90dB stimulus intensity.nce again, we can compare simulated and experimental VEMP waveforms, but now we look at similarities and differences between sessions and subjects, and relate them to the tissue transfer functions represented by the MUAPrs.

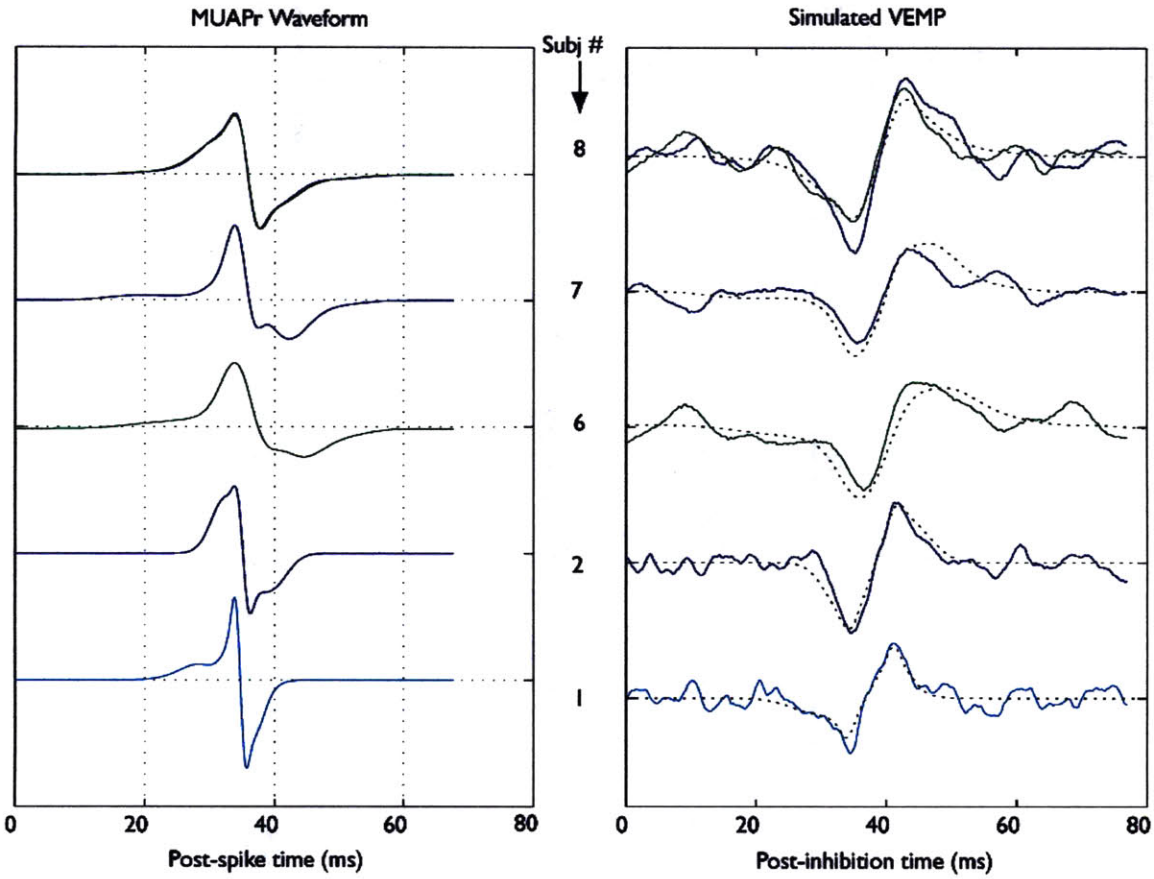

Figure 4.30 Selected MUAPr and corresponding synthetic VEMP waveforms

This figure shows a selection of the waveforms from Figure 4.29, illustrating the variety of the MUAPr shapes computed from the autocorrelations of the EMGs from different subjects/sessions (left), and the corresponding synthetic VEMP averages (right). The dotted line is the "theoretical" response formed by convolving the MUAPr waveform and the spike rate waveform consisting of the flat 6ms inhibition.

To illustrate the influence of the randomness inherent in the signal, we show (for Subject 8) two different synthetic VEMP averages where the MUAPr shape was virtually identical. Since all other simulation parameters are the same, the differences in VEMP arise from the statistical fluctuations in the spike counts over the inhibition interval, with a very small contribution from the additive noise.

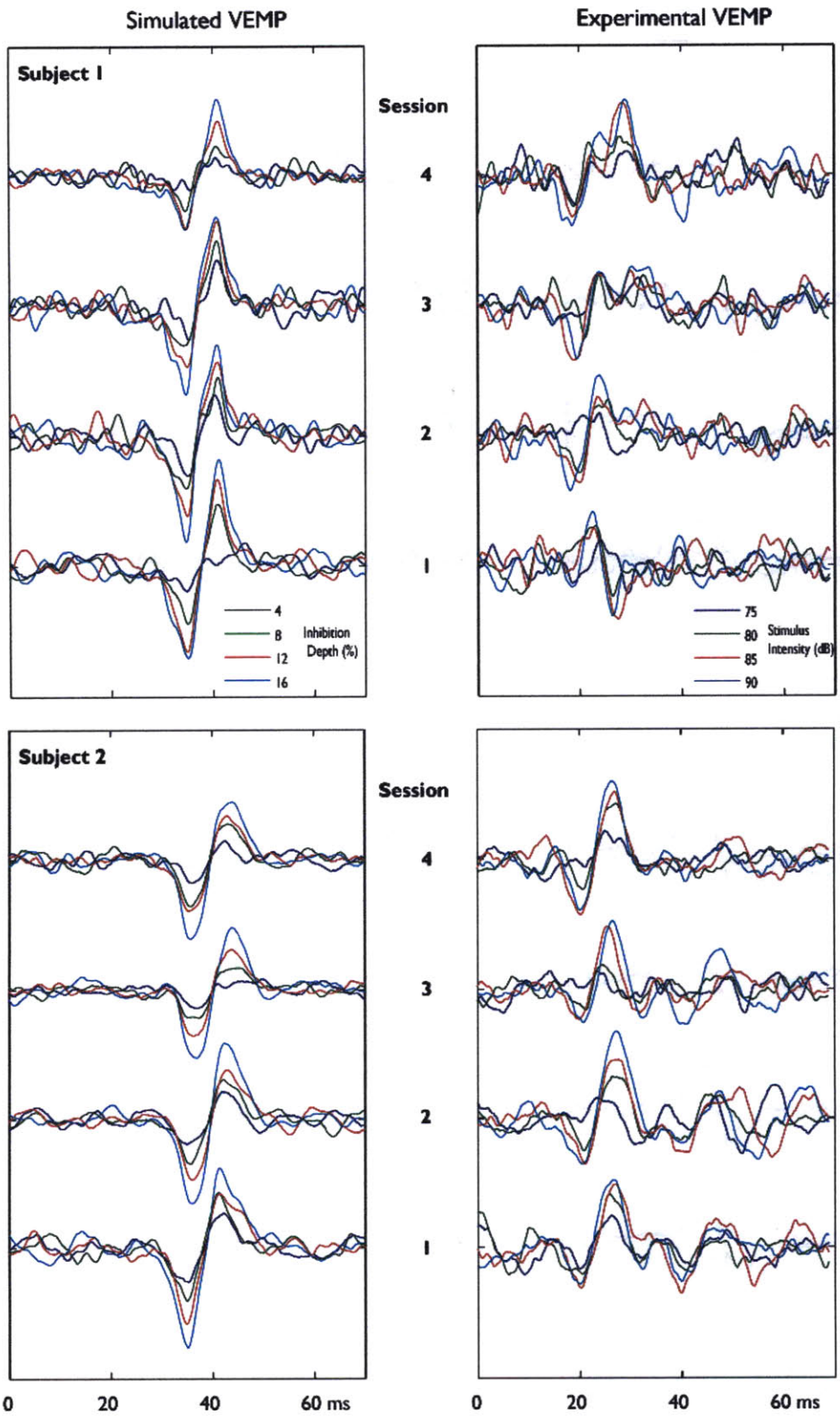

Figure 1.32 A, B (cont'd)

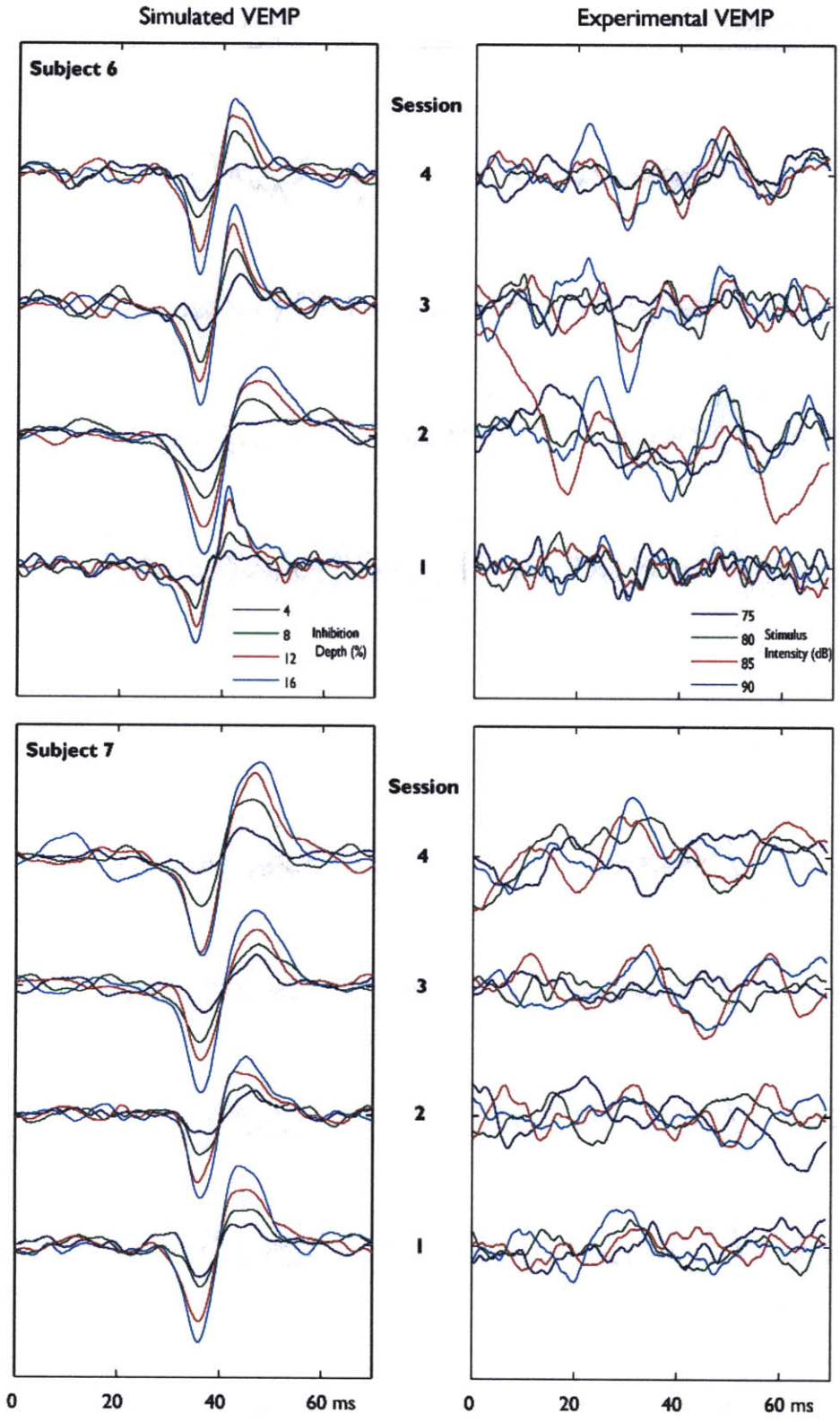

Figure 1.32 C, D (cont'd)

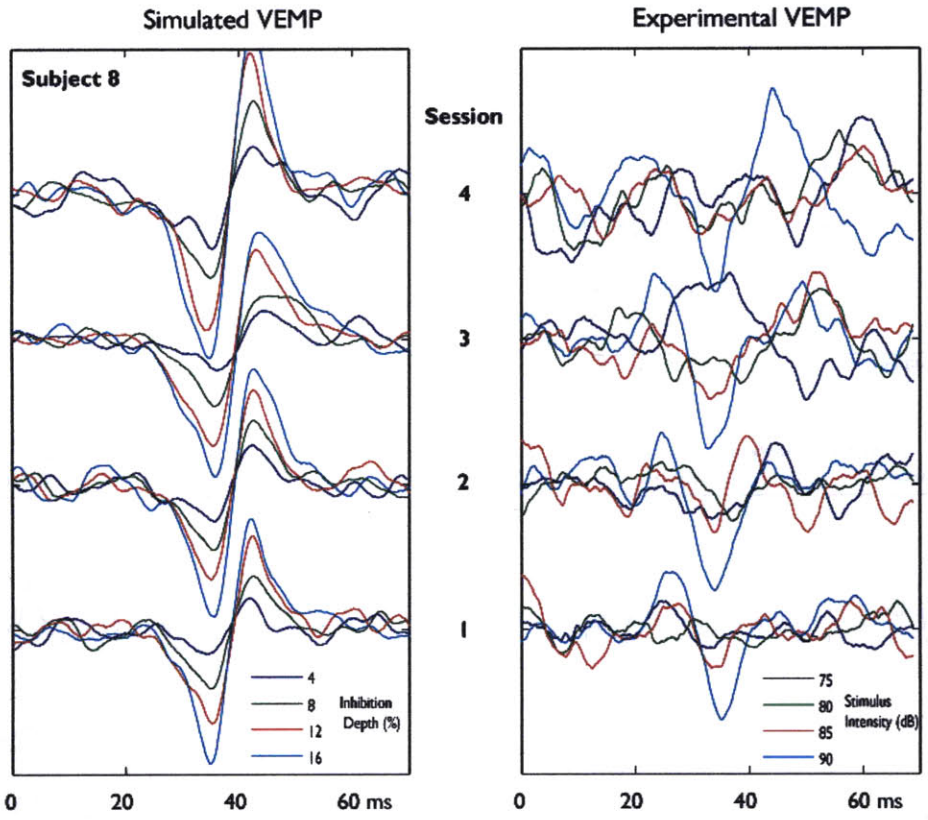

Figure 4.31 Growth of simulated and experimental VEMP with stimulus level

This figure consists of 5 panels (one for each subject studied), and in each panel, the left figure shows the synthetic VEMP responses, while the right figure shows the experimental VEMP. Each set of superimposed curves corresponds to a single session; and each curve in the set is the response computed at a given inhibition depth (left figures), or recorded at a given stimulus intensity (right figures). All simulations were done at a motor drive set to 75% MVC, and all recordings were with the subject exerting maximum contraction effort. Each curve represents the average of ~500 traces.

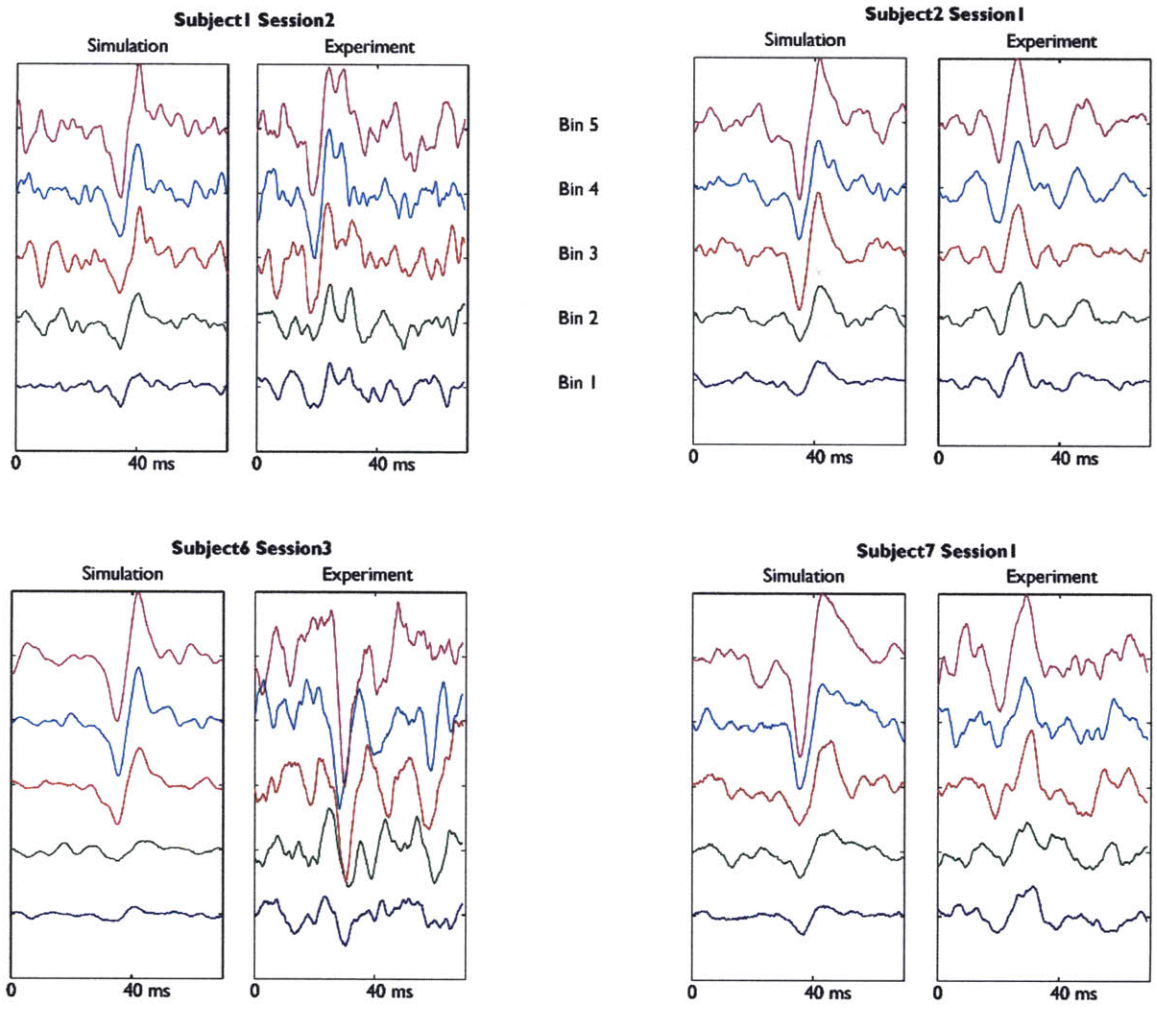

Figure 4.32 Growth of simulated and experimental VEMP with motor drive

For a selection of subjects and sessions, this figure shows sub-averages of simulated (left panels) and recorded (right panels) traces that have been grouped based on the range of filtered rms EMG associated with them. There are 5 such EMG ranges (bins) in each ensemble of 500 traces, Bin 1 corresponding to the 100 lowest EMG levels and Bin 5 being the top 100 EMG levels. The motor drive in the simulations is varied *pari passu* with changes in the EMG level of the corresponding experimental traces. The stimulus level for the recordings is 90dB, and the inhibition depth for simulations is 12%.

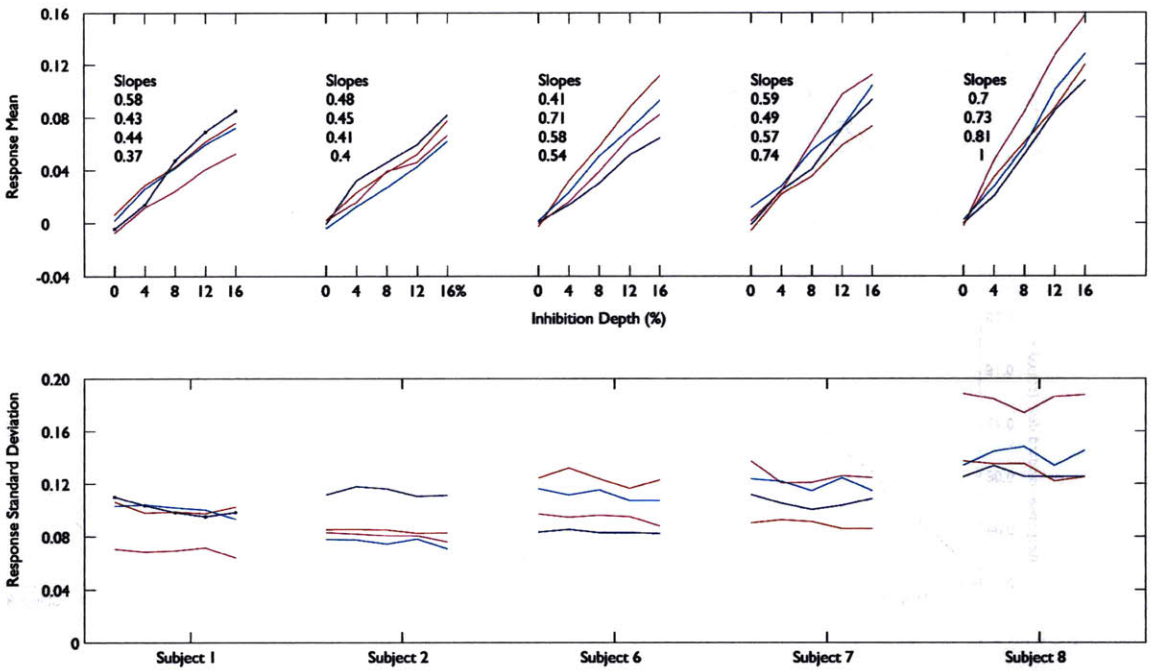

Figure 4.33 Simulation: Variation of mean VEMP response and std. dev. of response with inhibition depth

This figure shows the response growth with inhibition depth for the simulated VEMP (top panel) as well as the dependence on inhibition depth of the response variability (bottom panel). Each group of curves refers to a different subject, and each curve is the growth characteristic for a single session. The x-axis is the inhibition depth, ranging from 0 (no inhibition), to 0.16 (16%).

Each point is computed from an ensemble of 500 traces simulated at the specified inhibition depth and a motor drive of 75 %MVC. We compute the inner product of each trace in the ensemble with the simulated prototype response for the particular subject and session. The mean of these 500 inner products yields a point on one of the curves in the top panel, while the corresponding point in the bottom panel is the standard deviation of these inner products.

In the top panel, the insets indicate the slope of a linear fit to the 5 points of the response growth curve. The slopes for all 4 sessions are shown for each subject.

The units (nominally Volts, but with an undetermined scale factor) are the same for both top and bottom panels.

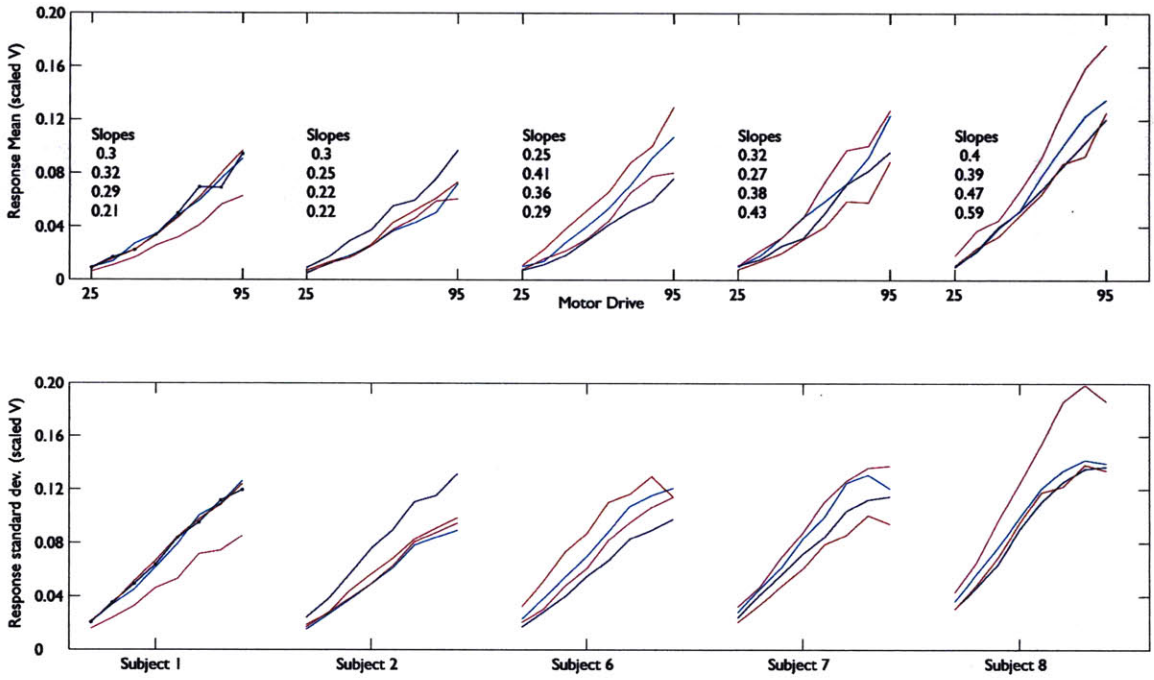

Figure 4.34 Simulation: Variation of mean VEMP response and std. dev. of the response with motor drive

The mean and standard deviation of the synthetic VEMP response level are shown as in the previous figure, but this time as a function of the motor drive.

As we expect from the qualitative observations in Figure 4.32, the signal level is seen to increase with increased motor drive. The relationship is not as clearly linear as the stimulus level dependence in the top panel of Figure 4.33, but is close to linear. We show the slopes of a linear fit to the data, as before.

Unlike the stimulus level dependency, we find that the variability of the response increases almost linearly with the motor drive over most of the simulated range of motor drives.

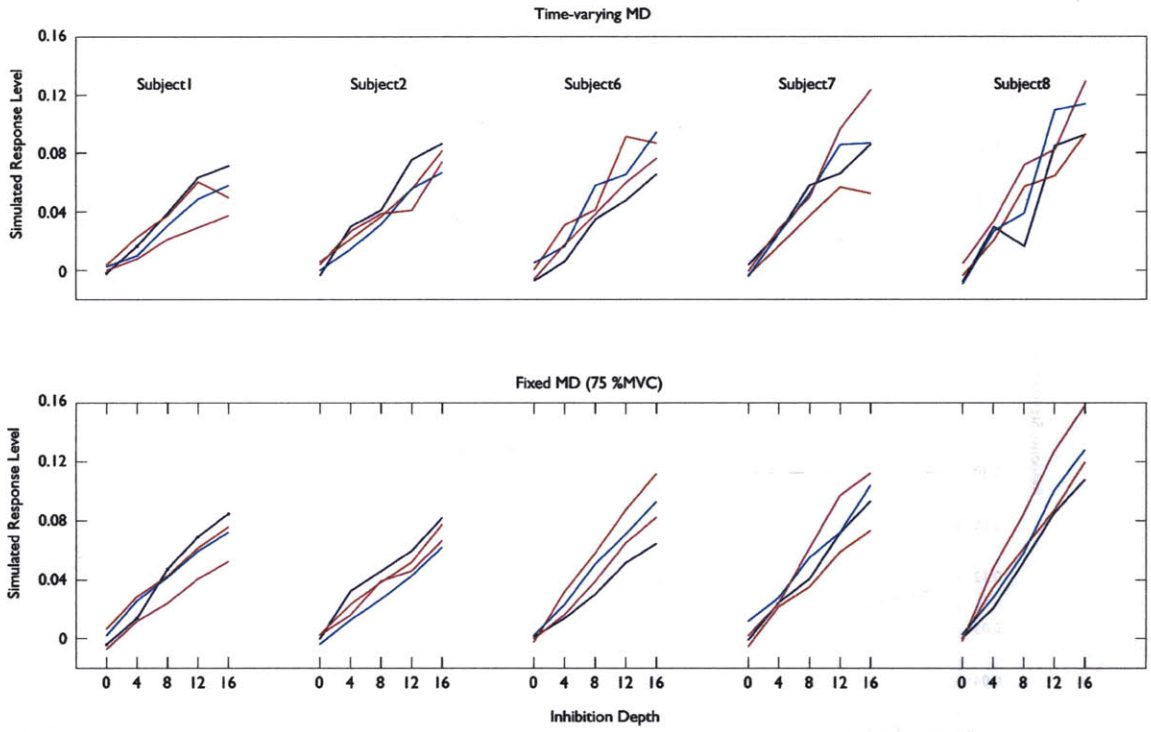

Figure 4.35 Response level growth functions (simulated VEMP): Comparison of fixed and variable motor drive.

This figure shows the response growth functions of simulated data for the case of fixed motor drive (bottom panel) and motor drive that is varied in the same manner as the experimental traces (top panel).

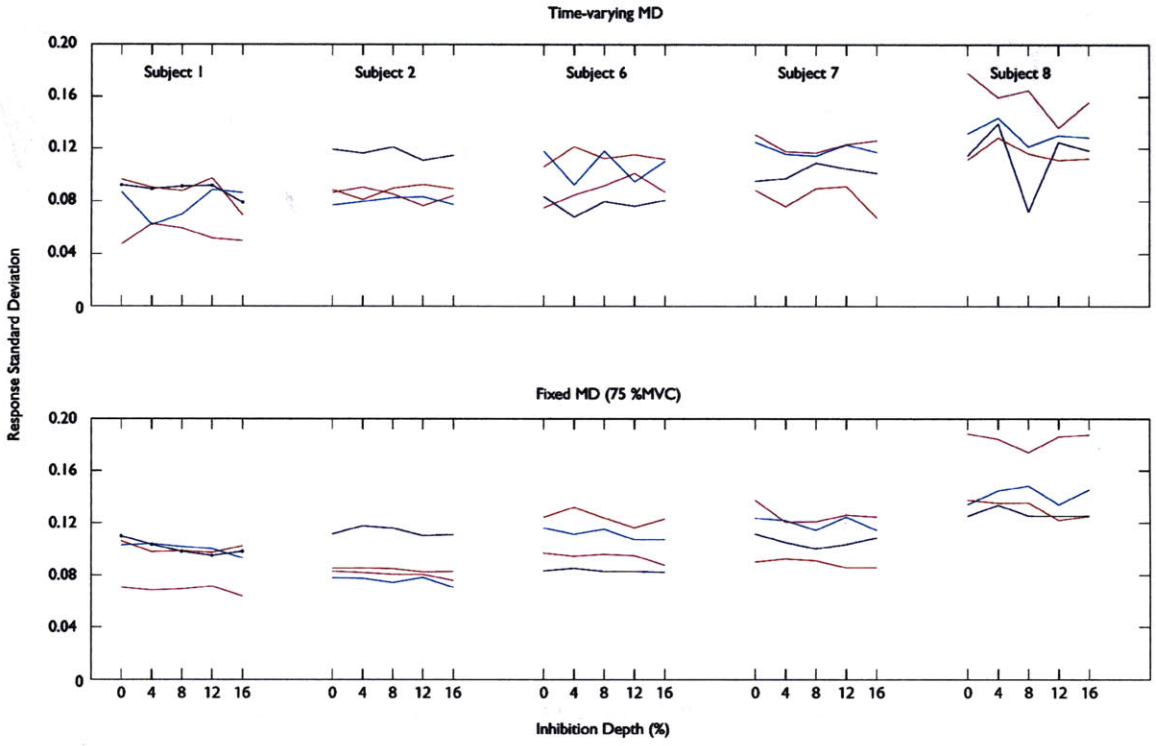

Figure 4.36 Response level variability (simulated VEMP): Comparison of fixed and variable motor drive.

Under fixed motor drive (bottom) and variable motor drive (top), we see similar values for the standard deviation of the response level across the trace ensemble. The variable drive does not appear to substantially increase the magnitude of the variability in response.

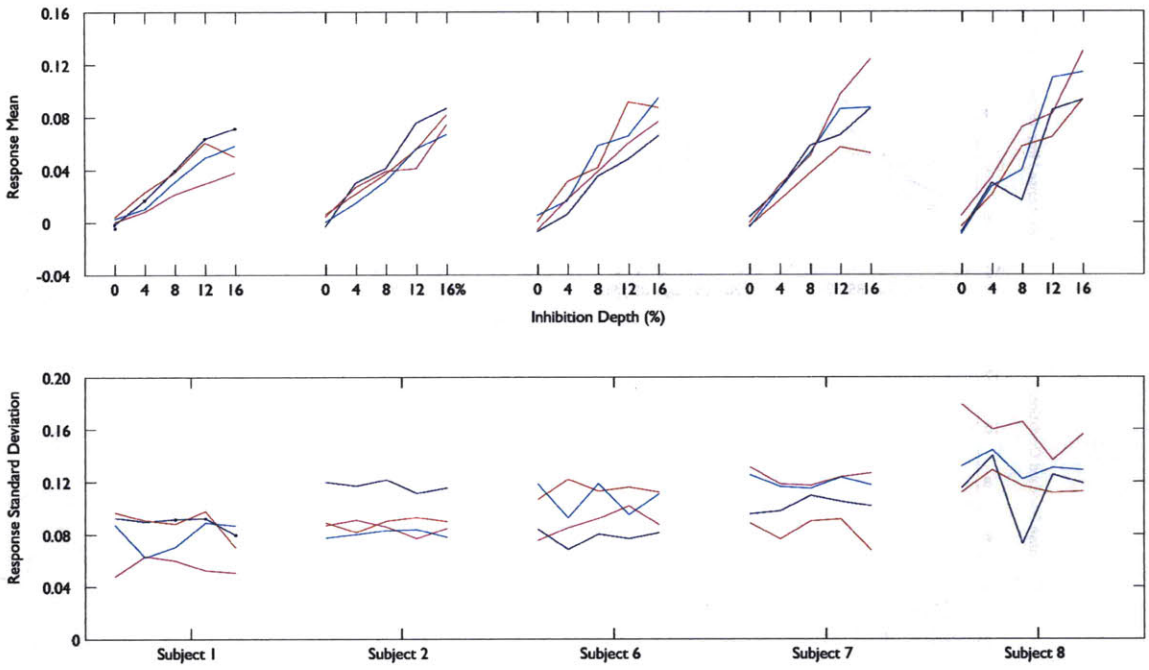

Figure 4.37 Simulation with variable drive: Growth of mean and std. dev. of the response level with inhibition depth

This figure shows the top panel of the previous two figures: it is the variable-motor-drive version of Figure 4.33

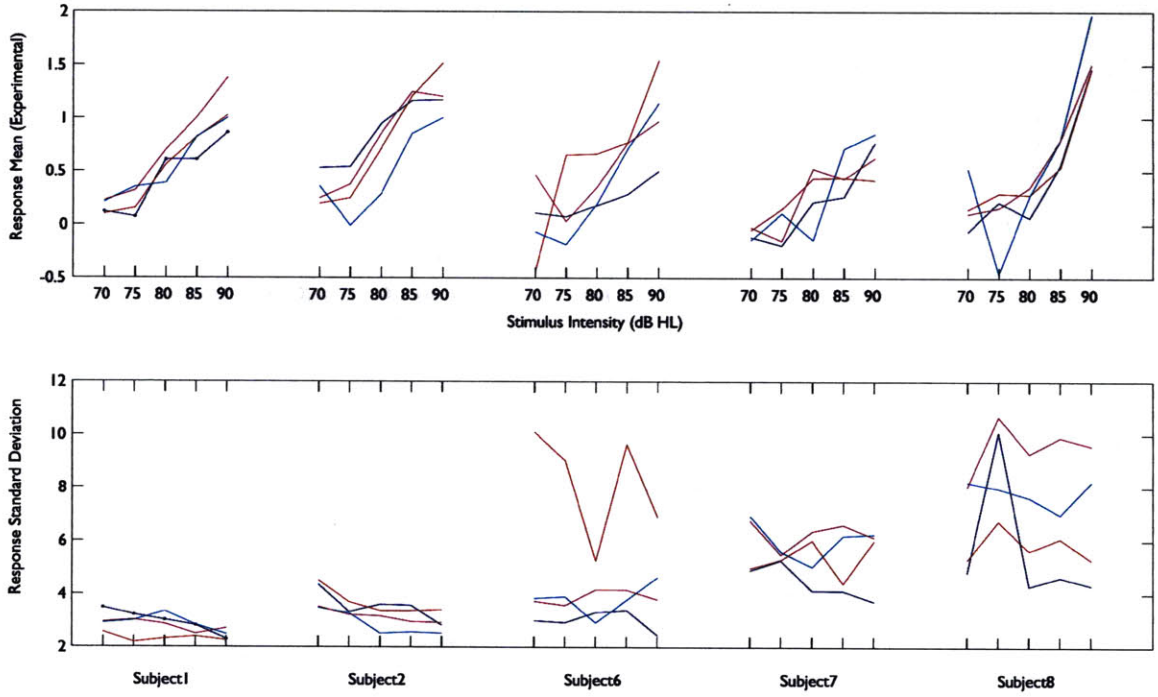

Figure 4.38 Experimental data: Variation of response mean and standard deviation with stimulus level

This figure replicates the analysis shown in Figure 4.33 for experimental data. The independent variable on the x-axis is the stimulus level instead of inhibition depth. The top panel shows the growth in mean VEMP response level as the stimulus level is increased, where the response level in each trace is computed as the inner product of the trace with a prototype waveform derived from the maximum stimulus-maximum contraction recording for the same subject/session. The bottom panel is the standard deviation of the response level estimates over the ensemble of traces. For each subject, each curve represents a different session. Each point on a curve represents one recording in each session, with the subject maintaining "maximum" contraction effort.

As in the simulation data, the scale on the ordinate is arbitrary, but identical in both panels.

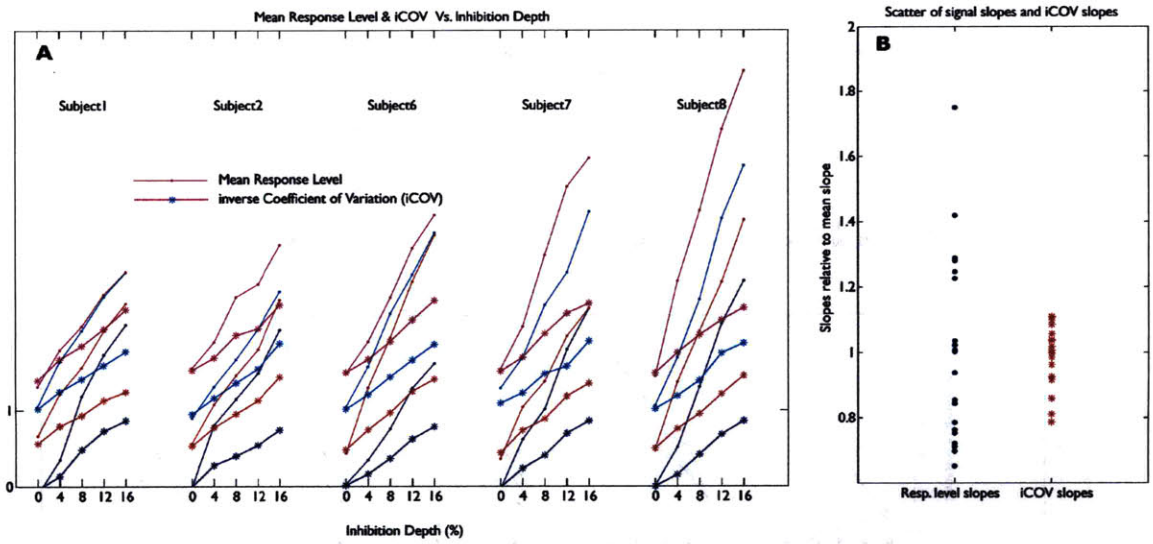

Figure 4.39 Simulation: Growth of the mean response and the iCOV with inhibition depth

The thin curves on panel A show the growth of the response level with inhibition depth, as in the top panel of Figure 4.33. The curves for different sessions of each subject have been offset slightly for clarity; as a result, we do not show a y-axis scale, only a 0-1V scale bar.. The thick lines show the growth of the ratio of the mean to standard deviation (inverse Coefficient Of Variation, or iCOV).

The two types of growth curves are seen to be approximately linear, and the slope of a linear fit can be computed in each case. We see that there is a greater diversity of slopes for the mean response characteristic than for the iCOV characteristic. In the panel B we show the spread of slopes: The slopes of each type of characteristic are computed for all 4 sessions and all 5 subjects. Each slope is then scaled by the mean of all the slope, and the results for each curve are shown as a function of the type of characteristic. The spread of the slope values about the mean is seen to be significantly larger for the response level curves than for the iCOV curves, i.e., the iCOV slope appears to be more robust to differences of subject and session.

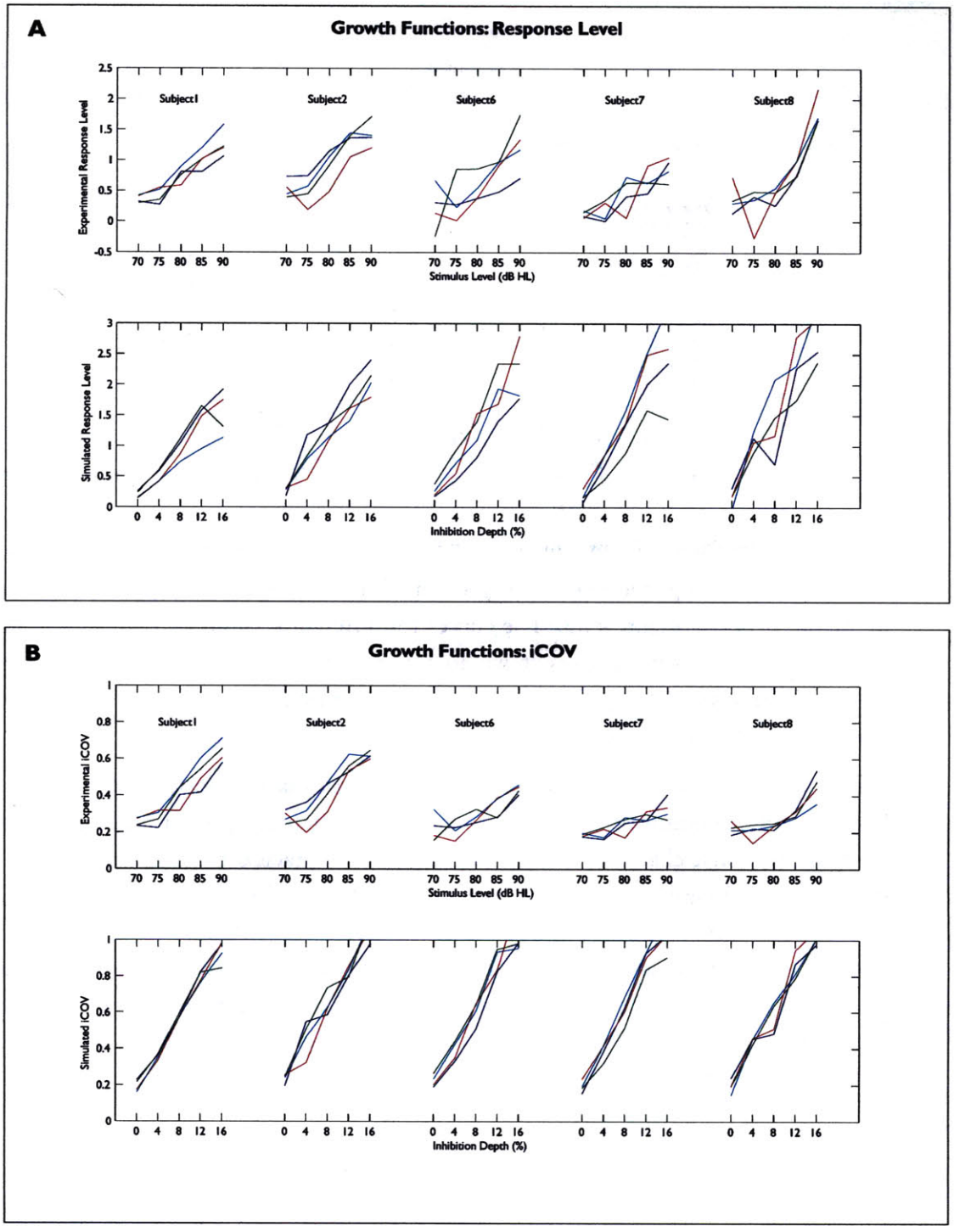

Figure 4.40 Growth of iCOV with stimulus level and inhibition depth

This figures shows a comparison of the growth curves of the response level (Fig. A) and iCOV (Fig. B). The top panels in each figure show experimental data as a function of stimulus intensity, while the bottom panels show simulation data as a function of inhibition depth.

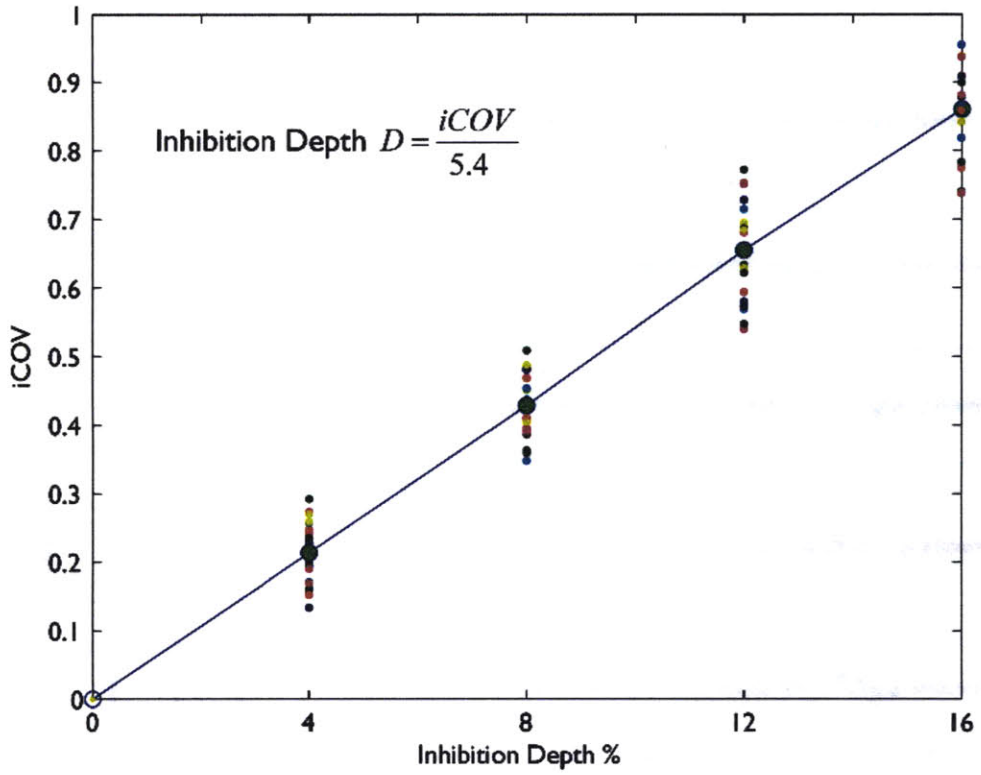

Figure 4.41 Relationship between iCOV and inhibition depth

At each value of inhibition depth between 0 and 16%, the small dots show the 20 iCOV values computed from the simulated trace ensembles (with variable motor drive) for each subject and session. The larger circles show the mean iCOV at each inhibition depth, and the line connecting these means shows the close to linear relationship between the simulation parameter (inhibition depth D), and the measured parameter (iCOV). A linear regression based on the pairs of iCOV and depth values is found to yield the relationship $D = \frac{iCOV}{5.4}$.

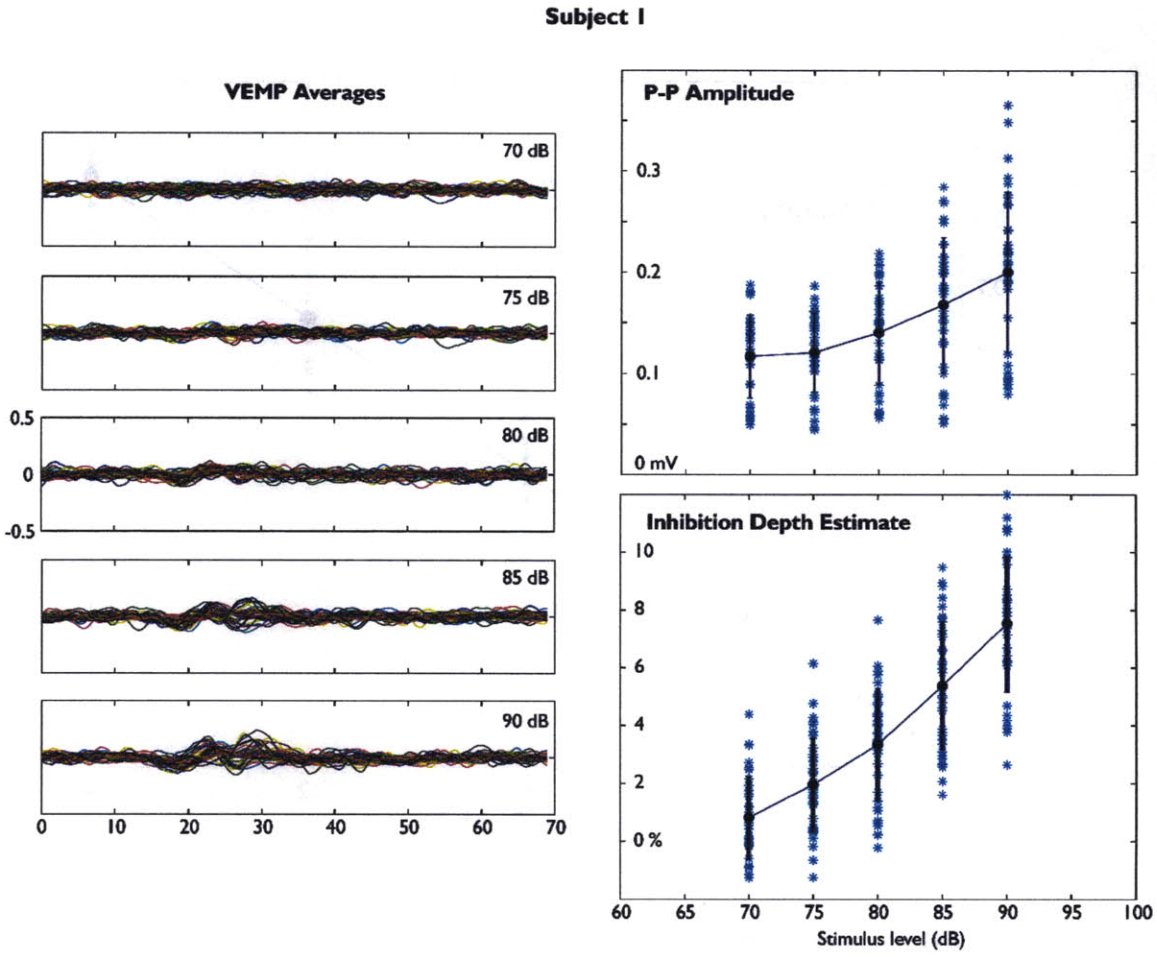

Figure 4.42 Comparison of traditional and proposed response magnitude estimates: Subject 1

At each stimulus intensity, the left panel shows the 36 VEMP averages, across all sessions for Subject 1. The right panels show growth curves of two response magnitude measures: the absolute peak-to-peak amplitude (top) and the inhibition depth estimate computed in Section 4.9 (bottom). The individual stars show the 36 values computed at each stimulus intensity, and the error bars represent 1 standard deviation about the mean. The solid line connects the mean values and represents the growth of the response magnitude with stimulus intensity.

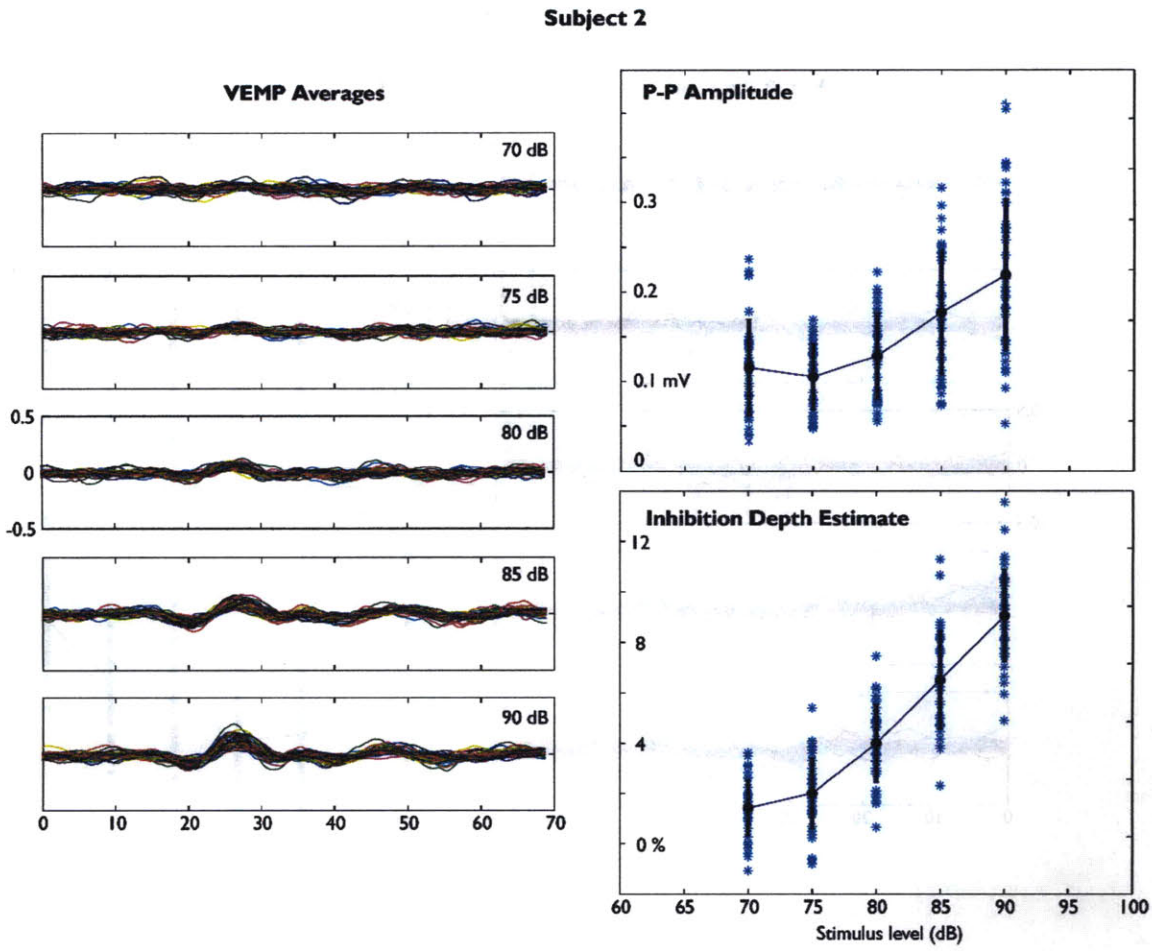

Figure 4.43 Comparison of response magnitude estimates: Subject 2 (See caption for Figure 4.42)

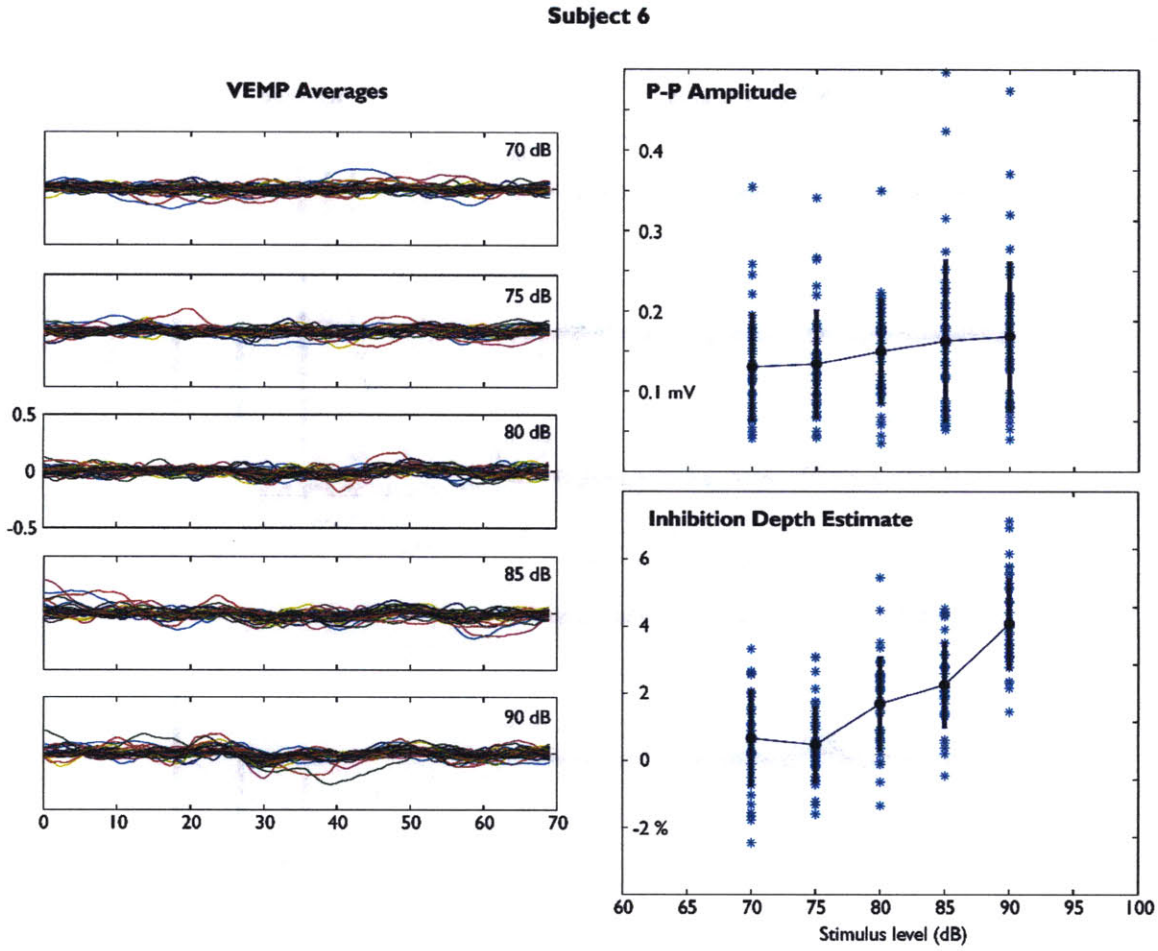

Figure 4.44 Comparison of response magnitude estimates: Subject 6 (See caption for Figure 4.42)

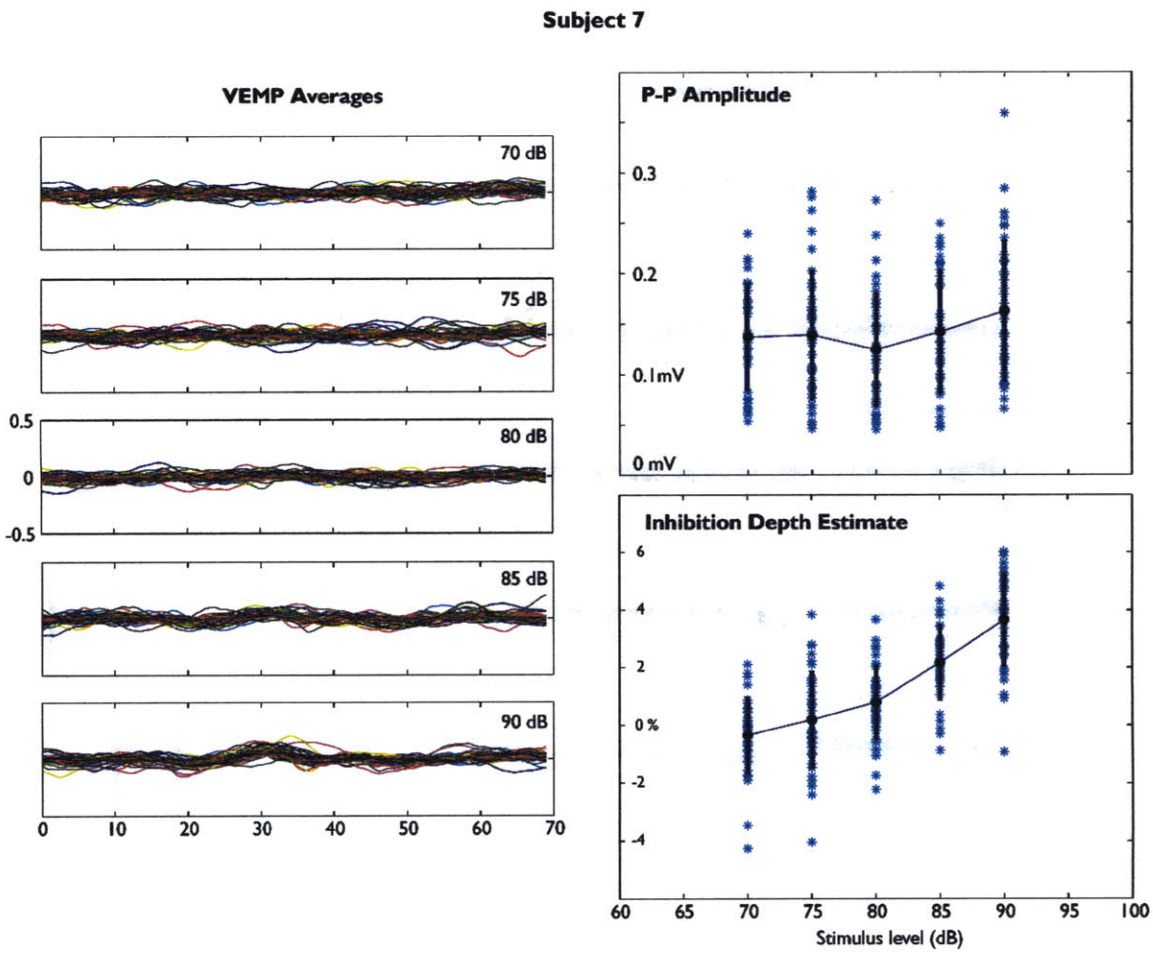

Figure 4.45 Comparison of response magnitude estimates: Subject 7 (See caption for Figure 4.42)

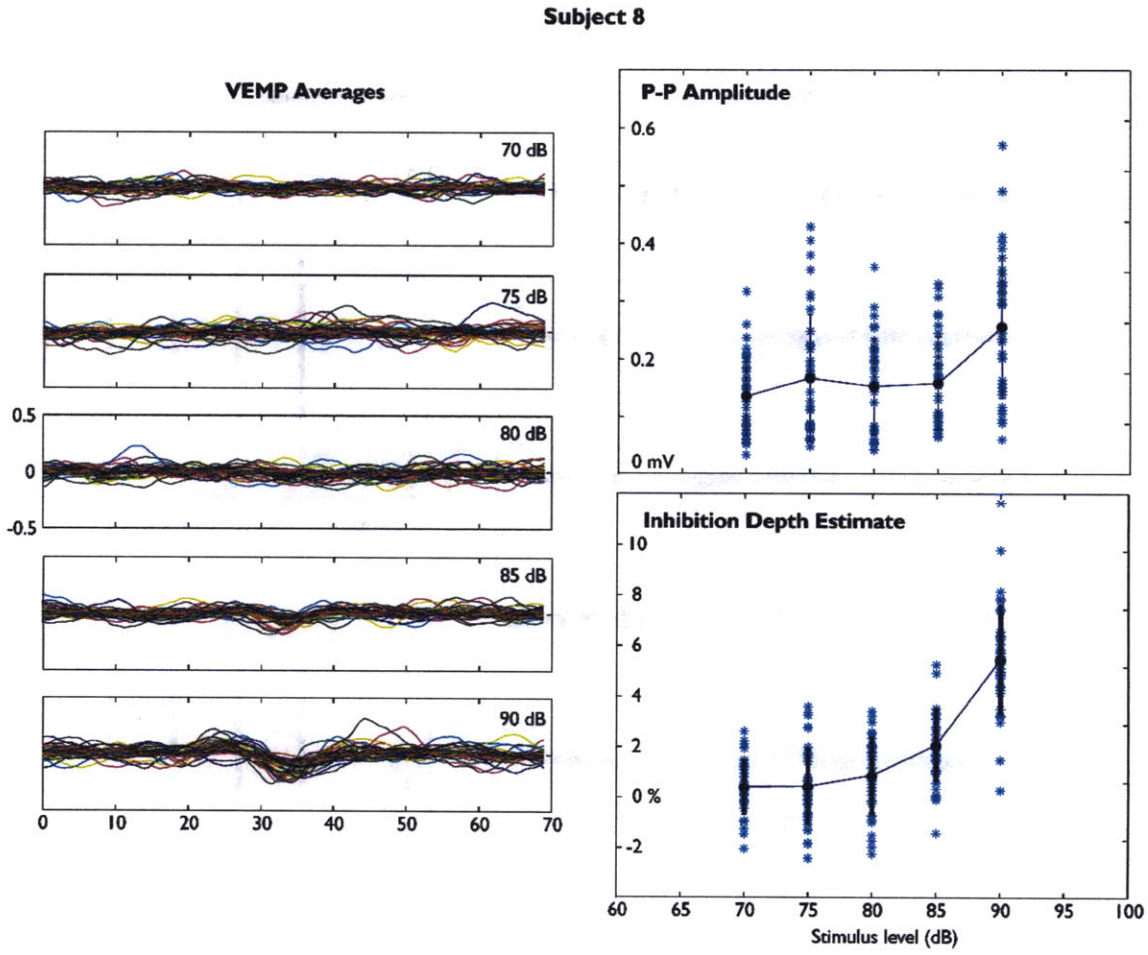

Figure 4.46 Comparison of response magnitude estimates: Subject 8 (See caption for Figure 4.42)

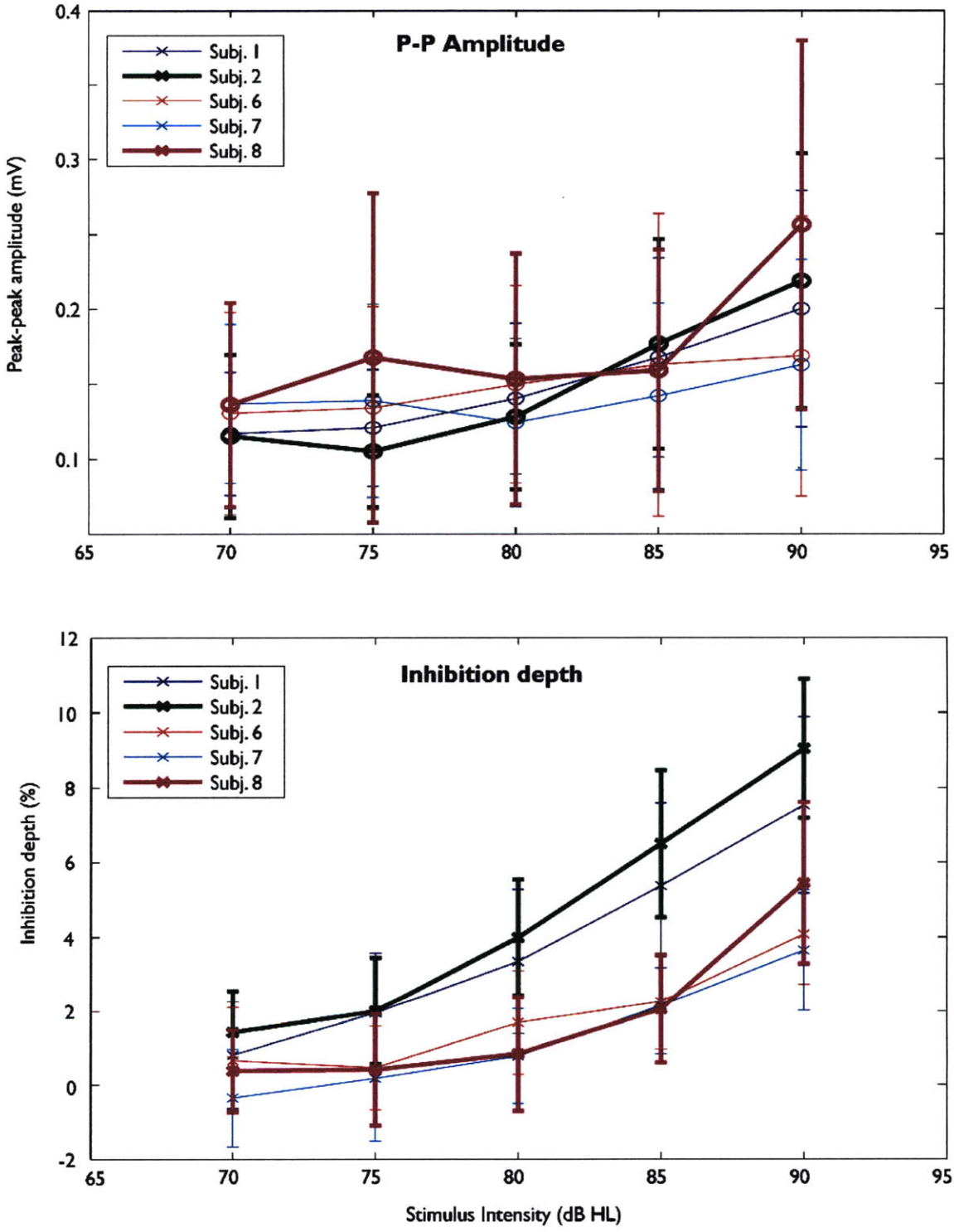

Figure 4.47 Performance of peak-to-peak amplitude and inhibition depth measures of VEMP response

4.13 References

1. Baloh, R.W. and V. Honrubia, *Clinical neurophysiology of the vestibular system*. Contemporary neurology series. 1979, Philadelphia: F. A. Davis Co. ix, 230 p.
2. Brookhart, J.M., V.B. Mountcastle, and H.W. Magoun, *The Nervous system (Handbook of Physiology)*. Vol. 5. 1977, Bethesda, Md.: American Physiological Society.
3. Highstein, S.M., R.R. Fay, and A.N. Popper, *The Vestibular System*. Springer Handbook of Auditory Research. 2004, New York: Springer. xvi, 560 p.
4. Hoffman, R.M., D. Einstadter, and K. Kroenke, *Evaluating dizziness*. American Journal of Medicine 1999; **107**(5):468.
5. Fife, T.D., et al., *Assessment: Vestibular testing techniques in adults and children: Report of the Therapeutics and Technology Assessment Subcommittee of the American Academy of Neurology*. Neurology 2000; **55**(10):1431.
6. Wuyts, F.L., et al., *Vestibular function testing*. Current opinion in neurology 2007; **20**:19.
7. Ashcroft, D.W. and C.S. Hallpike, *On the function of the saccule*. The Journal of Laryngology and Otology 2007; **49**(07):450.
8. Todd, N.P., F.W. Cody, and J.R. Banks, *A saccular origin of frequency tuning in myogenic vestibular evoked potentials? implications for human responses to loud sounds*. Hear Res 2000; **141**(1-2):180.
9. Didier, A. and Y. Cazals, *Acoustic responses recorded from the saccular bundle on the eighth nerve of the guinea pig*. Hear Res 1989; **37**(2):123.
10. McCue, M.P. and J.J. Guinan, *Acoustically Responsive Fibers In The Vestibular Nerve Of The Cat*. Journal Of Neuroscience 1994; **14**(10):6058.
11. Young, E.D., C. Fernandez, and J.M. Goldberg, *Responses of squirrel monkey vestibular neurons to audio-frequency sound and head vibration*. Acta oto-laryngologica 1977; **84**(5-6):352.
12. Wilson, V.J., et al., *The vestibulocollic reflex*. J Vestib Res 1995; **5**(3):147.
13. Wilson, V.J. and R.H. Schor, *The neural substrate of the vestibulocollic reflex. What needs to be learned*. Exp Brain Res 1999; **129**(4):483.
14. Routal, R.V. and G.P. Pal, *Location of the spinal nucleus of the accessory nerve in the human spinal cord*. J Anat 2000; **196 (Pt 2)**:263.
15. Falla, D., et al., *Location of innervation zones of sternocleidomastoid and scalene muscles - a basis for clinical and research electromyography applications*. Clinical Neurophysiology 2002; **113**(1):57.
16. Kamibayashi, L.K. and F.J.R. Richmond, *Morphometry of human neck muscles*. Spine 1998; **23**(12):1314.
17. Richmond, F.J.R., K. Singh, and B.D. Corneil, *Neck Muscles in the Rhesus Monkey. I. Muscle Morphometry and Histochemistry*. J Neurophysiol 2001; **86**(4):1717.
18. Blouin, J.S., et al., *Neural control of superficial and deep neck muscles in humans*. Journal of neurophysiology 2007; **98**(2):920.

19. Corneil, B.D., et al., *Neck muscles in the rhesus monkey. II. Electromyographic patterns of activation underlying postures and movements*. Journal Of Neurophysiology 2001; **86**(4):1729.
20. Burke, R., *Motor units: anatomy, physiology, and functional organization.*, in *Handbook of physiology: the nervous system, section 1*, V. Brooks, Editor. 1981, American Physiological Society: Bethesda, MD. p. 345-422.
21. Buchthal, F. and H. Schmalbruch, *Motor Unit Of Mammalian Muscle*. Physiological Reviews 1980; **60**(1):90.
22. Merletti, R. and P. Parker, *Electromyography: physiology, engineering, and noninvasive applications*. IEEE Press series in biomedical engineering. 2004, [Hoboken, NJ]: IEEE/John Wiley & Sons. xxii, 494 p.
23. Hogan, N. and R.W. Mann, *Myoelectric signal processing: optimal estimation applied to electromyography--Part I: derivation of the optimal myoprocessor*. IEEE Trans Biomed Eng 1980; **27**(7):382.
24. De Luca, C.J., *Physiology and mathematics of myoelectric signals*. IEEE Trans Biomed Eng 1979; **26**(6):313.
25. Farina, D. and R. Merletti, *A novel approach for precise simulation of the EMG signal detected by surface electrodes*. Ieee Transactions On Biomedical Engineering 2001; **48**(6):637.
26. Kushiro, K., et al., *Saccular and utricular inputs to sternocleidomastoid motoneurons of decerebrate cats*. Experimental Brain Research 1999; **126**(3):410.
27. Colebatch, J.G. and J.C. Rothwell, *Motor unit excitability changes mediating vestibulocollic reflexes in the sternocleidomastoid muscle*. Clinical Neurophysiology 2004; **115**(11):2567.
28. Rauch, S.D., et al., *Vestibular evoked myogenic potentials show altered tuning in patients with Meniere's disease*. Otology & neurotology 2004; **25**(3):333.
29. Welgampola, M.S. and J.G. Colebatch, *Characteristics and clinical applications of vestibular-evoked myogenic potentials*. Neurology 2005; **64**(10):1682.
30. Taylor, A.M., E.A. Christou, and R.M. Enoka, *Multiple features of motor-unit activity influence force fluctuations during isometric contractions*. Journal of neurophysiology 2003; **90**(2):1350.
31. Christakos, C.N., *A linear stochastic model of the single motor unit*. Biol Cybern 1982; **44**(2):79.
32. Christakos, C.N., *A study of the muscle force waveform using a population stochastic model of skeletal muscle*. Biol Cybern 1982; **44**(2):91.
33. Zhou, P. and W.Z. Rymer, *Factors governing the form of the relation between muscle force and the EMG: A simulation study*. Journal Of Neurophysiology 2004; **92**(5):2878.
34. Hamilton-Wright, A. and D.W. Stashuk, *Physiologically based simulation of clinical EMG signals*. Ieee Transactions On Biomedical Engineering 2005; **52**(2):171.
35. Zhou, P. and W.Z. Rymer, *Can standard surface EMG processing parameters be used to estimate motor unit global firing rate?* Journal of neural engineering 2004; **1**(2):99.
36. Farina, D., C. Cescon, and R. Merletti, *Influence of anatomical, physical, and detection-system parameters on surface EMG*. Biol Cybern 2002; **86**(6):445.
37. Wang, W., A. De Stefano, and R. Allen, *A simulation model of the surface EMG signal for analysis of muscle activity during the gait cycle*. Computers In Biology And Medicine 2006; **36**(6):601.

38. McGill, K.C., *Surface electromyogram signal modelling*. Med Biol Eng Comput 2004; **42**(4):446.
39. Agarwal, G.C. and G.L. Gottlieb, *Analysis Of Electromyogram By Fourier, Simulation And Experimental Techniques*. Ieee Transactions On Biomedical Engineering 1975; **BM22**(3):225.
40. Fuglevand, A.J., D.A. Winter, and A.E. Patla, *Models of recruitment and rate coding organization in motor-unit pools*. J Neurophysiol 1993; **70**(6):2470.
41. Deluca, C.J. and Z. Erim, *Common Drive Of Motor Units In Regulation Of Muscle Force*. Trends In Neurosciences 1994; **17**(7):299.
42. Coggshall, J.C., *Linear models for biological transducers and impulse train spectra: general formulation and review*. Kybernetik 1973; **13**(1):30.
43. Murofushi, T. and I.S. Curthoys, *Physiological and anatomical study of click-sensitive primary vestibular afferents in the guinea pig*. Acta Oto-Laryngologica 1997; **117**(1):66.
44. Masaki, Y., et al., *Cervical reflex induced by click stimuli in cats*. Acta Oto-Laryngologica 2002; **122**(6):607.
45. Cheng, P.W. and T. Murofushi, *The effect of rise/fall time on vestibular-evoked myogenic potential triggered by short tone bursts*. Acta oto-laryngologica 2001; **121**(6):696.
46. Cheng, P.W. and T. Murofushi, *The effects of plateau time on vestibular-evoked myogenic potentials triggered by tone bursts*. Acta oto-laryngologica 2001; **121**(8):935.
47. Duchene, J. and J.Y. Hogrel, *A model of EMG generation*. IEEE Trans Biomed Eng 2000; **47**(2):192.
48. Keenan, K.G., et al., *Influence of motor unit properties on the size of the simulated evoked surface EMG potential*. Experimental Brain Research 2006; **169**(1):37.
49. Fuglevand, A.J., et al., *Detection Of Motor Unit Action-Potentials With Surface Electrodes - Influence Of Electrode Size And Spacing*. Biol Cybern 1992; **67**(2):143.
50. Monster, A.W. and H. Chan, *Surface electromyogram potentials of motor units; relationship between potential size and unit location in a large human skeletal muscles*. Exp Neurol 1980; **67**(2):280.
51. Hughes, A.R. and J.G. Colebatch, *Surface Potentials Generated By Synchronous Activation Of Different Fractions Of the Motor Pool*. Muscle & Nerve 1996; **19**:836.
52. Coggshall, J.C. and G.A. Bekey, *A stochastic model of skeletal muscle based on motor unit properties*. Math. Biosci 1970; **7**:405.
53. Clamann, H.P., *Statistical analysis of motor unit firing patterns in a human skeletal muscle*. Biophys J 1969; **9**(10):1233.
54. Luca, C.J. and W.J. Forrest, *Some properties of motor unit action potential trains recorded during constant force isometric contractions in man*. Biol Cybern 1973; **12**(3):160.
55. Shiavi, R. and M. Negin, *Stochastic properties of motoneuron activity and the effect of muscular length*. Biol Cybern 1975; **19**(4):231.
56. Zhang, Y.T., P.A. Parker, and R.N. Scott, *Study of the effects of motor unit recruitment and firing statistics on the signal-to-noise ratio of a myoelectric control channel*. Med Biol Eng Comput 1990; **28**(3):225.
57. Hamilton, A.F., K.E. Jones, and D.M. Wolpert, *The scaling of motor noise with muscle strength and motor unit number in humans*. Exp Brain Res 2004; **157**(4):417.
58. McComas, A.J., *Motor Units-How Many, How Large, What Kind?* ISEK-XII 98:288.
59. Lillie, J.H. and B.A. Bauer, *Sectional anatomy of the head and neck: a detailed atlas*. 1994, New York: Oxford University Press. 212 p.

60. Enoka, R.M. and A.J. Fuglevand, *Motor unit physiology: some unresolved issues*. Muscle & nerve 2001; **24**(1):4.
61. Gath, I. and E. Stalberg, *In situ measurement of the innervation ratio of motor units in human muscles*. Exp Brain Res 1981; **43**(3-4):377.
62. Buchthal, F., C. Guld, and P. Rosenfalck, *Action Potential Parameters In Normal Human Muscle And Their Dependence On Physical Variables*. Acta Physiol Scand 1954; **32**(2-3):200.
63. Clancy, E.A., S. Bouchard, and D. Rancourt, *Estimation and application of EMG amplitude during dynamic contractions*. IEEE Eng Med Biol Mag 2001; **20**(6):47.
64. Papoulis, A. and S.U. Pillai, *Probability, random variables, and stochastic processes*. 4th ed. 2002, Boston: McGraw-Hill. x, 852 p.
65. Stein, R.B., E.R. Gossen, and K.E. Jones, *Neuronal variability: noise or part of the signal?* Nat Rev Neurosci 2005; **6**(5):389.
66. Harris, C.M. and D.M. Wolpert, *Signal-dependent noise determines motor planning*. Nature 1998; **394**(6695):780.
67. Clancy, E.A. and N. Hogan, *Probability density of the surface electromyogram and its relation to amplitude detectors*. IEEE Trans Biomed Eng 1999; **46**(6):730.
68. Henneman, E., *Relation Between Size Of Neurons And Their Susceptibility To Discharge*. Science 1957; **126**(3287):1345.

Chapter 5. Conclusions and future directions

The men of experiment are like the ant, they only collect and use; the reasoners resemble spiders, who make cobwebs out of their own substance. But the bee takes the middle course: it gathers its material from the flowers of the garden and field, but transforms and digests it by a power of its own. Not unlike this is the true business of philosophy; for it neither relies solely or chiefly on the powers of the mind, nor does it take the matter which it gathers from natural history and mechanical experiments and lay up in the memory whole, as it finds it, but lays it up in the understanding altered and digested.

~ Francis Bacon

Although it is fairly well understood that the mechanisms underlying VEMP are fundamentally different from those underlying neurogenic evoked potentials, the way VEMPs are acquired, processed and interpreted in the clinic today does not take these differences into account. The VEMP is largely studied from a phenomenological point of view, examining the response for features that are conserved over the course of the measurement and across the population, and looking for quantitative differences in these features between normal and pathological populations. The difficulties with this approach have been well documented: the response is extremely variable during a measurement, and those features that show the greatest promise for distinguishing populations (viz. amplitude and threshold) are also ones that show very large dispersion of values within each population.

We have approached the question of processing VEMP from a very different direction in this study. We try to understand what processes in the vestibular system give rise to the VEMP, and hypothesize a quantitative model to relate these processes and the response waveform. Using this model, we are able to ask the question: What is the best estimate of the parameters of the vestibular processes given only the surface measurements in response to each stimulus?

The experimental system we used to address this question was largely unchanged from the conventional clinical VEMP setup, but differed in the crucial respect that we could record the response to each stimulus presented. Thus, we were free to compute a variety of statistics on the measurements, and were not constrained to the sample mean computed by the waveform average in a conventional VEMP system..

Our approach to the estimation problem was to construct a computational analog of the physiological model, to examine its outputs and to find statistics – largely by examination – that correlated with parameters of the simulated vestibular processes. Thus, we did not directly answer the question above that sought an *optimal* solution to the estimation problem; we settled instead for a metric (the iCOV), that was simply *better* than the existing measure of VEMP amplitude in terms of intra-subject variability. More important than the

statistical performance of the metric, the use of a physiologically based model provides a framework for thinking about the iCOV metric and possible refinements to this metric in a systematic fashion. This allows us to define the several different directions for future development of the model-based analysis of VEMP. We now describe some of the proposed directions of future development

5.1 Future directions: signal processing

5.1.1 Analytical basis for iCOV

We discovered the relative independence of the iCOV metric from the subject- and session-specific characteristics and from contraction effort by examining the outputs of the computational model. We would like to understand the theoretical basis for this independence. To this end, we are in the process of developing an analytical description of a simplified version of the computational model, and obtaining an expression for the iCOV ratio.

Our analytical model assumes that the composite spiking process of the motor unit pool is characterized by a linear relationship between the mean rate and the variance of the spike counts in a unit time window: a relationship that was observed in the model (Figure 4.13). We define the units of the spike rate and the modulation depth so as to be unity at the maximum effort and stimulus intensity. Using the response obtained under these conditions as the template, we compute the inner product of this template with the traces at different values of motor drive and inhibition depth. When we compute the expressions for the mean and standard deviation of the inner product, we find that the iCOV reduces to a ratio of quadratic forms which is independent of the motor drive. The analysis also suggests that the iCOV could also become independent of the tissue transfer function under certain conditions. We are currently investigating the properties of a transfer function that would display this independence, and whether a physiologically realistic transfer function would satisfy these properties.

5.1.2 Improved estimators of inhibition depth

As we have seen, the iCOV metric was obtained by examination of the outputs of the computational model. The development of an analytical model, albeit a simplified one, opens the possibility of computing estimators of the inhibition depth that are *optimal* with respect to some statistical criterion, and thus take the modeling effort to its logical conclusion. An advantage of an analytically derived estimator is that one can establish confidence bounds on the estimate. However, such an estimator is only as good as the

accuracy of the statistical model underlying it, and as the models get more detailed, the estimation problem becomes more intractable.

5.1.3 Generalized forms of modulation

In developing the model of VEMP, we used an idealized representation of the internal vestibular response in the form of a rectangular function with a fixed inhibition duration and variable inhibition depth. In focusing on the inhibition depth as the quantity of interest, we have implicitly assumed that every pathological change in the saccule results in a reduction in the amplitude of the vestibular response. It is possible, however, that in some circumstances, the principal effect of the change is in the duration of the response. A generalization of the parameter estimation method to simultaneously estimate both parameters could provide greater insight into the physiological processes in different pathologies.

A further generalization could seek use the ensemble of response traces to estimate the entire time-course of the spike rate modulation following the stimulus. This problem is of potential interest in a variety of applications beyond VEMP, where the underlying process is a point process, but only filtered observations are available, and we are interested in short term changes in the rate of the point process. There have been relatively few studies of this type of parameter estimation, but problems of this type arise in such diverse areas as seismology, neurophysiology, water-flow modeling and optical detection.

5.2 Future directions: clinical applications

An immediate follow-up to the study described in this thesis is to apply the inhibition depth estimate to a variety of identified vestibular pathologies. We propose to implement the estimation algorithm in real time on a version of the clinical VEMP system and perform a systematic clinical study on subjects recruited from the patient population at one or more centers for diagnosis and treatment of vestibular disorders. We expect to learn the normative ranges of the inhibition depth in each population, and study differences in derived parameters such as thresholds, tuning curves, and level functions.

We also propose to explore the application of these methods to other situations where the underlying mechanism is the variation in the rate of a point process, but only filtered observations are available. Examples include assessment of neuromuscular tremor, control of motor prostheses using surface signals, and in neurophysiology, for studying ion channel dynamics from membrane potential measurements.